Solenoid Operated Variable Valve Timing for Internal Combustion Engines

Girish Parvate-Patil

A Thesis

in

The Department

of

Mechanical and Industrial Engineering

Presented in Partial Fulfillment of the Requirements

For the Degree of Master of Applied Science at

Concordia University

Montreal, Quebec, Canada

April, 2005

Your file Votre référence
ISBN: 0-494-04425-X
Our file Notre référence
ISBN: 0-494-04425-X

ABSTRACT

In internal combustion engines, particularly for spark ignition (SI) engines, valve events and their timings put forth a major influence on the engine overall efficiency and its exhaust emissions. Because the conventional SI engine has fixed timing and synchronization between the camshaft and crankshaft, a compromise results among engine efficiency, performance, and its maximum power. By using variable valve timing (VVT) technology it is possible to control the valve lift, phase, and valve timing at any point on the engine map, in order to enhance the engine overall performance. To get full benefits from VVT, various types of mechanisms have been proposed and designed. Some of these mechanisms are in production and they have shown significant benefits for improving the engine performance. During the last two decades, remarkable developments have been seen in Electromagnetic valve actuators (EMVA) to obtain VVT.

Electromagnetic valve actuators, which incorporate solenoids, are increasingly becoming the actuator of choice in industry lately, due their ruggedness, low cost, and relative ease of control. Latest application of solenoid incorporating permanent magnet based EMVA's are under going research and development. This application presents challenges that require the improvement of the static and dynamic characteristic of the EMVA. Some of the challenges include, but not limited to, are attaining quiet operation, reduced bounce, less energy consumption, trajectory shaping, and high actuation speeds. In this study, effects of variable valve timing strategies on gasoline and diesel engines are discussed and analyzed. Also the static characteristics of a solenoid incorporating a permanent magnet as its core are developed, and validated with experiments. The permanent magnet core solenoid is novel in that a single electromagnet can provide bi-direction motion of the core motion. Its application to VVT can provide infinite position control and timing, force control such as to reduce impact forces, and latching capabilities, providing a novel actuator to the automotive industry.

DEDICATION

To my beloved Parents

I kept walking horizon was nearby
I kept going horizon was nearby
I was going on and on, still horizon was nearby
I stood, looked back, realized; I traveled thousands of miles,
still horizon was nearby
I had a look at all my past, felt so nice, felt like I am at horizon
I kept going because horizon was nearby

--- Girish

ACKNOWLEGEMENTS

This thesis has made one of the greatest contributions in developing my academic career.

I am greatly thankful to my supervisors, Dr. Henry Hong and Dr. Brandon Gordon who were there to help me during my research endeavour. I do appreciate their kindness, selflessness, patience and encouragement. I just couldn't have done it without their persistent guidance.

I appreciate my loving wife, Pooja, for her support and help during my thesis work.

I am grateful to John Elliott, Robert Oliver and Gilles Huard of the Department of Mechanical and Industrial Engineering, for their technical support. I also would like to thank some of my friends who have inspired me and have greatly contributed to my success in graduate school.

The author would like to thank the Natural Sciences and Engineering Research Council of Canada (NSERC) for the funding of this research project.

Girish Parvate-Patil

TABLE OF CONTENTS

LIST OF FIGURES

FIGURE **PAGE**

LIST OF TABLES

NOMENCLATURE

i - Applied current (A)

i_m - Magnetizing current (A)

i_e - Exciting current (A)

$i_e - i_m$ - Core loss component of current

l_C - Length of magnet core reluctance (19×10^{-3} m)

l_m - Length of the magnet (38×10^{-3} m)

l_x - Length of air gap at pole end (m)

l_y - Length of air gap at boss end (2×10^{-3} m)

r - Radius of the magnet (9×10^{-3} m)

x - Solenoid core gap (m)

y - Solenoid core fixed air gap (m)

A - Pole face area of the magnet (4.92×10^{-4} m^2)

A_C - Area of magnet core reluctance (2.54×10^{-3} m^2)

A_x - Area of air gap reluctance (m^2)

BDC - Bottom dead center

Bm - Magnetic flux density (T)

B_0 - External magnetic field (T)

BSFC - Brake specific fuel consumption

B_r - Residual magnetism (T) [1.45 T for NdFeB]

BsHs - Saturation point

B_z - Magnetic flux density at distance (T)

C.I. - Compression ignition

CO - Carbon Monoxide

EEVC - Early exhaust valve closing

EEVO - Early exhaust valve opening

EIVC - Early intake valve closing

EIVO - Early intake valve opening

EGR - Exhaust gas recirculation

EMVA - Electromagnetic valve actuator

EVC - Exhaust valve closing

EVO - Exhaust valve opening

F_{mag} - Force of attraction due to magnet (N)

F_{total} - Force due to solenoid coil and permanent magnet (N)

Hc - Coercive force (N)

HC - Hydrocarbons

Hm - Magnetic field intensity

IVC - Intake valve closing

IVO - Intake valve opening

LEVC - Late exhaust valve closing

LEVO - Late exhaust valve opening

L_i - Leakage inductance (mH)

LIVC - Late intake valve closing

LIVO - Late intake valve opening

$L(\phi, x)$ - Coil inductance (mH)

M - Magnetization of permanent magnet ($kJT^{-1}m^{-3}$)

N - Total number of coil windings

NOx - Nitrogen oxides

R_C - Variable resistance across the coil (Ω)

R_i - Variable resistance across the coil (0.60Ω)

RGF - Residual gas fraction

TDC - Top dead center

UBHC - Unburned Hydrocarbons

V - Applied voltage across the solenoid terminal (V)

VVA - Variable valve actuation

VVT - Variable valve timing

V_ϕ - Induced voltage across the coil due to changes from the magnetic flux (V)

dA - Area of element of through which field passes volume in the field

dV - Element of permanent magnet volume in the field

μ_C - Permeability of magnet

μ_0 - Permeability of air ($4\pi \times 10^{-7}$ $WbA^{-1}m^{-1}$)

ϕ - Magnetic flux (Wb)

$-\nabla \bullet M$ - Magnetic volume charge density

$n \bullet M$ - Magnetic surface charge density

CHAPTER 1

INTRODUCTION

1.1 General

A major goal of engine manufacturers is to minimize specific fuel consumption and emissions from engines. One solution is by the independent actuation of the inlet and exhaust valves at any position of the piston, with no more need for a camshaft. A major disadvantage of conventional SI engines results from the energy losses during the inhaling of the sub-atmospheric gases during the suction stroke and expelling of exhaust gases to atmosphere during the exhaust stroke. These pumping losses depend upon the opening and closing position of the throttle valve. The losses are high when the throttle valve tends to close and are low at wide-open throttle. Thus, the pumping losses are inversely proportional with the engine load. Without a throttle valve, control of the air-fuel mixture can be realized by variation of the intake valve-opening period; therefore, variable valve timing (VVT) has great potential for reducing pumping losses.

Residual gas fraction (RGF) is controlled by the valve overlap and cannot be changed for various speeds and loads. The fixed valve events of conventional cam controlled engines compromises the engine for better performance under all operating conditions. The inlet valve timing is the most important parameter for optimizing the engine volumetric efficiency, whereas the exhaust valve timing controls the RGF, which reduces exhaust NO_X emission. For the engine to operate efficiently and effectively over its entire operating range and conditions, the valve events should be able to vary with speed and load anywhere on the engine map. By using variable valve actuation (VVA) technology it is possible to control the

valve lift, phase, and valve timing at any point on the engine map, in order to enhance the engine overall performance.

Electromagnetic variable valve actuators, which incorporate solenoids, are increasingly becoming the most popular type of actuators being used in automobile industry, due to their low cost, ease of control, reduced complexity, and relatively high force density per unit mass. Solenoids have a relatively large force to weight ratio and high-speed characteristics, and thus they have been useful for valve actuation. This application presents some challenges and efforts need to concentrate towards quiet operation, reduced bounce, less energy consumption, desired trajectory shaping, and high actuation speed. The electromagnetic valve actuator is supposed to facilitate the concept of variable valve actuation (VVA), which is intended to replace the conventional camshaft-driven valve train. The use of the electromagnetic variable valve actuation, coupled with electronic control would be capable of variable valve timing and lift, providing an additional degree of freedom and control over the entire engine operation.

In this thesis the effects of variable valve timing on four-stroke gasoline and diesel engines are studied, and the basic model for the solenoid operated valve actuator is developed. The design of the actuator consists of using a permanent magnet core which replaces the original steel iron core of the solenoid. This device is designed to produce bidirectional motion and force when it is energized.

1.2 Valve-Train Mechanism

Located along the camshaft are cams which are egg-shaped eccentric lobes, one lobe for each valve. Each lobe has a follower as shown in fig. 1.1. As the camshaft is rotated, the follower is forced up and down as it follows the profile of the cam lobe. The followers are connected to the engine's valves through various types of linkages called pushrods and rocker arms. The pushrods and rocker arms transfer the reciprocating motion generated by the camshaft lobes to the valve. The valves are maintained closed by springs. As the valve is opened by the camshaft, it compresses the valve spring. The energy stored in the valve spring is then used to close the valve as the camshaft lobe rotates out from under the follower.

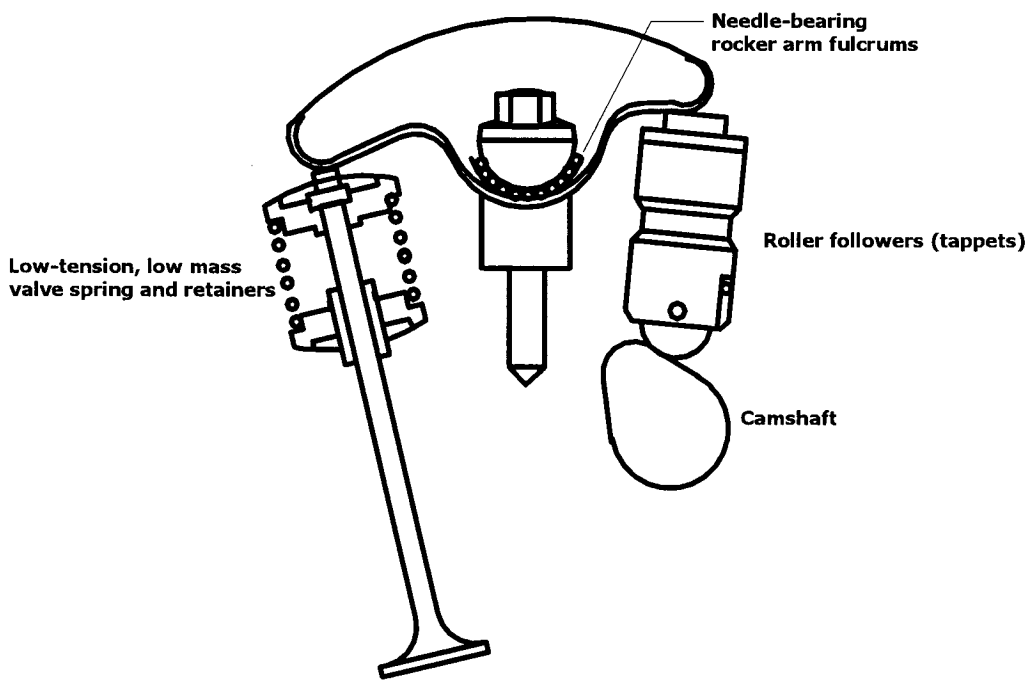

Fig. 1.1. Conventional low friction valve train mechanism

The Design of valve train mechanisms is crucial and is one of the most difficult automotive components to design because the mechanism must always perform properly under all loads and speeds during the entire engine operating range. At low engine speeds the forces create the primary load on the valve train, while at high speeds the addition of inertia forces plays an important role to create higher loads. As a function of engine speed, the valve train must actuate the engine intake and exhaust valves in proper sequence and profile to allow the fuel-air mixture and exhaust through the combustion chamber for optimal engine performance in terms of ignition, power, efficiency, and pollution control.

At a typical part load throttle engine operating condition, the mechanical friction of a conventional four-cylinder engine consumes approximately 22 % of the indicated power. Reduction in valve train friction can improve the engine thermal efficiency and thereby reduce vehicle fuel consumption. To understand the nature and magnitude of engine friction losses require a frictional analysis of the engine on a component-by-component basis.

Valve train friction can be significantly reduced by spring load reduction, and by the use of roller tappet and rocker arm/fulcrum needle bearings. A significant part of the valve train friction, approximately 50%, can be eliminated with roller cam followers, as the type shown in fig. 1.1. It is known that contact stresses are higher at lower engine speeds, and this fact coupled with the difficulty for the complete oil film formation for lubrication may lead to the cam/follower wear.

By using electromagnetic mechanisms to directly actuate the intake and exhaust valves, the camshaft and the complexity of the mechanical valve train system are no longer required.

Engines operated by electromagnetic valve actuators (EMVA) are called 'Camless Engines'. Since the EMVA is completely independent of the camshaft, valve timing, lift and phase can be varied according to all engine requirements. To vary the valve events optimally and reliably, feedback control strategies operated by robust microprocessor based electronic systems are necessary. Depending on the type and make of the engine, fig. 1.2 shows the possible arrangement for an EMVA system.

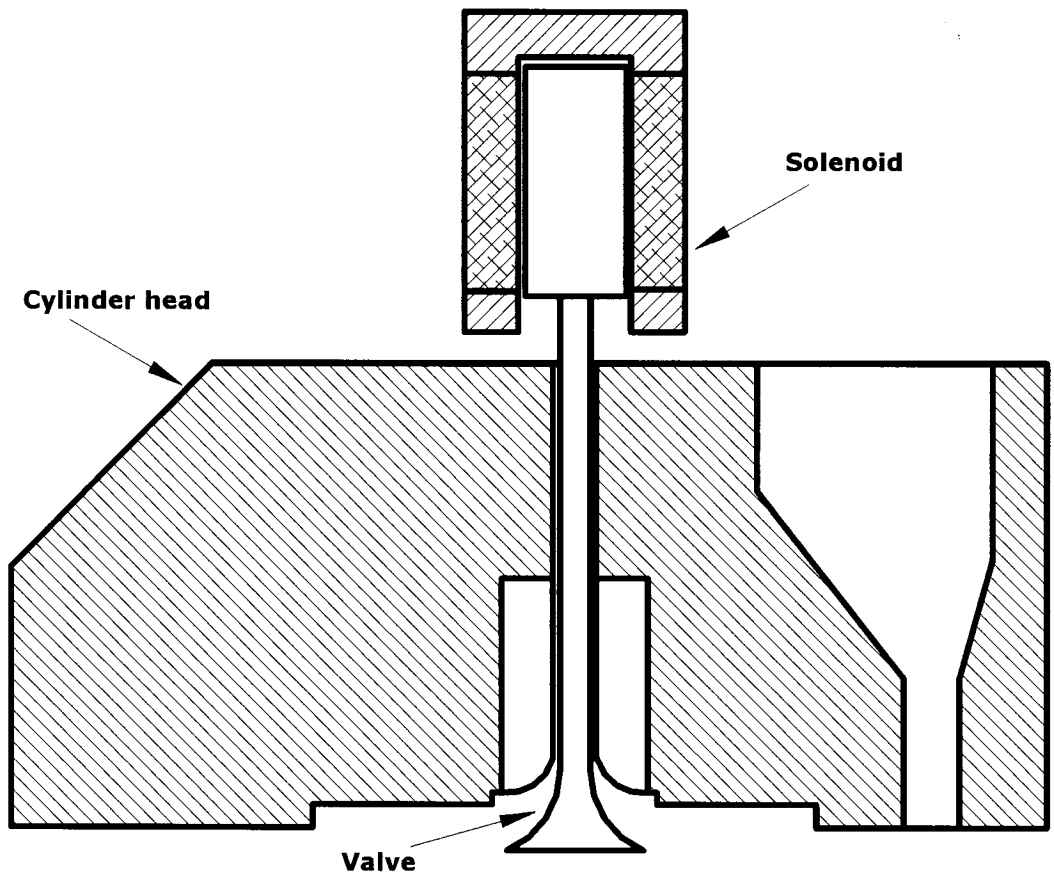

Fig. 1.2. Overhead mounted solenoid operated valve mechanism

1.3 REVIEW OF PREVIOUS WORK

This section reviews the literature in the technology of intake and exhaust strategies of VVT and their effects on the engine performance and emissions.

1.3.1 Role of Variable Valve Timing in Gasoline and Diesel Engine.

A major disadvantage of conventional SI engines results from the energy loss due to the inhaling of the sub-atmospheric gases during the suction stroke and expelling of exhaust gases during the exhaust stroke. These pumping losses depend upon the opening and closing position of the throttle valve. The losses are high when the throttle valve tends to close and are low at wide-open throttle. Thus, the pumping losses are inversely proportional to the engine load. Without a throttle valve, control of the air-fuel mixture can be realized by variation of the intake valve-opening period; therefore, the VVT has great potential for reducing pumping losses in gasoline engines.

At low speeds, the pumping losses in gasoline engines are much greater than those of diesel engines because of the throttle intake system. In diesel engines, control of load is obtained by regulating the quantity of fuel injected. Unlike gasoline engines, diesel engines do not have a throttle to control the air-fuel mixture. Thus, due to the absence of the throttle valve, pumping losses at part load are much less. Also, the application of a turbocharger at low speeds reduces the pumping losses by providing air boost.

The compression ratio is a very important parameter in diesel engines. For high speeds as well as at cold starting, the diesel engine needs a high compression ratio. Due to this high compression ratio, the clearance between the piston and valves, at TDC, is very small. Thus,

this is one of the mechanical constraints that must be considered in the control of intake and exhaust valves. In the case of medium speed diesel engine, the compression ratio is not as high as in high-speed diesel engines. These engines are used in marine applications, rail transportation, and power generation sets, where exhaust emissions is of main concern.

Several benefits of VVT when applied to diesel engines have been realized in recent years. One of the major benefits is the reduction of NOx by manipulation of exhaust valve timing. Also, improvements in torque and volumetric efficiency could be gained by varying the intake valve timing. The fixed valve events for conventional cam controlled engines compromises the engine for better performance under all operating conditions. The inlet valve timing is the most important parameter for optimizing the engine volumetric efficiency, whereas the exhaust valve timing controls the residual gas fraction (RGF), which reduces exhaust NOx emission. RGF can be controlled by the valve overlap and can be changed for various speeds and loads by the application of VVT. To operate the engine efficiently and effectively over its entire operating range and conditions, the valve events should be able to vary with speed and load anywhere on the engine map.

1.3.2 Variable Valve Timing for Four-Stroke Gasoline Engine.

Tuttle [5] tested the concept of the late intake valve closing (LIVC) system on a single cylinder SI engine with three modified cams. He reported that there was a 40 % reduction in pumping losses during part load conditions, a 1 % loss in torque from the maximum best torque values, and a 24 % reduction in NO_X emissions at mid load with no changes in hydrocarbons (HC).

Asmus [6] stated that the volumetric efficiency increases by delaying the intake valve closing at higher speeds because the mixture high flow momentum continues to charge the cylinder even though the piston is traveling upwards. But late intake valve closing will penalize the volumetric efficiency at lower speeds because the intake manifold and cylinder pressures are equal at BDC and will result in some of the fresh charge to be pushed back into the intake manifold.

According to Rabia *et al.* [7], the knocking onset in LIVC engines was found to increase with decreasing engine speed. This is because the air-fuel density is lower and the mixture is richer, which decreases the flame speed and thus enhances knocking. The LIVC engines demand more spark advance as compared to conventional engines especially at part loads, because the mixture is permitted a sufficient amount of time to auto-ignite. By advancing the spark it is possible to avoid auto-ignition. The maximum pressure inside the cylinder of LIVC engines was found to be lower than that in conventional engines. This is because the amount of effective mixture left for combustion after the intake stroke is less in LIVC engines. Similarly, Ahmad *et al.* [8] reported that LIVC systems present difficulties because at very low loads the ignition can occur before the intake valve has been closed.

Saunders *et al.* [9] used two methods for improving the engine efficiency. One is VVT by LIVC to reduce the pumping losses, and the other is variable compression ratio (VCR) to increase the expansion ratio. The combination of these two methods results in an Otto-Atkinson cycle engine. Such an engine type was obtained by modifying a 4-cylinder inline, 1275 cc, 8.8 compression ratio (CR) engine. They obtained LIVC by using a secondary camshaft driven by a variable-geometry timing-belt. VCR was obtained by using different

length connecting rods, modifications to the cylinder head and by using gaskets. According to the authors, it was not clear whether VCR could give further improvements expected in terms of the Otto-Atkinson cycle, relative to LIVC alone. The authors claimed that 13 % bsfc (brake specific fuel consumption) could be obtained by using LIVC. By using LIVC with VCR, bsfc can be improved up to 20 %. To obtain LIVC + VCR combination engines require much hardware modifications, which result in a high cost engine.

Blakey *et al.* [10] reported that if LIVC is combined with a VCR device, further fuel savings could be realized. The LIVC serves the purpose of reducing the pumping losses, and the VCR is to vary the amount of air-fuel mixture according to load and speed conditions. This combined strategy results up to 20 % of fuel consumption savings over a conventional engine at low speeds/loads.

Blakey *et al.* [11] performed further LIVC/VCR (Otto-Atkinson Cycle) engine experiments. The tests were performed on a Ford 2.0 liter DOHC 16 valve engine. To obtain LIVC they used a two-camshaft arrangement with pushrods, which practically leads to complexity and friction increase in the valve mechanism. The design restricted the system from getting the full benefits of fuel efficiency, and a 6.7 % bsfc reduction was reported.

Ma [12] tested the LIVC concept for a multi-intake valve engine. He stated that it is easy to arrange for the second intake valve to be phased with a variable delay from the first intake valve to produce a prolonged intake-opening period. He suggested that LIVC is a practical and applicable concept to engines.

Seiichi *et al.* [13] investigated the effects of the over expansion cycle with late closing of

intake valves on the engine performance. It was reported that substantial compression ratio variations occurred with the intake valve closure timing. Experiments were performed on a large single cylinder engine with a stroke volume of 650 cc with four kinds of expansion ratio from 10 to 25, and four sets of intake valve closure timing from 0 to 110 degree of crank angle. It was concluded that improvement of both indicated and brake thermal efficiency reaches up to 16 %, which is much higher than ever reported by the authors. It was also mentioned that by increasing the expansion ratio tends to increase the friction work due to the increased cylinder pressure. This friction work diminishes the engine efficiency.

Shiga *et al.* [14] obtained LIVC control by using two types of camshafts. One was the original camshaft and the second was geometrically half early closing. The LIVC strategy was applied on a 4-stroke, 1-cylinder SI liquid-cooled DOHC 4-valve, 249 cc engine. It was claimed that EIVC can improve the thermal efficiency by 7 % at expansion ratios greater than 16.

Soderberg *et al.* [15] tested LIVC strategies with symmetric and with asymmetric valve events. It was mentioned that tumble inside the cylinder is induced by the symmetric valve event, whereas swirl is induced by the asymmetric valve event. It was noted that early intake valve closing (EIVC) supported a longer flame development period but faster combustion occurs. This might be due to the low lifts of the intake valve which helps to atomize the fuel droplets by shearing flow. EIVC results in a more stable combustion as compared to that of LIVC.

Soderberg *et al.* [16] developed a cylinder head for cross flow to compare throttled and unthrottled operations using LIVC. This type of cylinder head improves the swirl rate. Also, it assists LIVC operation during intake valve opening by providing sufficient room to open. The LIVC strategy was applied on a single cylinder version of the 5-cylinder, 2.5-liter B5254FS Volvo engine with two overhead camshafts. By using LIVC for reducing pumping losses they found that residual gases also increased. This is because the intake and exhaust valves are operated by the same camshaft, which, to satisfy phasing requirements of the intake valve timing to get LIVC also influences the phasing of the exhaust valve timing. The authors claimed that at part load fuel conversion efficiency was improved up to 9 %, combustion efficiency was improved by 2 %, and NO_X was reduced.

Saunders *et al.* [17] implemented the LIVC concept on an Austin A series engine. They switched between unthrottled LIVC and conventional throttled load control. To achieve LIVC, they implemented a second camshaft above the rocker arm to directly control the intake valve. Although the indicated thermal efficiency was less, there was a 7 % improvement in fuel efficiency, and a maximum fuel economy gain of about 11% at half load. They did not report the increase in friction losses and the effects due to the second overhead camshaft.

Elord *et al.* [18] obtained LIVC control by developing a device that could phase shift the valve timing of an engine. A four cylinder, Fiat DOHC engine, was used for the test program. It was noted that the mixture charge was being returned to the carburetor. Fitting a one-way reed-valve between the carburetor and the intake manifold can solve this problem.

Haugen *et al.* [19] tested the LIVC concept by designing a third camshaft and placed it above the original intake valve camshaft. This was implemented on a 1988 Oldsmobile Quad 4, a 2.3-liter 16-valve DOHC 4-cylinder engine. According to their invention, they obtained 6.3 % reduction in bsfc, NO_X emission were reduced, whilst HC emissions increased. It was mentioned that exhaust noise levels decreased because of the low cylinder pressure. But there was an increase in noise during the intake stroke due to the gas backflow into the intake manifold. No details were given about the extra friction losses that could occur by the additional third camshaft. It should be noted more moving parts makes the system complex.

To get delayed overlap, Stein *et al.* [20] used a dual equal variable camshaft timing (VCT) strategy to equally phase shift the intake and exhaust valves. They tested this concept on a 2.0-liter, 4-valve engine by retarding the valve events by 30 degrees. It was stated that EGR helps to reduce NO_X, unburned HC, and pumping losses. Reduction in NO_X occurs because of the temperature drop inside the cylinder; re-burning of exhaust gases reduces the HC; and, pumping losses reduce because of the high cylinder pressure during the intake stroke. They also mentioned that higher octane is not required for LIVC with the dual equal VCT strategy because the compression ratio is reduced due to LIVC and thus results in a lower gas temperature at the end of the compression stroke.

Ham *et al.* [21] studied the engine simulation model to check the effects of changing the maximum intake valve lift to control in-cylinder turbulence intensity and burn-rate. It was found that intake valve closing is the most sensitive parameter for changing the breathing characteristics of an engine, that delaying IVC causes the volumetric efficiency to increase at high engine speed while penalizing it at low speeds. To obtain high volumetric efficiency it is always advantageous to use variable valve actuation devices that could vary both lift and

duration. But further experimental studies are necessary to check the validity of the above conclusions.

Tuttle [22] tested the EIVC concept on a single cylinder SI engine. He used three modified cams to vary the inlet valve events. He reported a 40 % reduction in pumping losses as compared to a conventional engine. Also reported was a 7 % reduction in fuel consumption with 24 % reduction in NO_X at half load. He also mentioned that at part load, the cylinder gas temperature was lower, the heat transfer was lower, but HC emission was higher. The reduction in NO_X and the increase in HC emissions take place because combustion temperatures in EIVC engines are lower due to the lesser amount of air-mixture that is burnt during the combustion process. The proposed system requires more number of cams, which leads to complexity in the VVT mechanism.

Urata *et al.* [23] manufactured an engine equipped with a newly developed hydraulic variable valve train (HVVT) and tested it for EIVC. The tests were performed on a 4-cylinder inline, 2156 cc, 9.4 CR engine. It was reported that the fuel consumption could be reduced by about 7 %, while meeting the US EPA emission standards. Also, pumping losses can be reduced by up to 80 %. They also stated that EIVC lowers the gas temperature in the cylinder during the compression stroke because there is a less amount of air-mixture to burn.

Gray [24] noted from previous experiments that EIVC and small overlap result in the best fuel efficiency for given loads. According to Gray, the reasons are unclear, but they might be related to the lower residual gases from the small overlap. He also stated that, when compared to SI engines, the high-speed diesel engine needs a higher compression ratio. The

clearance between the cylinder head and piston at TDC is smaller for higher compression engines. Small clearances would restrict the variation of valve displacements for any VVT system. This is true only for overhead mounted valves; he did not discuss the subject of side-mounted valves.

Hans *et al.* [25] studied the load control by using the intake valve for air-fuel mixture control. They concluded that through early closing of the intake valve, at the time when the piston reaches its highest speed, air oscillation would occur with high amplitude in the intake manifold system even at low engine speed and low load. By controlling the charge by the intake valve leads to the absence of vacuum in the intake manifold, and the pulsations in the intake manifold lead to wall deposits of the fuel and to bad mixture preparation. Therefore, VVT for throttle control needs higher performance of the mixture preparation system.

Stivender [26] controlled the air-fuel mixture by varying the lift of the intake valve. For small valve lifts, the turbulence intensity increases and the liquid fuel passing through such an aperture undergoes almost explosive atomization due to the large shear forces to which it is subjected. He also mentioned that the increase in intensity of the predominantly small-scale turbulence in the charge was the primary objective in proposing the method for engine throttling.

Moro *et al.* [27] reported that, it is possible to decrease the engine torque from its maximum value by simply controlling the amount of EGR by using late exhaust valve closing (LEVC). To get full benefits of control of torque and reduction of pumping losses it is advantageous to combine LEVC with EIVC. Because EIVC reduces the pumping losses, by combining these

two strategies complete engine load control could be achieved. The approach by the authors was based on thermodynamics consideration only, taking account the mechanical losses, valve lift timings and combustion duration effects.

According to Diana *et al.* [28] the shape and the valve lift timing affect both pumping losses and air motion inside the cylinder. They compared flow characteristics for different VVA systems by using 1D code for the simulation of the inlet and exhaust phases, and fluid dynamic 3D code to evaluate the mixing phenomena inside the cylinder. They adopted two strategies. One was EIVC in which opening of the intake valve takes place at TDC but closes early with respect to a conventional engine. The second was EIVC-C (centered early intake valve closing) in which the valve opens late and closes early with respect a conventional engine. For all and any time period from the start of intake valve opening to the end of closing, it was symmetrically centered about a predefined crank angle. They mentioned that EIVC is more beneficial than EIVC-C because, by opening the valve near to TDC it is possible to get effective air-fuel mixture at the end of the compression stroke with lower pumping losses, pressure and temperature. The authors also mentioned that the combustion process deteriorates because of lower levels of turbulence inside the combustion chamber when the engine is throttled. This sentence contradicts with other authors. In fact, throttling always assist for creating turbulence.

Sellnau *et al.* [29] designed a two-step VVA system and combined it with the EIVC strategy. They used a modern 4-valve SI, 10.3 CR DOHC V6 engine for simulation. Because the valves are actuated in two steps by a hydraulic control mechanism, the valve lift friction is reduced, and using slider elements it is possible to reduce the cost of the system. It was stated

that pumping losses are greatly reduced in EIVC because the cylinder undergoes decompression and recompression at a lower effective compression ratio, which results in lower average pressure and temperature to assist in the reduction of NOx emissions. They concluded that the two-step EIVC with dual independent cam phasing gives 8 % fuel economy, while three-step EIVC with dual independent cam phasing gives 9 % fuel economy.

Vogel *et al.* [30] made tests on a Ford 'Zetec', 4-cylinder, 2.0-liter engine by fitting a secondary valve assembly between the cylinder head and the original intake manifold of the engine. The main purpose was to implement VVT (EIVC) with the use of the secondary valve. They obtained EIVC by shutting the secondary valve abruptly during the downward motion of the piston, which limits the air-fuel mixture admitted into the cylinder. It was concluded that this strategy saved 70 % in pumping losses, the fuel economy can be improved by 4 %, and the roughness of the engine is reduced. How the secondary valve was actuated was not described, but the authors mentioned that the secondary valve concept is a "fail safe" design. They also mentioned that according to tests conducted, the power required to actuate the secondary valve was more than the power saved in terms of fuel economy.

If the LIVC strategy is compared with EIVC, then in case of LIVC the manifold pressure is high because part of the air-fuel mixture from the cylinder goes back into the intake manifold. For the EIVC strategy, the manifold pressure is also high but is caused by the restriction of the closing intake valve (i.e.: pressure buildup due to stopping of the inertia flow). Higher manifold pressure results in more fuel droplets to be admitted into the cylinder. More droplets, which are not vaporized, cause poor combustion. EIVC engines can overcome

this penalty because of its higher intake air-fuel mixture velocity during the intake phase. This higher velocity creates turbulence for good fuel vaporization. On the other hand, LIVC engines do not use the valve to throttle the flow and thus there is no change in the incoming air-fuel mixture velocity. The flow losses for LIVC engines tend to be higher when compared to EIVC because of the air-fuel mixture reverse flow.

Badami *et al.* [31] performed experiments on a 2-cylinder, 4-stroke, 594 cc, 7.5 CR, air-cooled engine. Experiments were to test the effects of spark advance and changes in air-fuel ratio by variable valve overlap by adopting the LIVO strategy by using a passive electro-hydraulic link for the valve operation. They claimed that combinations of spark advance (from 10° to 5°) and variable valve overlap results in a 6 % reduction in fuel consumption when a fixed mass of fuel was delivered, and that a 20% reduction was achieved at a fixed throttle position. HC reduces by more than 40 % but cyclic irregularities of the engine speed increases. Thus, to reduce engine cyclic irregularities, it is recommended that the spark advance be limited, and use LIVO to reduce the overlap. The authors did not mention the effects of LIVO on pumping losses.

Law *et al.* [34] adapted two methods by using variable valve timing for the control of auto-ignition (CAI). For testing purposes they used only one active cylinder (450 cc, 10.5 CR) from a 1.8 L 4-cylinder engine. The valves were actuated by an electro-hydraulic active valve train (AVT) for the purpose to recirculate and vary the amount of exhaust gases to reduce NOx, as well as to control auto-ignition.

1.3.3 Variable Valve Timing for Four-Stroke Diesel Engines

Lancefield et al. [41] tested a modern European 2.2 L, 4-clynider, 4-valve per cylinder diesel engine to investigate the effects of a variable duration cam system. They made minor changes to the cylinder head and cam drive arrangement to perform tests for low and medium engine speeds. They reported that brake specific fuel consumption (BSFC) reduces by using EIVC and LIVC strategies, and claimed that by valve event optimization at low speeds, the torque can be increased up to 16.4 %.

Tai et al. [42] tested a 2.7 litre, V6, 4-valve per cylinder, light duty turbocharged diesel engine with an electromagnetic camless valvetrain. The valvetrain mechanism was hydraulically operated and electronically controlled. They claimed that after optimization of the intake valve closing, torque improvement was observed at low and medium speeds, whereas torque decreased at high speeds, and there were insignificant changes in fuel consumption. They also claimed that by optimizing in combination the intake valve closing and the exhaust valve opening, torque improvements occur at low and medium speeds but the fuel consumption increases. They suggested that future work should include the studies of internal EGR, the effects of variable intake valve lift, the profile and timing on in-cylinder swirl, and the effects on peak cylinder pressure by LIVC.

Endo et al. [43] investigated the pumping losses and volumetric efficiency of an EP100-II, compression ratio 15.5, 6-cylnder turbocharged diesel engine. They claimed that pumping losses and volumetric efficiency could be improved at higher engine speeds if valve-opening areas are larger. They also investigated the effects of inertia charging on pumping losses and

volumetric efficiency by determining the relationship between the intake valve timing and the amplitude and phase of the intake air pulsation.

The compression release is a method to reduce the engine power by opening the exhaust valve well before the exhaust stroke to release the compression. Hu. et al. [44] developed a variable valve actuation system for compression release of diesel engine retarding and tested it with a prototype VVA system on a 6-cylinder, 14-15 litre engine. During the test, diesel engine retarding power is achieved by releasing the compressed air charge near the TDC of the compression stroke. They claimed that by using VVA for the brake valve events, results in maximum cylinder pressure and optimally efficient compression release. The engine rpm can be reduced by avoiding or delaying the opening of exhaust valve during the exhaust stroke, this method is called as brake valve event. According to the results they also claimed that 84 % of the system retarding potential is extracted by using VVA system versus 55-72% with an exhaust cam driven engine brake.

Benajes et al. [45] studied the effects of intake valve pre-lift on a 6-cylider heavy-duty turbocharged diesel engine by means of a wave action model, which solves the general flow equations by means of the finite difference method. According to the authors, an intake valve pre-lift is an appropriate technique in order to produce internal EGR. The valve overlap increases due to the intake valve pre-lift which results in an increase of backflow produce EGR. They also suggested in order to produce internal EGR by intake valve pre-lift, additional measures, such as fuel-delivery adjustments or turbocharger modifications, should be undertaken.

Stas [46] tested a high-speed turbocharged diesel engine to show how the exhaust blowdown period affects the pumping work. He concluded that, during the blowdown period the cylinder pressure may drop well under the ambient pressure level, and this pressure still remains below the subsequent intake pressure level. This phenomenon of dropping down the pressure is called the Kadenacy effect, which can reduce exhaust pumping losses. The reduction in exhaust pumping loss occurs because the exhaust stroke proceeds at a lower pressure level. He claimed that the thermal efficiency increases by 3 % if the Kadenacy effect is used.

Charlton et al. [47] investigated the effects of VVT on a highly turbocharged, compression ratio 12.93, 6-cylinder, 39.42-litre diesel engine through a computer simulation. According to their results the best load acceptance characteristics for high speeds was obtained with a valve overlap of 120 degrees crank angle, and for low speeds it was 80 degrees crank angle. They suggested that it is essential to increase the valve overlap as rapidly as possible to its maximum value to obtain optimum transient response. This is because rapid increase of the valve overlap increases the mass flow through an engine.

1.3.4 Electromagnetic Valve Actuators.

Quite a few models and mechanisms have been proposed by various authors to capture the static and dynamic characteristics of an electromagnetic solenoid. Some are discussed in the following section.

Lequesne et al. [49] used the finite element method (FEM) to develop a mathematical model of a solenoid. The model predicts force levels, coil inductance, and the effects of eddy currents losses.

Vaughan et al. [50] proposed a nonlinear magnetic model for a solenoid operated proportional valve. To obtain the transient magnetic characteristic, which represents magnetic hysteresis and saturation, a series of experiments were performed. In their experimental analyses they did not consider the thermal effects on the system.

Masaud et al [51] developed a model for solenoid-controlled servo valves based on the model by Lequence et al [49]. The series of experiments were done by using different step voltages at different armature positions. A curve fitting technique was used for force and flux versus positions for different fixed armature positions. In this model they considered hysteresis and saturation but thermal effects and flux leakage were neglected.

Cheung et al. [52] developed a mathematical model that approximates the linear and saturation regions of a solenoid by a first order and a second order function, respectively. This involves identifying the constants in the empirical equation for reluctance when the current and flux linkage have a linear relationship. This is done using simple relationships derived from fundamental linear magnetic principles. A saturation boundary is defined, above which the flux current relationship is nonlinear. This region is approximated as a parabola and parameters of the parabola are identified using curve fitting techniques. The model includes identifying leakage inductance as well. Experimental data was generated by feeding a sinusoidal voltage into the coil. The model does not include hysteresis.

Lequesne [53] presented a different configuration of the Electromechanical Valve (EMV), where the magnetic force is produced by two permanent magnets attached at the boss end and a pair of coils below these two permanent magnets. Motion is produced by the oscillation of two springs supporting a steel plunger and the plunger is latched at the end of its travel by the permanent magnet, with no current flowing. The plunger is unlatched by energizing the coil with current so as to produce a magnetic field that opposes that produced by the permanent magnet. The expression for the magnetic force is represented as a surface integral of the magnetic field strength calculated by finite element method. Modeling of eddy currents was taken into account since this represented core losses. The finite element model was validated with experimental data.

Wang et al. [54] developed a model that considers the saturation of the solenoid coil. The linear part was modeled by using linear magnetic theory and the parameters of the system were calculated by using a curve fit technique. The saturation region of the coil was modeled by a polynomial function, which depends on current and position. The inductance and rate of change of flux were considered as a nonlinear function, which is dependent on position and current. The thermal effects, inductance and bouncing of the valve were not taken into consideration.

Hoffman et al. [55] modified the model done by [51]. The improvement of the model included a design of controlling accurate valve closing and opening with very small contact velocity for soft landing. To control the valve position a tracking controller was combined with a feedforward and feedback controller. The feedforward controller calculates the

required trajectory, while the feedback controller was designed by using the state feedback method.

1.3.5 Thesis Objectives

The research program of this thesis will concentrate on the following items:

1. Review and analysis of variable valve timing strategies.
2. An assessment of intake and exhaust valve strategies for variable valve timing.
3. Effects of late intake valve closing on four stroke gasoline engines.
4. Analysis of variable valve timing events and their effects on single cylinder gasoline and diesel engine by studying individual valve events strategies. This study also covers the effects of valve events on engine performance and emissions.
5. Study of solenoid force and current characteristics, by replacing conventional iron core with strong permanent magnetic core.
6. Development and experimental validation of the mathematical model for dynamic current and force response of the solenoid at fixed permanent magnet core positions.
7. Drawing conclusions and making recommendations for further investigation into variable valve timing strategies and its variable valve actuation mechanisms.

CAHPTER 2

INTAKE AND EXHAUST STRATEGIES

2.1 Various Intake and Exhaust Strategies

2.1.1 General Valve Opening and Closing

The main characteristic of conventional cam operated engines is that the intake valve always performs the same displacement at a well-defined crankshaft angle and is independent of the engine working conditions. Variable Valve Actuation (VVA) can enable the varying of valve events as per engine speed and load requirements. Valve events for the conventional SI engine are discussed below, as referred to fig.2.1

Intake Valve Opening (IVO)-

The inlet valve opens and the air-fuel charge is sucked into the cylinder as the piston moves downward from top dead center (TDC). It continues until the piston reaches its bottom dead center (BDC). Generally, opening of the intake valve takes place at around 10 degrees before TDC during the exhaust stroke. Opening of the inlet valve represents the start of the intake stroke as well as the start of intake and exhaust valve overlap.

Exhaust valve closing (EVC)-

The exhaust valve closes when most of the burned gases have been expelled to the exhaust manifold. This is the end of the exhaust stroke as well as the end of valve overlap. Closing of the exhaust valve takes place at around 10 degrees after TDC during the intake stroke.

Intake valve closing (IVC)-

Closing of the inlet valve represents the end of the intake stroke and the start of the compression stroke. The inlet valve closes at around 50 degrees after BDC during the compression stroke.

Exhaust valve opening (EVO)-

Opening of the exhaust valve represents the end of the expansion stroke and the start of the exhaust stroke. The exhaust valve opening takes place at around 60 degrees before BDC.

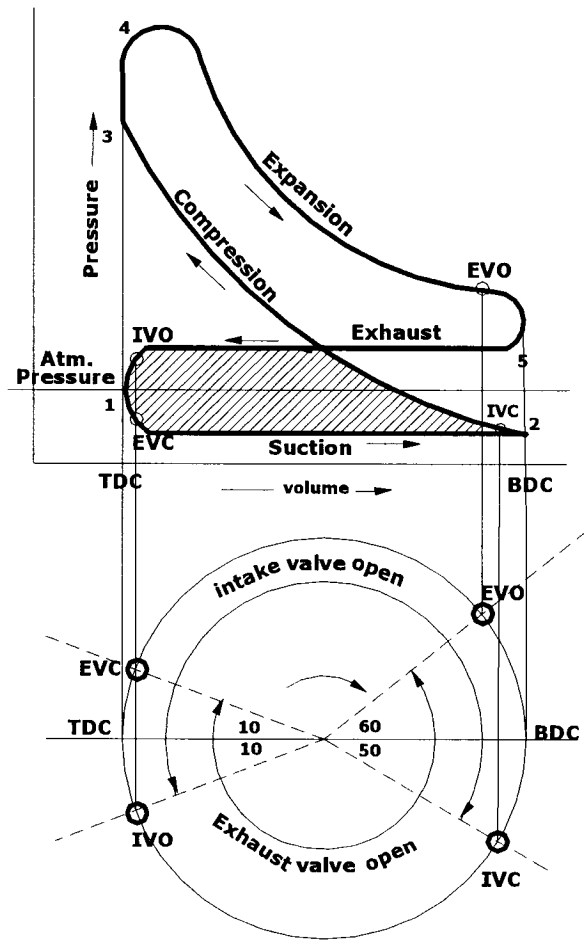

Fig. 2.1 Valve timing diagram in relation with PV diagram for conventional four stroke SI engine

Various intake and exhaust strategies are:

1. Late intake valve closing (LIVC)
2. Early intake valve closing (EIVC)
3. Late intake valve opening (LIVO)
4. Early intake valve opening (EIVO)
5. Early exhaust valve opening (EEVO)
6. Late exhaust valve opening (LEVO)
7. Early exhaust valve closing (EEVC)
8. Late exhaust valve closing (LEVC)

In the above discussion the angles of opening and closing of inlet and exhaust valves are taken as baseline angles representative to any conventional cam operated SI engine.

The combinations of some of the above strategies are also possible. Later in this thesis, the above-mentioned strategies are discussed with the help of the GT-Power computer simulation model results for a low speed single cylinder engine.

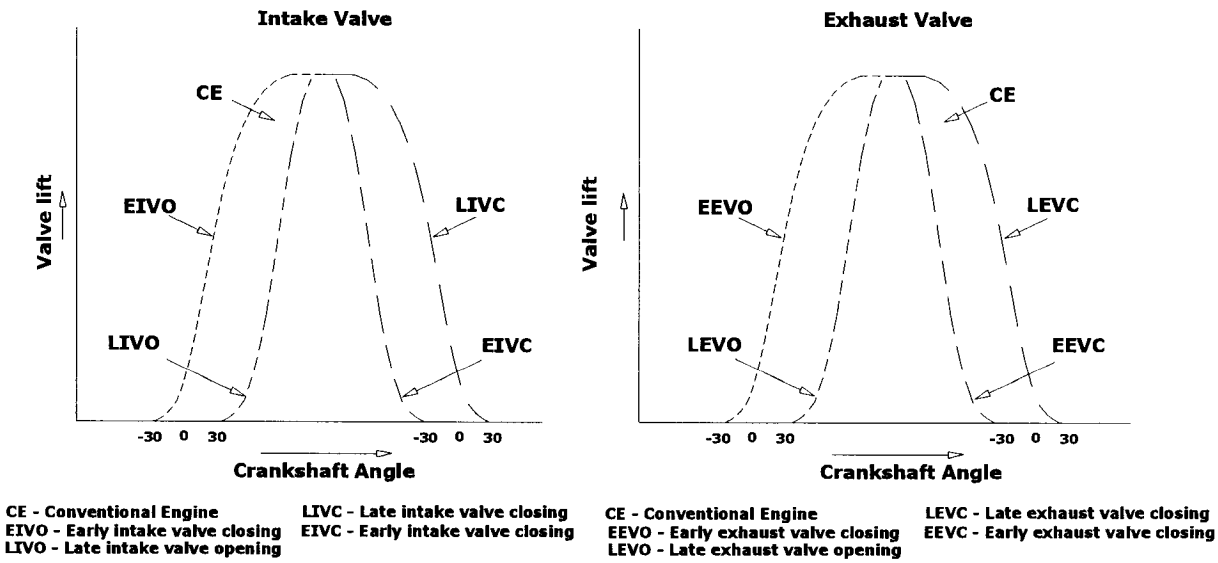

Fig. 2.2 Various valve events and their range of opening and closing with respect to crank angle

Fig. 2.2 shows a pictorial representation of these possible valve events in comparison with a conventional engine (CE). Idealized PV diagrams of various intake and exhaust strategies for four stroke SI engines are shown in figures 2.3 to 2.10, and are discussed in the following. Note that the negative loops (pumping losses) have been exaggerated for illustrative purposes. Any effects on the positive loop are not considered.

2.1.2 Late intake valve closing (LIVC) – Fig. 2.3

The closing of the intake valve represents the end of the intake stroke and the start of the compression stroke. The inlet valve closes at around 60 degrees after BDC during the compression stroke.

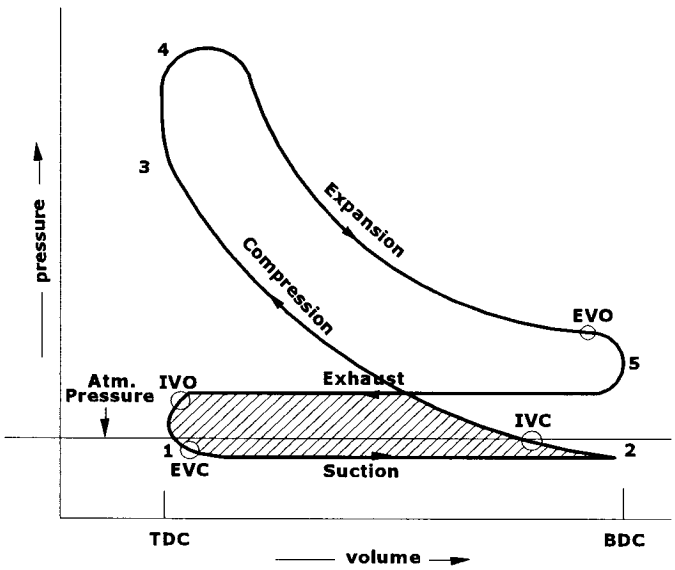

Fig.2.3 PV diagram for LIVC engine

In the LIVC system, the closing of the intake valve is delayed towards the end of the compression stroke. In a conventional engine, during the induction stroke the intake valve opens and the charge is admitted into the combustion chamber. During the compression stroke the intake valve closes and the charge gets compressed. But in LIVC, the inlet valve remains open for a little longer time during part of the compression stroke so that some of the

charge is expelled back into the intake manifold. The pressure of the entrapped charge is little more than the atmospheric pressure. During the subsequent induction stroke the entrapped charge gets readmitted at a pressure above that of the air-fuel mixture in conventional engines. This means that the suction pressure line deviates very little from the atmospheric line. Thus, the negative area is reduced which results in reduced pumping losses as shown in fig. 2.3. In other words, the vacuum created in a LIVC engine during suction of the air-fuel mixture is not too low, which results in less force (work) required to complete the induction stroke.

As shown in fig. 2.4a, during the suction stroke, pressure CE_P inside the cylinder for the conventional engine is less than atmospheric pressure A_P. Figure 2.4b shows that the pressure LE_P inside the cylinder for the LIVC engine is less than atmospheric pressure A_P, but more than the pressure CE_P inside the conventional engine.

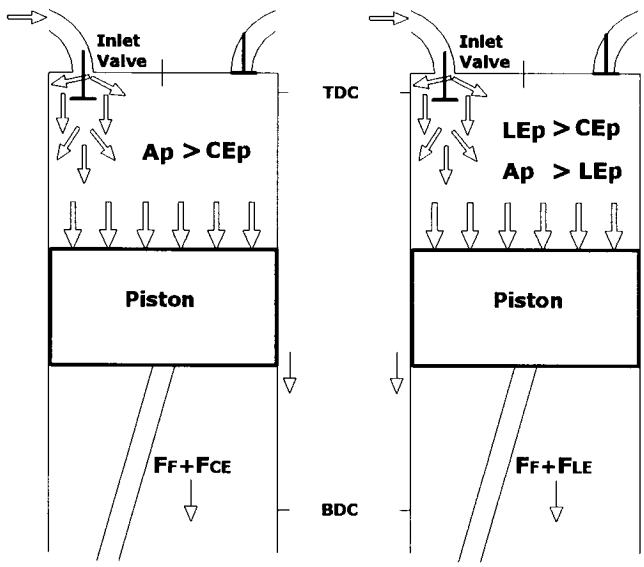

a) b)

Fig. 2.4. a) Conventional engine, b) LIVC engine

Due to increase in pressure inside the LIVC engine, the force required for the piston to work against vacuum is less with respect to conventional engines, that is $F_{LE} < F_{CE}$, which results in a saving of pumping work during the suction stroke. The research work of this section is published in [3].

2.1.3 Early intake valve closing (EIVC) – Fig. 2.5

The EIVC system is based on closing of the intake valves when the desired fresh air-fuel mixture has been introduced. In this way, when low load and low speed conditions are required, only a desired and limited fraction of the intake stroke is used to introduce the mixture from the manifold. Then, the valve is closed and in the remaining intake stroke the cylinder is isolated. This partial intake stroke is the result of early intake valve closing which reduces the amount of air-fuel mixture admitted inside the engine cylinder. The work (or pumping losses) required for admitting this limited amount of air-fuel mixture is less than respect to conventional engines.

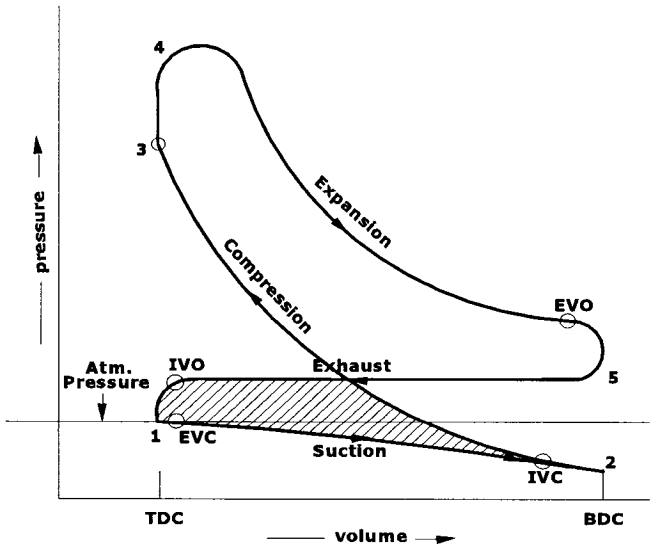

Fig. 2.5 PV diagram for EIVC engine

EIVC also results in some pumping losses due to the low lift of the valves. This drawback

can be improved by using variable valve mechanisms that enable faster valve lifts [36].

The idealized PV diagram for an EIVC engine is shown in figure 2.5. The area below the atmospheric line is a portion of the negative pumping work, which is greatly reduced with respect to a conventional engine.

2.1.4 Late intake valve opening (LIVO) – Fig. 2.6

Opening of the intake valve is the beginning of the induction stroke as well as the start of the valve overlap period. Normal opening of the intake valve takes place at around 10 degrees before TDC. Late opening of the intake valve tends to cause no flow connection between the cylinder and the intake manifold unless there is a pressure gradient between them. Further delay in the LIVO actually causes the cylinder pressure to dip momentarily below the intake manifold pressure [6]. The pumping losses will be increased because of the greatly reduced cylinder pressure in the first part of the intake stroke.

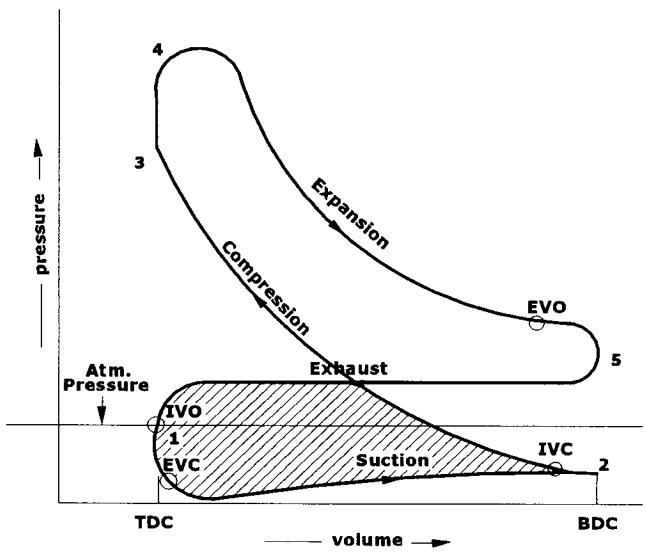

Fig. 2.6 PV diagram for LIVO engine

As shown in fig.2.6, the suction line of the PV cycle is more negative with respect to a conventional engine cycle. Even though pumping losses increase, there is no detrimental

effect on the volumetric efficiency. This is because all the air-fuel mixture is brought into the cylinder with high velocity during the remaining suction stroke after the intake valve opens. This high velocity creates turbulence for the air-fuel mixture, which assists for good combustion, and is considered as a good technique to reduce unburned hydrocarbons (UBHC) emissions.

2.1.5. Early intake valve opening (EIVO) – Fig. 2.7

In conventional engines, the opening of the intake valve occurs at around 10 degrees before TDC. Early opening well before the end of the exhaust stroke means increasing the duration of the valve overlap. Some amount of burnt gases will go back into the intake manifold because of the cylinder-intake manifold pressure gradient [32]. This backflow is also used for internal exhaust gas recirculation (EGR), which is helpful to reduce NOx [33]. In addition, EIVO allows the exhaust gases to be in contact with the low-pressure intake system for a longer period of time. Thus, the manifold exhaust gases are recycled back into the cylinder at a lower temperature and leads to a reduction in NOx.

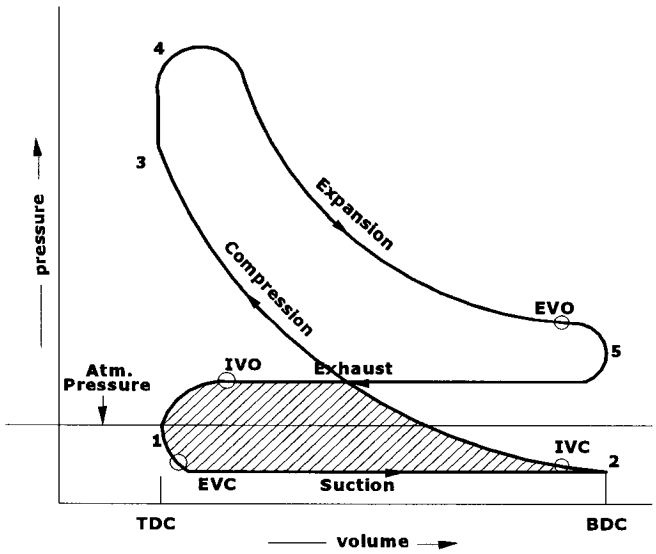

Fig. 2.7 PV diagram for EIVO engine

During EIVO the large intake reverse flow diverts exhaust products temporarily into the intake system, and is later returned into the cylinder along with the new fuel-air mixture. The main cause of reverse flow is due to the pressure gradient between the cylinder and intake manifold. Because some of the exhaust gases go into the intake manifold, this means less burnt gases are being expelled during the exhaust stroke. Thus, the pumping losses are reduced, as shown in the reduction of the negative loop in the PV cycle of fig. 2.7.

2.1.6. Early and late exhaust valve closing (EEVC and LEVC) – Fig. 2.8 and Fig. 2.9

The closing of the exhaust valve takes place at around 10 degrees after TDC. It is the end of the exhaust stroke as well as the end of valve overlap.

Closing of the exhaust valve occurs after TDC, which allows backflow of burnt gases from the exhaust manifold back into the cylinder. During idle, burnt gas backflow is more dominant because of the high-pressure gradient in the intake manifold and combustion chamber. Whereas, during part-load and wide-open throttle the pressure gradient is considerably lower.

Also, because of valve overlap, some of the burnt gases may pass into the intake manifold during the exhaust stroke. During the suction stroke these gases will be returned to the cylinder and will add to the trapped cylinder burnt byproducts. Also, the exhaust valve reverse flow that normally follows the exhaust outflow returns burnt gases to the cylinder, and thus further increases the residual fraction. EEVC may prevent total or partial overlap from occurring. No backflow of exhaust gases can occur from the exhaust manifold to the intake manifold when there is no overlap, but some amount can occur with partial overlap.

The amount of backflow is determined by the amount of valve overlap.

Law *et al.* [34] adapted two methods by using variable valve timing for the control of auto-ignition (CAI). For testing purposes they used only one active cylinder (450 cc, 10.5 CR) from a 1.8 L 4-cylinder engine. The valves were actuated by an electrohydraulic active valve train (AVT) for the purpose to recirculate and vary the amount of exhaust gases to reduce NOx, as well as to control auto-ignition.

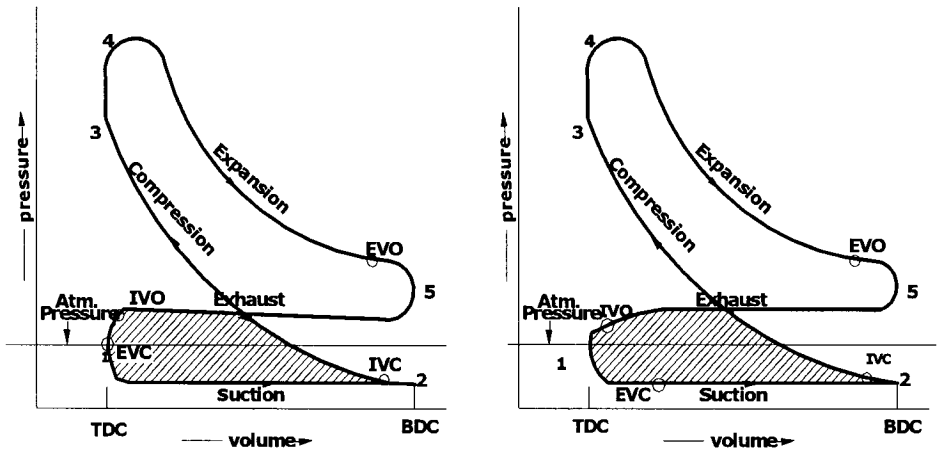

Fig. 2.8 & 2. 9. PV diagrams for EEVC & LEVC engine respectively.

In method one, EEVC strategy was used so that the exhaust gases trapped inside the cylinder could be later mixed with the subsequent fresh air-fuel mixture. The authors indicated that because of EEVC, a small amount of pumping losses occurred due to the compression and expansion of trapped residual gases. In method two, exhaust gas recirculation was obtained by valve overlap since some exhaust gases reenter into the cylinder and then mix with the fresh air-fuel mixture. Unlike the first method, the authors did not mention any valve timing strategy to vary the valve overlap. Method one is said to be sequential because exhaust gases are first trapped and then the fresh air-fuel mixture enters later; while method two is said to

be simultaneous because recalling of exhaust gases and entering of the fresh charge are at same time during the valve overlap. By the methods of controlling auto-ignition, 90 % reduction in NO_X was also achieved.

For LEVC, the period of valve overlap also increases. During the suction stroke some of the burnt gases from the exhaust manifold flows back into the intake manifold [6], which thus reduces the quantity of fresh air-fuel mixture (reduces volumetric efficiency). Also, it reduces the pumping losses during the intake of the new fresh charge because the intake manifold pressure is high, as shown in fig. 2.9.

In the case of LEVC, there is more exhaust gas backflow because of the increase in overlap. A simultaneous but smaller increase in intake valve reverse flow also occurs, due to the increased valve overlap duration.

At high speeds, more valve overlap is beneficial for scavenging of the residual gas, which gives higher power output. But more overlap is detrimental for idle quality due to the larger amount of residual gases going back into the intake manifold. Backflow can be prevented by reducing the overlap, which results in an increase in torque at idle speed (low speed). But, this will reduce the volumetric efficiency at higher speeds.

In case of LEVC, some amount of the unburned and burned gas mixture is retrieved from the exhaust manifold during valve overlap. This retrieved mixture once again goes through the combustion process with the combustion of the new air-fuel mixture, which results in the

reduction of unburned gases. But still, according to Siewert [32], LEVC is less effective in reducing HC emissions as compared to EEVC.

2.1.7. Early and late exhaust valve opening (EEVO and LEVO) - Fig. 2.10 and 2.11

EEVO occurs well before the end of the expansion stroke. This early timing provides better scavenging of burned gases, but it causes a reduction in the expansion work (see fig. 2.10) and thus reduces the output power of the engine. Therefore, it is detrimental to open the exhaust valve too early. However, there would be a reduction in the pumping work required to evacuate the cylinder after the piston passes through BDC. This is due to the decrease in the mass of exhaust gas during the exhaust stroke. This reduction in mass would require less force to expel them out.

According to Asmus [6], in EEVO engines, if the cylinder pressure during the exhaust stroke does not rise appreciably above the exhaust manifold, the pumping losses will be minimized.

Siewert [32] tested a single cylinder engine for EEVO strategy. According to Siewert, EEVO results in an increase of exhaust hydrocarbons composed more of the unsaturated (saturated carbons means carbons which contain maximum amount of oxygen) types since early valve opening interrupts the completion of cylinder hydrocardon reactions. Similarly, the increase in CO indicated its oxidation in the cylinder has also been curtailed by early EVO. It was noted that NOx was reduced because the exhaust gases dilute the fresh charge and thus decrease the combustion temperature. Because of the air-fuel dilution, the strength of the mixture reduces and causes the fuel consumption to increase.

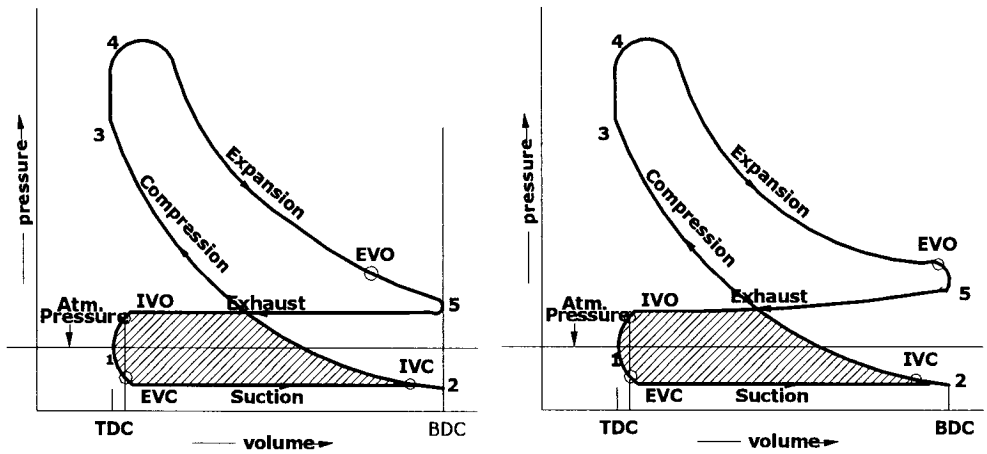

Fig. 2.10 & 2,11. PV diagrams for EEVO & LEVO engine respectively

LEVO reduces the power output because the majority of the work is from the exhaust stroke that is used to expel the burnt gases from the engine cylinder. Thus, a greater pumping loss results (see fig. 2.11). Unburned HC are also affected by exhaust valve opening timing. In case of LEVO, gases get more time to blow- down, which helps for good cylinder oxidization [20].

More exhaust valve opening delays causes a greater amount of the residual gases to be expelled during the overlap period. Then, there is the possibility of the exhaust gas to flow into the intake manifold during the overlap period, and then will flow back into the cylinder during the intake stroke. This flow reversion is also called the "internal exhaust recirculation" process, which is used to reduce NO_X.

2.2 Engine Model Simulation and Analysis for Cam Operated Dependent Actuator for Four Stroke Gasoline Engine

The following section presents the analysis and computer simulation (GT-Power) results to predict the gas flow dynamics through the intake and exhaust valves for a single cylinder variable valve timed engine. For both the intake and exhaust valves, variable valve timing is acquired by either advancing or by retarding the cam profile to obtain the phase shift. The research work of this section is published in [2].

GT-Power is computer aided engineering (CAE) software package for engine simulation studies, which features an object based code design with unique geometrical elements. It is designed for steady state and transient simulations for a wide range of engine issues like VVT. It represents the flow and heat transfer in the piping and in the other components of an engine system. In this section the effects of variable valve timing (VVT) events on gasoline engine performance are described. An investigation into the effects of inlet and exhaust valve gas dynamics done and in particular, effects on the pressure-volume cycle and reverse flow through the intake and exhaust valves are studied. The engine specifications are as shown in table 2.1.

Figures 2.12 a. and 2.12 c. show the valve lift and phase profiles for intake and exhaust valves, respectively, for a conventional cam operated engine. Figure 2.12 b shows the air-fuel mass flow through the intake valve into the engine cylinder. During the compression stroke after BDC and during the valve overlap period, possible back flow can occur. Figure 2.12 d, shows the mass flow through the exhaust valve out of the engine cylinder. Again, possible

back flow can occur during valve overlap.

Table 2.1 Engine Specifications

Type of engine: 4-stroke
Number of cylinders: single cylinder
Engine speed: 1000 rpm
Bore and stroke: 100 mm respectively
Compression ratio: 9.5
TDC clearance height: 3mm
Inlet valve reference diameter: 45.5 mm
Inlet valve opening timing: 10 degrees before TDC
Inlet valve closing timing: 60 degrees after BDC
Inlet cam phase shift: 30 degrees for retard and advance
Maximum valve lift: 10.2 mm
Exhaust valve reference diameter: 37.5 mm
Exhaust valve opening timing: 60 degrees before BDC
Exhaust valve closing timing: 20 degrees after TDC
Exhaust cam phase shift: 30 degrees for retard and advance

The 1-cylinder 4-stroke engine model was simulated for four cases of valve timing strategies, as listed in the following:

Case I - Early intake valve opening and early intake valve closing (EIVO + EIVC)

Case II - Late intake valve opening and late intake valve closing (LIVO + LIVC)

Case III - Early exhaust valve opening and early exhaust valve closing (EEVO + EEVC)

Case IV - Late exhaust valve opening and late exhaust valve closing (LEVO + LEVC)

2.2.1 Case I- Early Intake Valve Opening and Early Intake Valve Closing (EIVO + EIVC)

In this case, 30 degrees of cam shift advances the intake valve timing. There were no changes made in the exhaust valve timing. Figure 2.13a shows the phase shift advanced for the intake valve. The corresponding air-fuel mass flow and their dynamic changes are shown in fig. 2.13b.

By EIVO, the duration of the overlap period increases and thus the amount of back flow also increases (see fig.2.13b). On the other hand by EIVC, backflow during the compression stroke is lower because the air-fuel mass has less time to flow back through the inlet valve to the intake manifold (see fig.2.13b).

For this case, with a given engine speed, and by changing only the intake valve timing while keeping the exhaust valve timing unchanged (see fig.2.13a and fig.2.13b), there is not much significant difference in exhaust gas dynamics as shown in fig.2.13d.

The PV diagram of fig.2.17b shows lower pumping losses for an EIVO + EIVC engine with respect to a conventional engine as shown in fig.2.17a. These simulation results agree with references [22,23,24,25,26,27,28,29,30,31,32] as previously discussed.

2.2.2. Case II- Late Intake Valve Opening and Late Intake Valve Closing (LIVO + LIVC)

In this case, shifting of the cam profile by 30 degrees retards the inlet valve timing. No changes were made to the exhaust valve timing. Figure 2.14a shows the retard in phase shift

for the inlet valve timing and the corresponding air-fuel mass flow dynamics is as shown in fig.2.14b.

LIVO prevents partial or full valve overlap, which results in very low or no backflow to occur during this period, as shown in fig.2.14b. In case of LIVC, the closing of the intake valve is delayed towards the end of the compression stroke. Due to this late closing some of the air-fuel mass flows back into the intake manifold (see fig.2.14b). The amount of back flow is more with respect to a conventional engine.

For this case, although there was no change made in the exhaust valve timing, LIVC still produces significant effects on the exhaust gas dynamics because of air-fuel mass back flow. Because there is more backflow during the compression stroke, less air-fuel mass are left for combustion. This results in less burnt gases produced after combustion, as shown in fig.2.14d. The PV diagram of fig.2.17c shows an increase in the pumping losses with respect to a conventional engine. This is because the reduction of pumping losses by LIVC is overshadowed by the increase due to LIVO. Simulation results for this case agree with the discussions from references [5,6,7,8,9,10,11,12,13,14,15,16,17,18,19,20,21]

2.2.3 Case III- Early Exhaust Valve Opening and Early Exhaust Valve Closing (EEVO + EEVC)

In this case, the exhaust valve timing is advanced by 30 degrees on the cam shift, as shown in fig.2.15c. No changes were made to the intake valve timing, as shown in fig. 2.15a. Figure2.15c shows the timing advance in phase shift for the exhaust valve, and fig.2.15d shows the corresponding flow of burnt gases.

Even though EEVO provides better scavenging for the burnt gases, it also reduces the expansion work during the power stroke. Figure 2.15d indicates that the quantity of mass flow rate during the power stroke is less with respect to a conventional engine.

EEVC reduces the partial or total overlap, which reduces or prevents the backflow, as shown in fig.2.15b and fig.2.15d. Because of EEVC, the total amount of burnt gases may not escape out of the engine cylinder during the exhaust stroke. In fig.2.15b it is noticeable that the exhaust stroke is computed before TDC by closing the exhaust valve earlier.

In the case of EEVO + EEVC, the pumping losses are more and the expansion work is lower as shown in fig.2.17d, than that in a conventional engine as shown in fig.2.17a. During the end portion of EEVC, the exhaust gases get a smaller area to flow out of the cylinder through the exhaust valve opening. This flow restriction may increase the pumping losses. Whereas, in the case of EEVO, opening of the exhaust valve cuts down part of expansion stroke, which results in the reduction of the expansion work (fig.2.17d). The simulation results agree with references [6,31], as previously discussed.

2.2.4 Case IV- Late Exhaust Valve Opening and Late Exhaust Valve Closing (LEVO + LEVC)

In this case, the exhaust valve timing is retarded by 30 degrees as shown in fig.2.16c. No changes were made to the inlet valve timing as shown in fig.2.16a. Figure 2.16c shows the phase shift being retarded for the exhaust valve, and the corresponding flow of burnt gas dynamics is shown in fig.2.16d.

For this case of LEVO, the majority of work shifts to the exhaust stroke (see fig.2.16d). Due to this shift, a more complete blow-down takes place and no loss occurs in the expansion work during the power stroke. LEVC increases the valve overlap period, which causes backflow during this period (see fig.2.16 b and fig.2.16d). As shown in fig. 2.17e, in the case of LEVO complete expansion work takes place, whereas, pressure increases at an early stage.

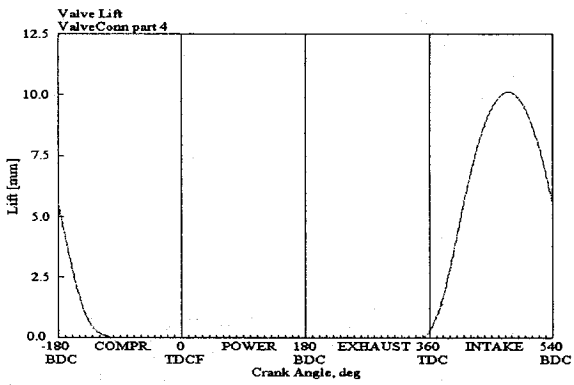

a. Intake valve lift and phase for conventional cam operated engine

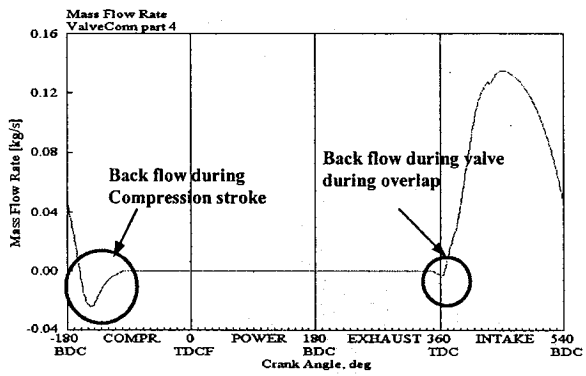

b. Flow of air-fuel mass through the intake valve into an engine cylinder. Possible back flow can occur during valve overlap and closing time of intake valve after BDC

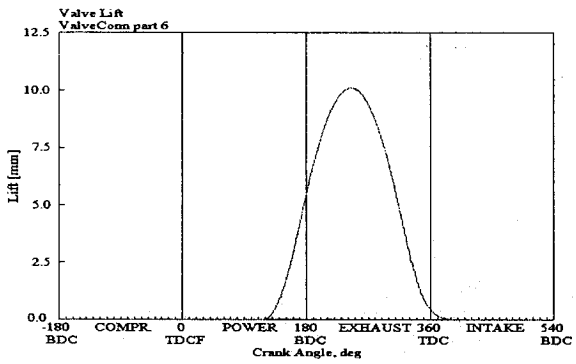

c. Exhaust valve lift and phase for conventional cam operated engine

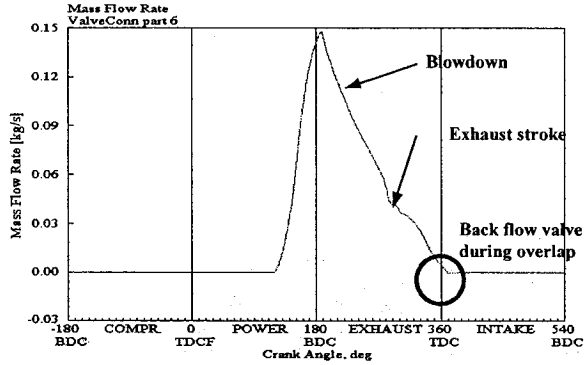

d. Flow of burnt mass through the exhaust valve out of an engine cylinder. Possible back flow can occur during valve overlap.

Fig. 2.12 Conventional cam operated four stroke SI Engine

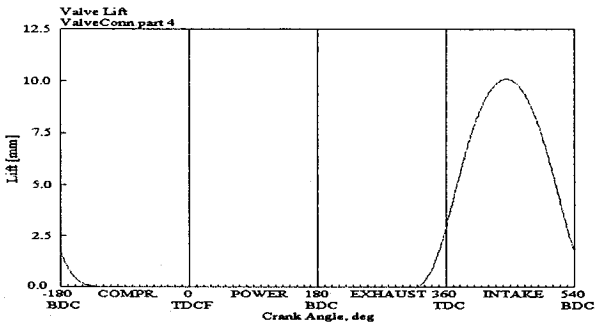

a) Intake valve lift and advanced phase shift

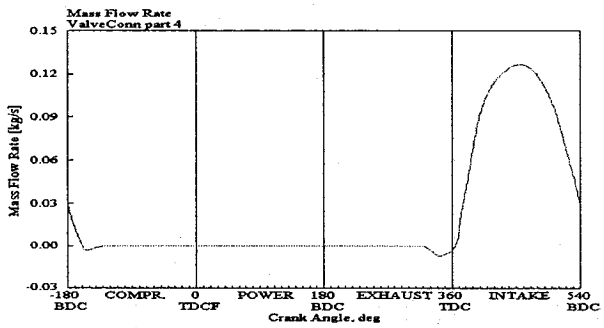

b) Flow of air-fuel mass

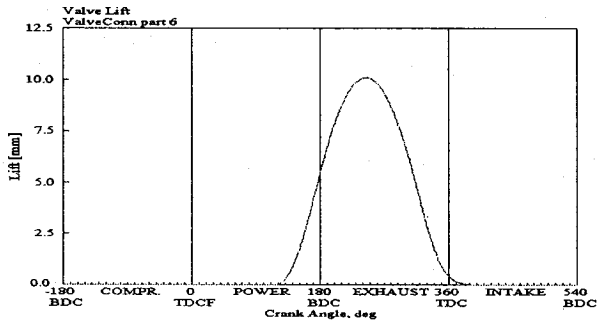

c) Exhaust valve lift and phase

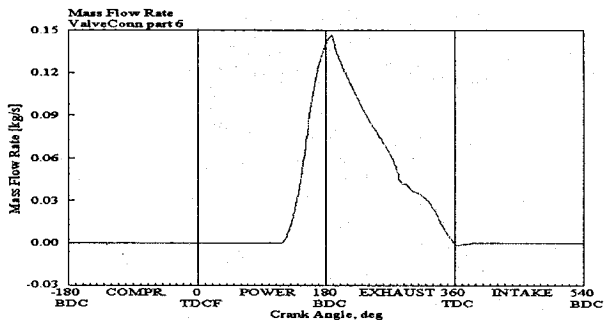

d) Flow of burnt mass

Fig. 2.13. EIVO + EIVC ---- Advancing Intake cam by 30 degree phase shifting

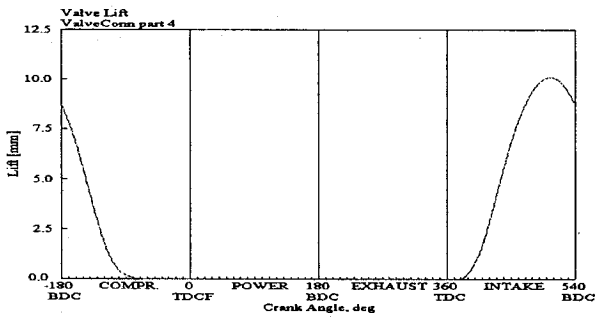

a) Intake valve lift and retarded phase shift

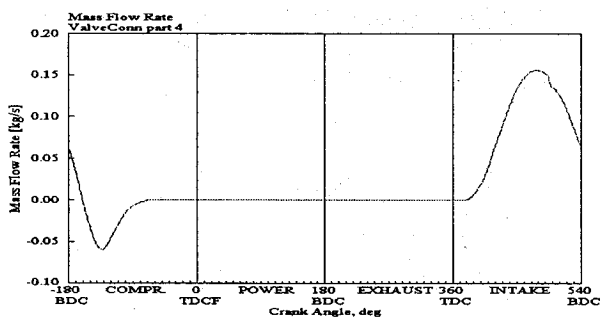

b) Flow of air-fuel mass

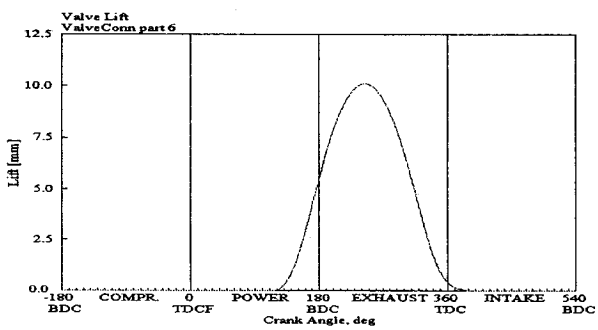

c) Exhaust valve lift and phase

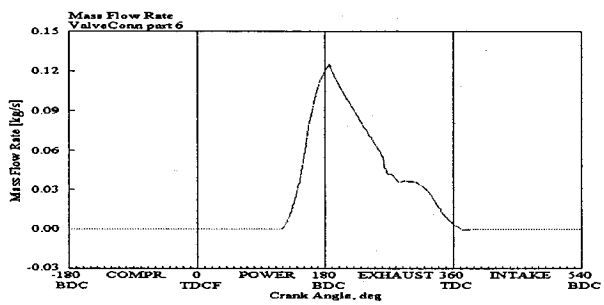

d) Flow of burnt mass

Fig. 2.14. LIVO + LIVC ---- Retarding Intake cam by 30 degree phase shifting

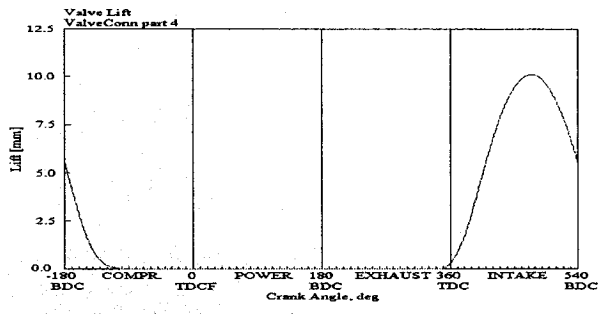

a) Intake valve lift and phase

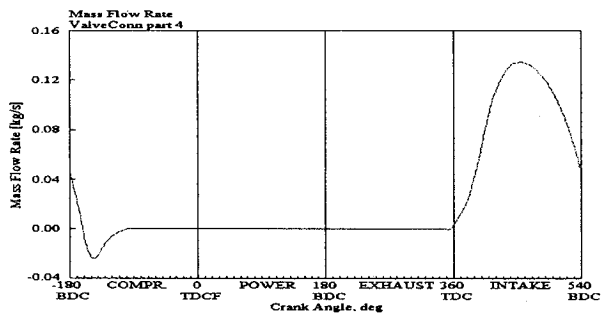

b) Flow of air-fuel mass

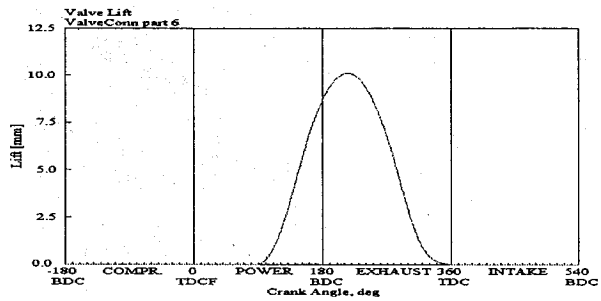

c) Exhaust valve lift and advanced phase shift

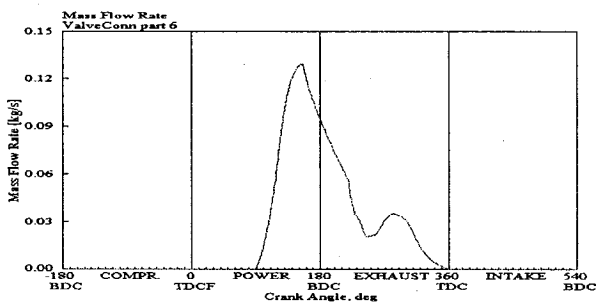

d) Flow of burnt mass

Fig. 2.15. EEVO + EEVC ---- Advancing Exhaust cam by 30 degree phase shifting

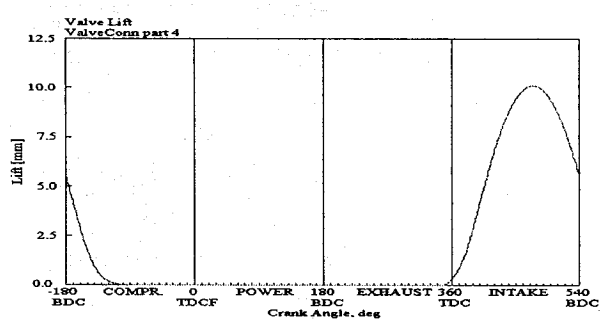

a) Exhaust valve lift and phase

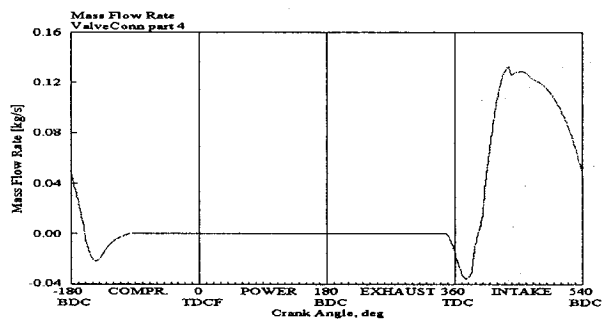

b) Flow of air-fuel mass

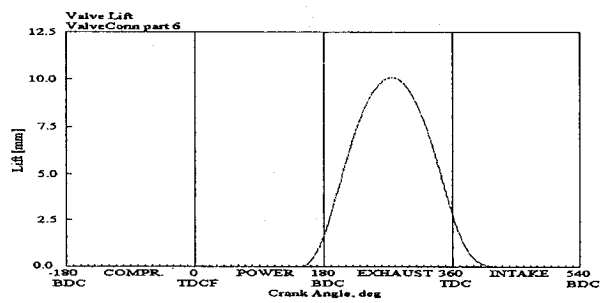

c) Exhaust valve lift and retarded phase shift

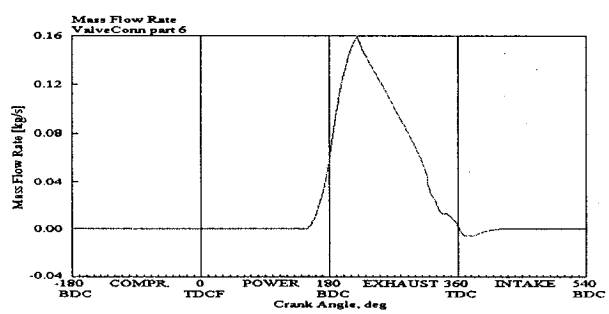

d) Flow of burnt mass

Fig. 2.16. LEVO + LEVC ---- Retarding Exhaust cam by 30 degree phase shifting

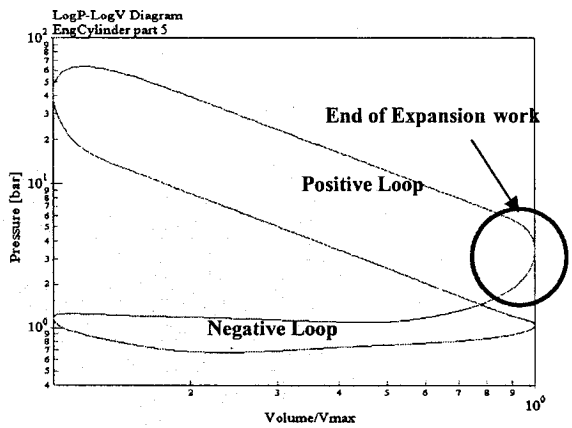

a. Pressure-Volume diagram for Conventional Engine

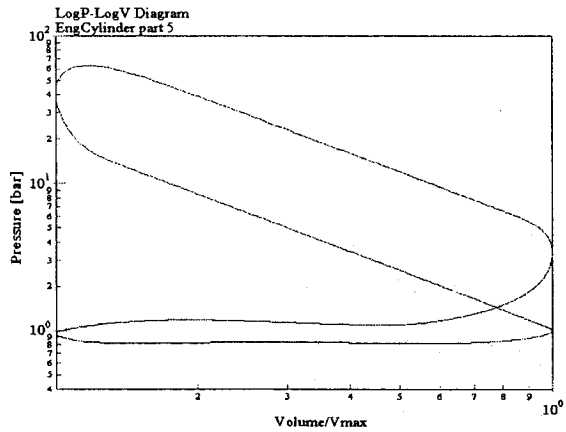

b. Pressure-Volume diagram for EIVO + EIVC Engine (Case I)

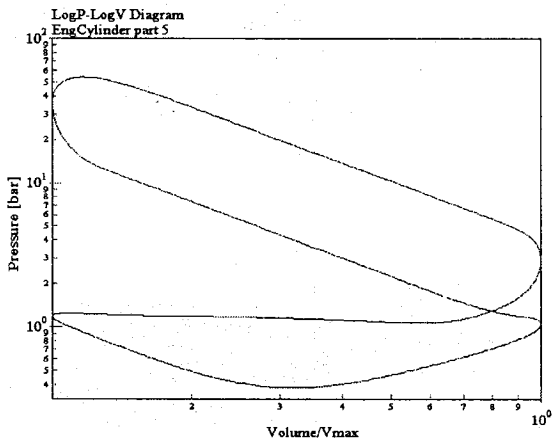

c. Pressure-Volume diagram for LIVO + LIVC Engine (Case II)

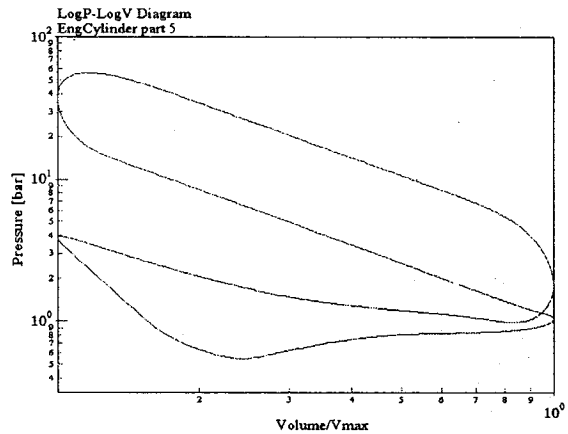

d. Pressure-Volume diagram for EEVO + EEVC Engine (Case III)

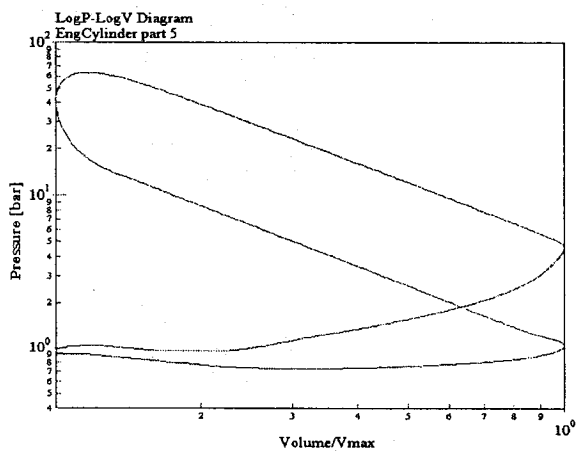

e. Pressure-Volume diagram for LEVO + LEVC Engine (Case IV)

Fig 2.17. Log P-Log V diagrams for SI engine (Phase shifting)

2.3 Engine Model Simulation and Analysis for Solenoid Operated Independent Actuator for Four Stroke Gasoline Engine

The following section presents the analysis and computer simulation results to predict the gas flow dynamics through the intake and exhaust valves for a single cylinder variable valve timed engine. For both the intake and exhaust valves, variable valve timing is acquired by either advancing or by retarding the closing or opening timing of the intake and exhaust valves. The valves used on this engine are solenoid operated. The research work of this section is published in [4].

Table 2.2 Engine Specifications (solenoid operated SI engine)

Type of engine: 4-stroke, Single cylinder, 4000 rpm
Bore and stroke: 100 mm respectively
Compression ratio: 9.5
TDC clearance height: 3mm
Solenoid operated intake and exhaust valves
Inlet valve reference diameter: 45.5 mm
Inlet valve opening timing: 10 degrees before TDC
Inlet valve closing timing: 50 degrees after BDC
Inlet valve lift (maximum): 4.2 mm
Exhaust valve reference diameter: 37.5 mm
Exhaust valve opening timing: 60 degrees before BDC
Exhaust valve closing timing: 10 degrees after TDC
Exhaust valve lift (maximum): 5 mm

Figure 2.18 shows the PV diagram for an engine used for modeling purposes, with conventional opening and closing of intake and exhaust valves (see Table 2.2 for valve timings). Figures 2.19a and 2.19c show the valve lift and phase profiles for the intake and exhaust valves, respectively, for a conventional (solenoid valve actuated) engine. Figure 2.19b shows the air-fuel mass flow through the intake valve into the engine cylinder. During the compression stroke after BDC and during the valve overlap period, possible backflow can occur. Figure 2.19d shows the mass flow through the exhaust valve out of the engine cylinder. Again, possible backflow can occur during the valve overlap.

For discussion purposes with respect to late and early opening and closing of the intake and exhaust valves, 50 degrees of margin is kept with respect to the standard base line angles of the conventional cam operated SI engine. The 1-cylinder 4-stroke engine model was simulated for all eight valve-timing strategies, as listed in the following:

2.3.1 Case I - Early Intake Valve Closing (EIVC)

Early intake valve closing is obtained by closing the inlet valve 50 degrees earlier, as shown in fig. 2.20a with respect to a conventional engine. There were no changes made in exhaust valve timing. The corresponding air-fuel mass flow and their dynamic changes are shown in fig. 2.20b.

Due to early closing of the inlet valve, backflow during the compression stroke can be reduced or avoided (fig. 2.20b). Early closing of the inlet valve limits or cuts down the admission of air-fuel mixture during the suction stroke and hence reduces the volumetric efficiency as well as pumping losses of the engine, as shown in fig. 2.28a.

2.3.2 Case II - Late Intake Valve Closing (LIVC)

Late intake valve closing is obtained by closing the inlet valve 50 degrees later with respect to a conventional engine. Figure 2.21a shows the late closing of the inlet valve, and fig.2.21b shows the corresponding air-fuel mass flow dynamics.

In case of LIVC, the closing of the intake valve is delayed towards the end of the compression stroke. Due to this delay some of the air-fuel mass flows back into the intake manifold (see fig.2. 21b). The amount of backflow is more as compared to a conventional engine.

Although there were no changes made in the exhaust valve timing, LIVC still produces significant effects on the exhaust gas dynamics because of the air-fuel mass backflow. Because there is more backflow during the compression stroke, this results in less air-fuel mass left for combustion and thus less burnt gases are produced after combustion (see fig. 2.21d).

Pumping losses for LIVC are lower as shown in fig. 2.28b, which agrees with the pervious discussion in the section under LIVC. LIVC reduces the effective compression ratio and thus has a negative effect (reduces) on the volumetric and thermal efficiencies.

2.3.3 Case III - Early Intake Valve Opening (EIVO)

The intake valve opens 50 degrees earlier with respect to a conventional engine. No changes were made to the exhaust valve timing, as shown in fig.2.22c. Figure 22a shows the early opening of the inlet valve, and fig.2.22b shows the corresponding air-fuel mass flow. By EIVO, the duration of the valve overlap period increases and thus the amount of backflow

also increases during this period. Pumping losses are reduced as shown in fig.2 28c, which agrees with the pervious discussion in the section under EIVO. Figure 2.22d shows that there are not much significant changes in the exhaust gas dynamics due to intake valve timing variation. This is because the suction stroke starts well before TDC (fig. 2.22a). But, it is observed that there are fluctuations in the flow of fresh air-fuel mixture at the beginning of the intake stroke, which maybe due to the pressure gradient between the cylinder and exhaust manifold.

2.3.4 Case IV - Late Intake Valve Opening (LIVO)

Late opening of the inlet valve is obtained by 50 degrees delayed opening with respect to a conventional engine. LIVO prevents partial or full valve overlap, which results in very low or no backflow, as shown in fig. 2.23b. The suction of the air-fuel mixture starts after the intake valve opens, away after BDC. This late opening increases the vacuum inside the cylinder, and results in higher pumping losses (fig. 2.28d). Late opening of the intake valve creates turbulence for the incoming air-fuel mixture, which helps homogenous combustion.

2.3.5 Case V - Early Exhaust Valve Closing

Early exhaust valve closing is obtained by closing the exhaust valve 50 degrees earlier than in a conventional engine. EEVC reduces the partial or total valve overlap period, and results in the reduction or prevents exhaust backflow (figs. 2.24b and 2.24d). Because of EEVC, the total amount of burnt gases may not escape out of the cylinder during the exhaust stroke. In fig. 2.24d it is noticeable that the exhaust stroke is completed well before TDC by closing the exhaust valve early. In such a situation, normal scavenging due to the exhaust stroke does not take place, which results in some residual gases to stay in the cylinder. It may be noted in fig.

2.24b that backflow into the intake manifold can occur while the piston is approaching TDC because the exhaust valve was closed early.

During the end portion of EEVC, the exhaust gases have a smaller exhaust valve opening area to flow out of the cylinder. This flow restriction may increase the pumping losses as shown in fig 2.28e. Pumping losses also increase because of the compression and expansion of trapped residual gases.

2.3.6 Case VI - Late Exhaust Valve Closing (LEVC)

Late exhaust valve closing is obtained by closing the exhaust valve 50 degrees later, as shown in fig 2.25c, than in a conventional engine. LEVC increases the valve overlap period, which allows backflow to occur (fig.2.25d). This is the reason why LEVC is one of the good methods to create internal EGR. As shown in fig. 2.28f, pumping losses are lower.

2.3.7 Case VII - Early Exhaust Valve Opening (EEVO)

Early exhaust valve opening is obtained by opening the exhaust valve 50 degrees earlier than in a conventional engine. Even though EEVO provides better scavenging for the burnt gases, it also cuts down part of the expansion stroke, which results in the reduction of the expansion work, as shown fig.2.28g. The mass flow rate during the exhaust stroke is more as shown in fig.2.26d, than in a conventional engine

Because of early opening, the pressure gradient between the cylinder and the exhaust manifold is insufficient to create a strong blow-down. This is why some of the work is transferred to exhaust stroke and results in an increase of the pumping losses, as shown in

fig.2.28g.

2.3.8 Case VIII - Late Exhaust Valve Opening (LEVO)

Late exhaust valve opening is obtained by opening the exhaust valve 50 degrees later with respect to a conventional engine. For this case the majority of work shifts to the exhaust stroke, as shown in fig.2.27d. A stronger blow-down takes place and no loss occurs in the expansion work during the power stroke, as shown in fig.2.28h. Late opening of the valve cases greater expansion work and increases the pumping losses at the beginning of the exhaust stroke (see fig. 2.28h).

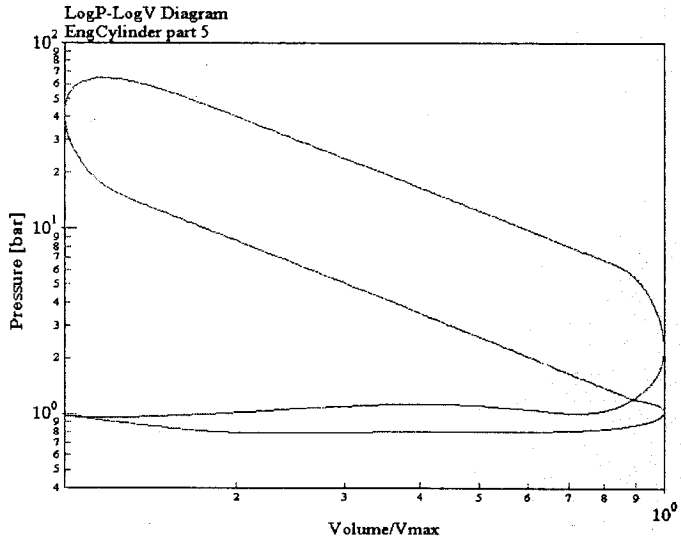

Fig. 2.18 P-V diagram for solenoid valve operated SI engine

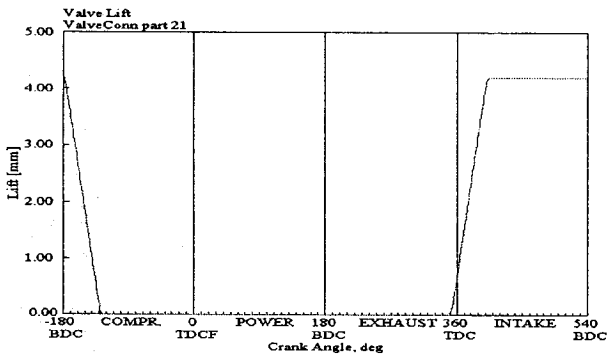

a) Intake valve lift and phase for base engine

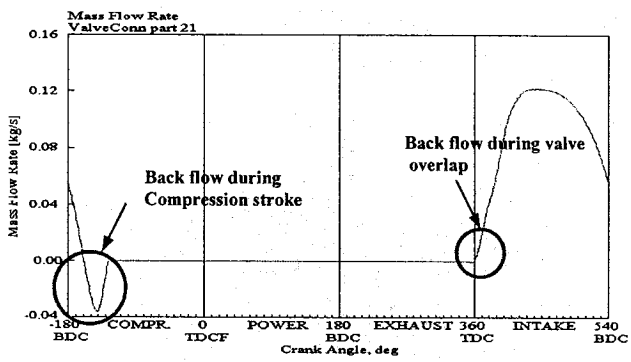

b) Flow of air-fuel mass through the intake valve into an engine cylinder. Possible backflow can occur during valve overlap and closing time of intake valve after BDC.

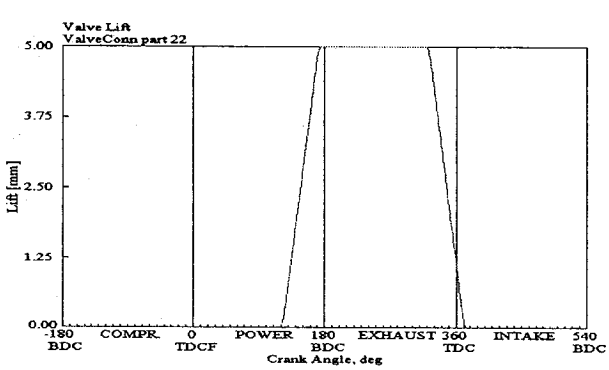

c) Exhaust valve lift and phase for baseline engine

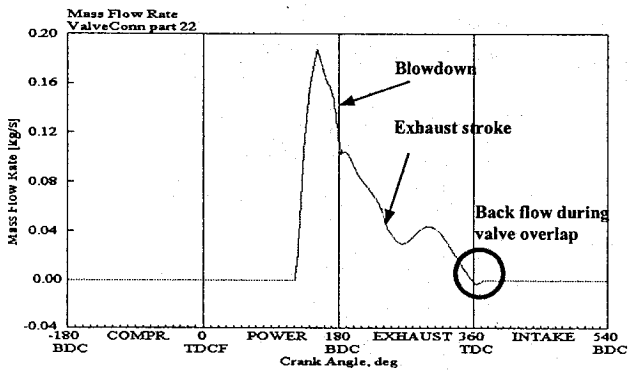

d) Flow of burnt mass through the exhaust valve out of an engine cylinder. Possible backflow can occur during valve overlap.

Fig. 2.19 For Solenoid valve operated SI engine

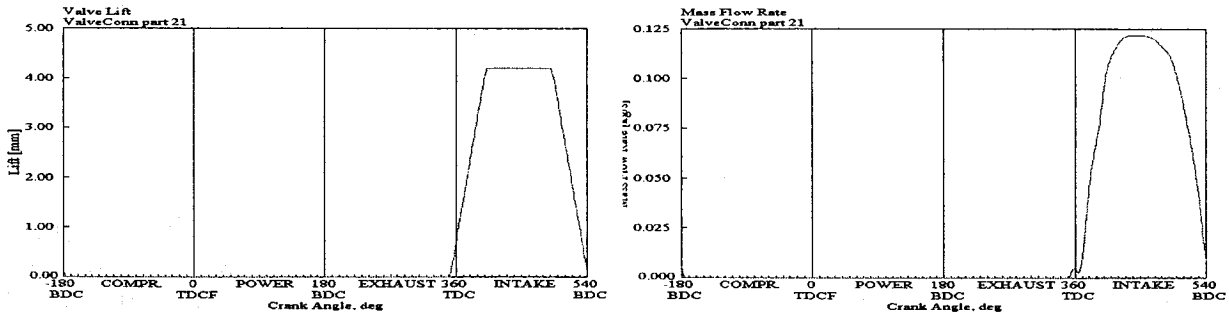

a) Intake Valve lift

b) Flow of air-fuel mass

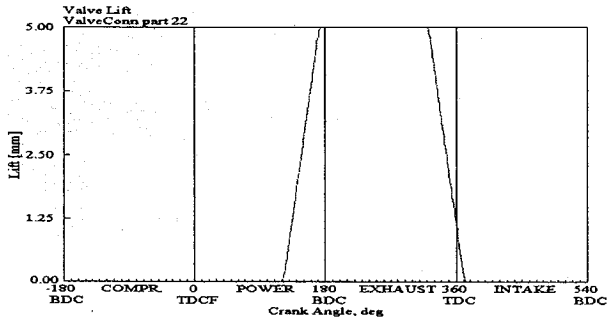

c) Exhaust valve lift

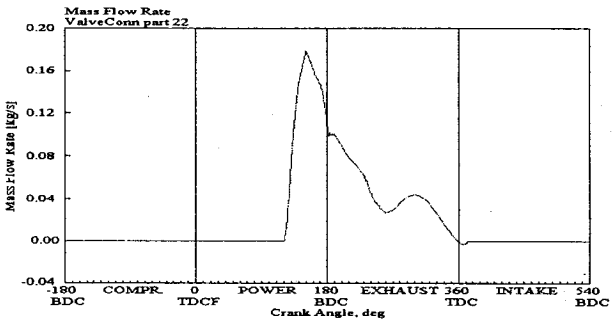

d) Flow of burnt mass

Fig. 2.20 Early Intake Valve Closing

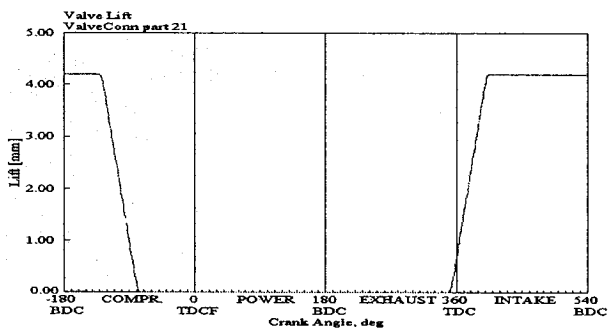

a) Intake Valve lift

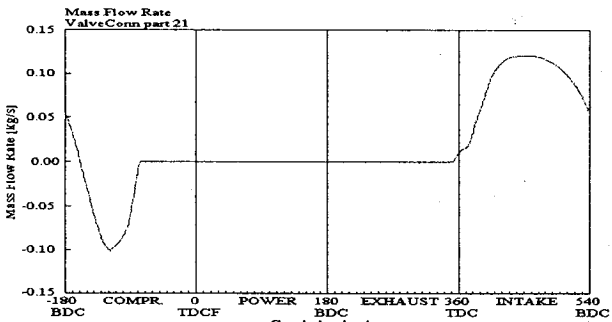

b) Flow of air-fuel mass

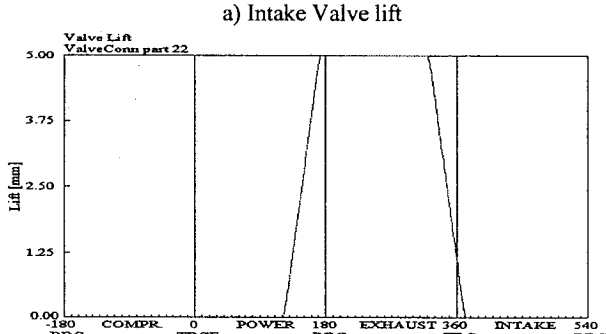

c) Exhaust valve lift

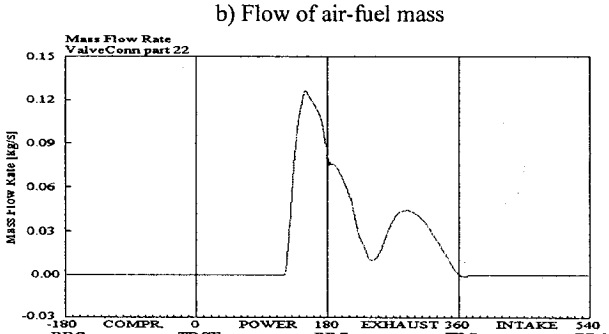

d) Flow of burnt mass

Fig. 2.21 Late Intake Valve

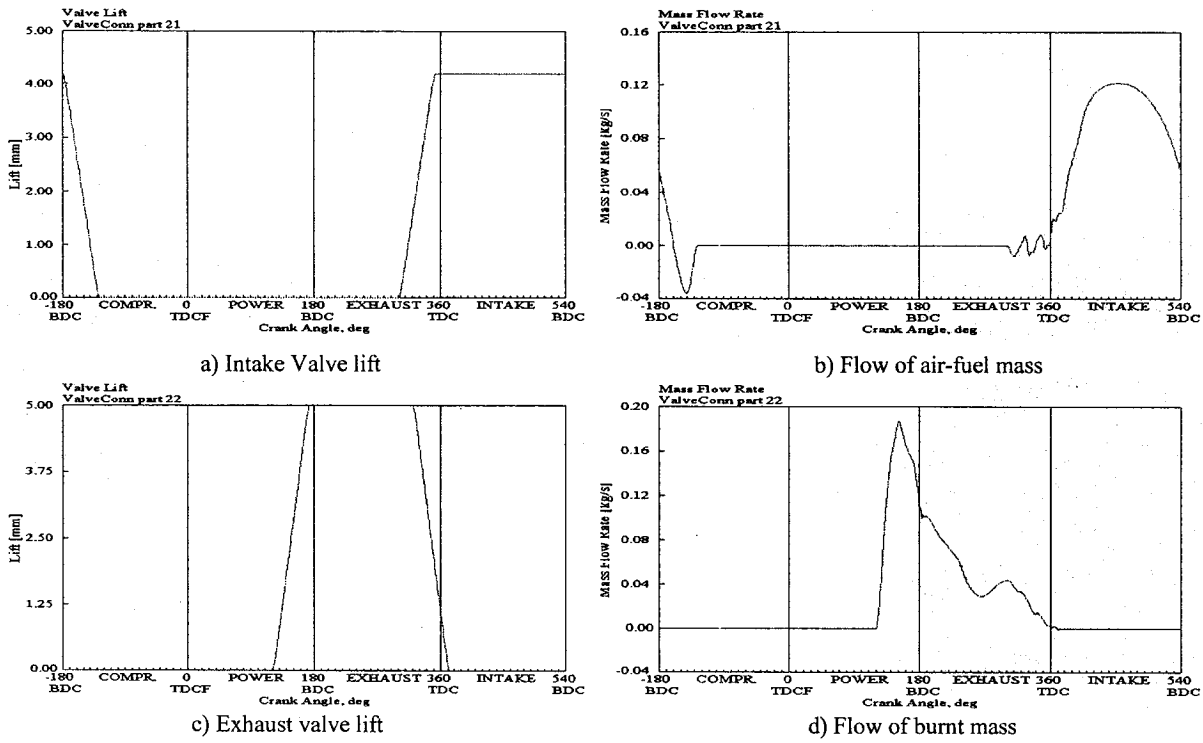

a) Intake Valve lift

b) Flow of air-fuel mass

c) Exhaust valve lift

d) Flow of burnt mass

Fig. 2.22 Early Intake Valve Opening

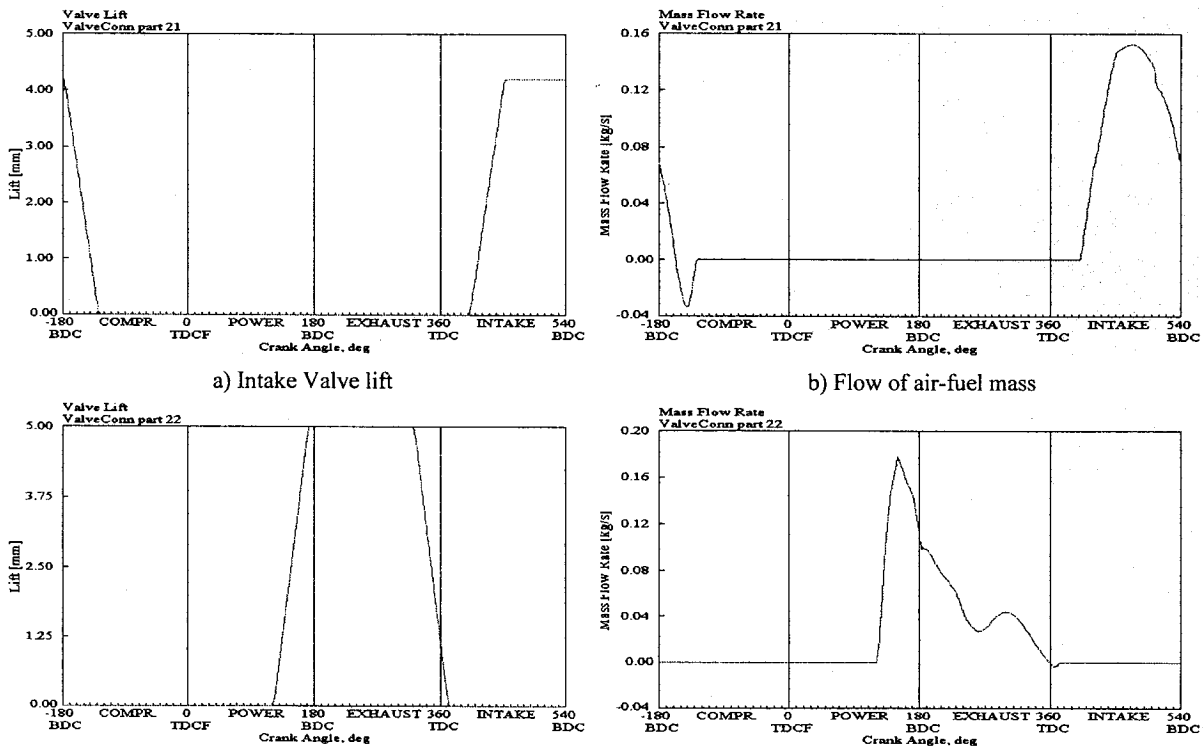

a) Intake Valve lift

b) Flow of air-fuel mass

c) Exhaust valve lift

d) Flow of burnt mass

Fig. 2.23 Late Intake Valve Opening

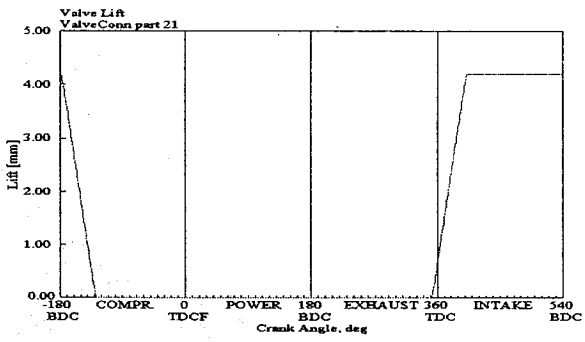

a) Intake Valve lift

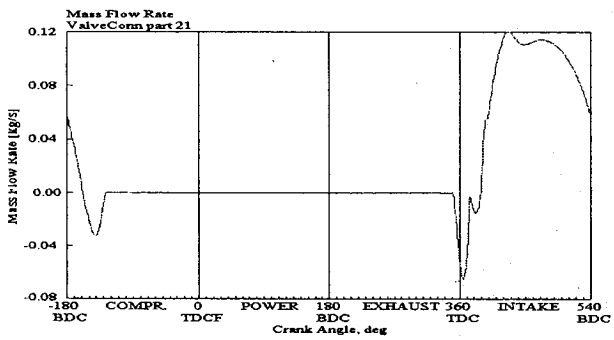

b) Flow of air-fuel mass

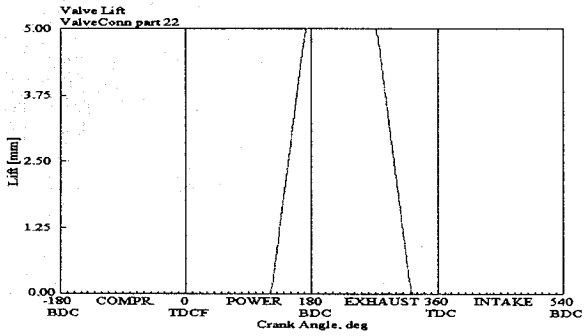

c) Exhaust valve lift

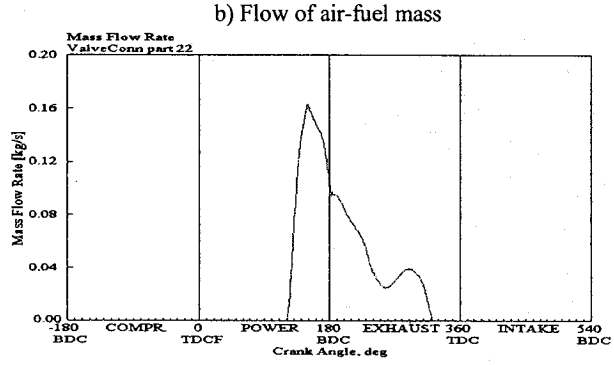

d) Flow of burnt mass

Fig. 2.24 Early Exhaust Valve Closing

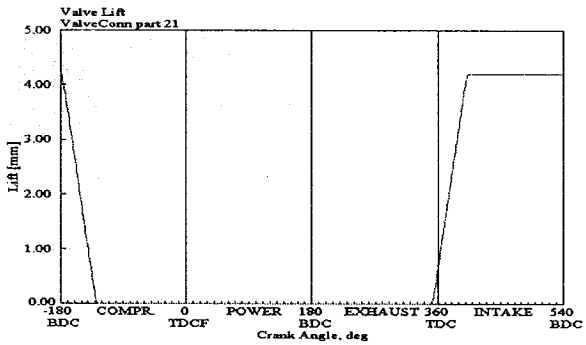

a) Intake Valve lift

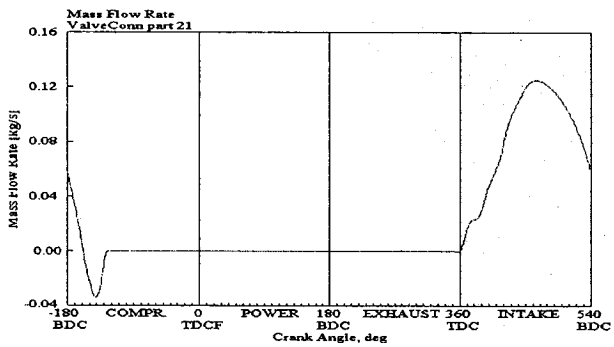

b) Flow of air-fuel mass

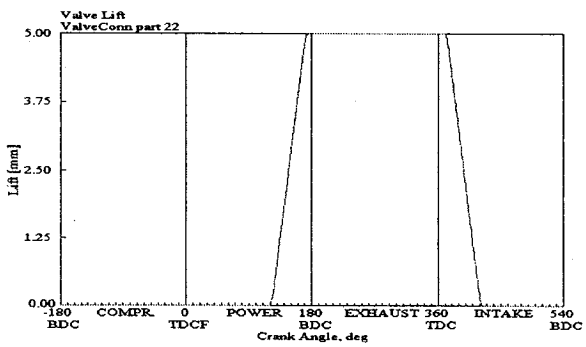

c) Exhaust valve lift

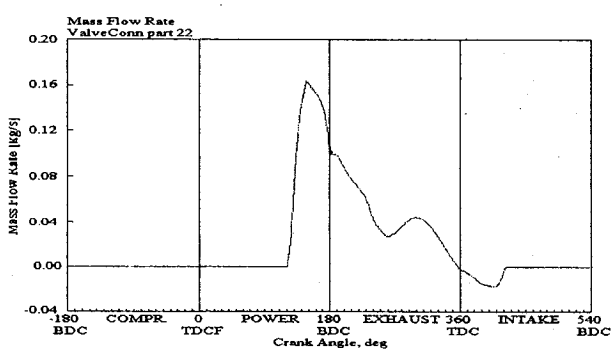

d) Flow of burnt mass

Fig. 2.25 Late Exhaust Valve Closing

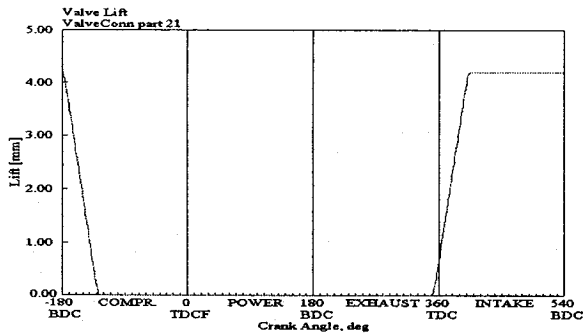

a) Intake Valve lift

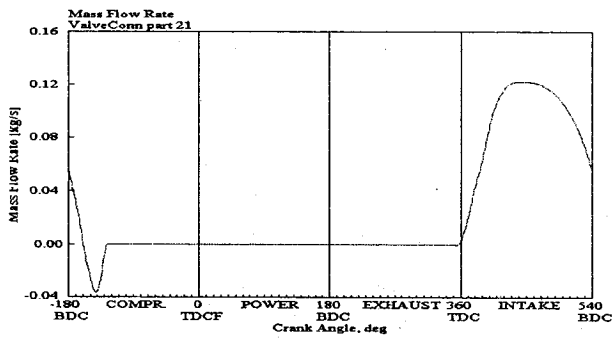

b) Flow of air-fuel mass

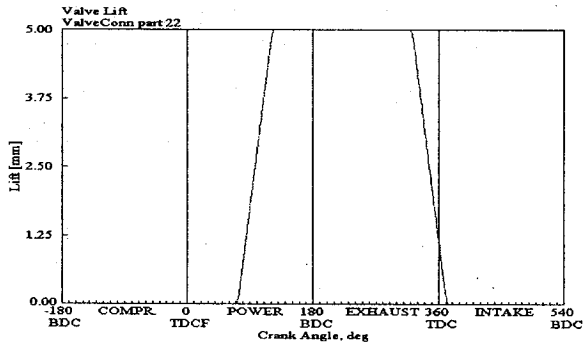

c) Exhaust valve lift

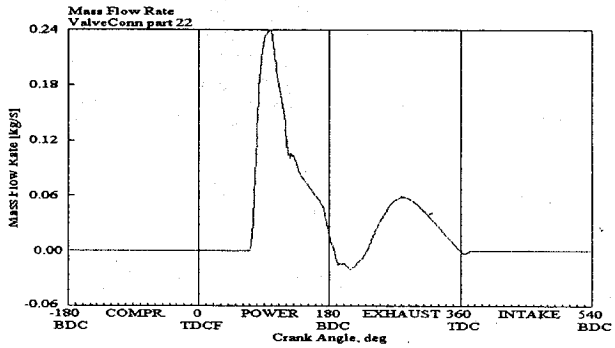

d) Flow of burnt mass

Fig. 2.26 Early Exhaust Valve Opening

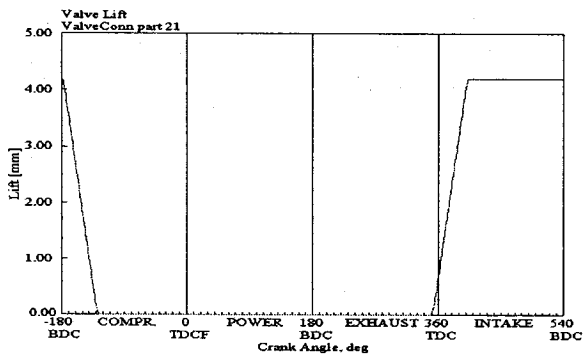

a) Intake Valve lift

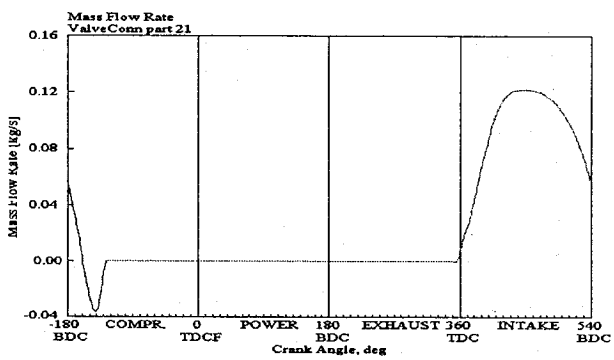

b) Flow of air-fuel mass

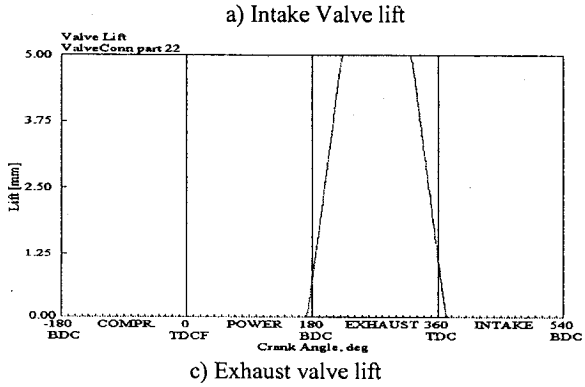

c) Exhaust valve lift

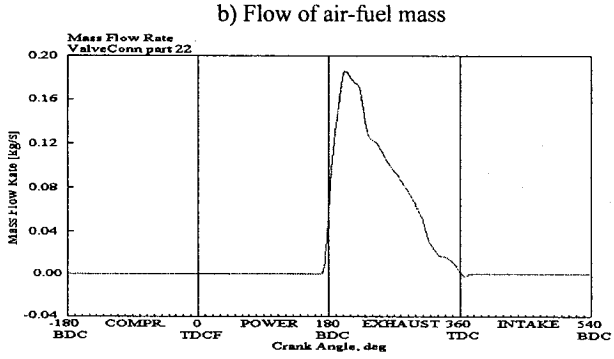

d) Flow of burnt mass

Fig. 2.27 Late Exhaust Valve Opening

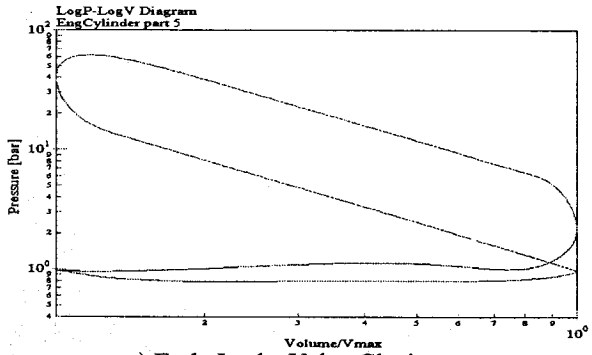

a) Early Intake Valve Closing

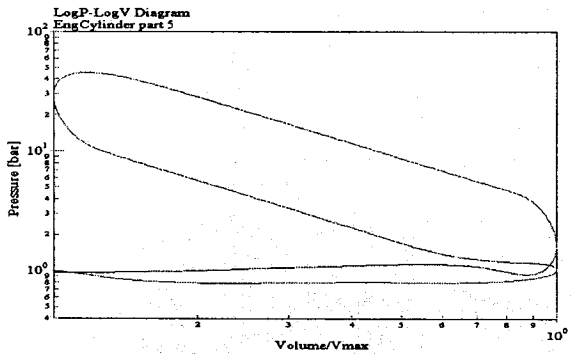

b) Late Intake Valve Closing

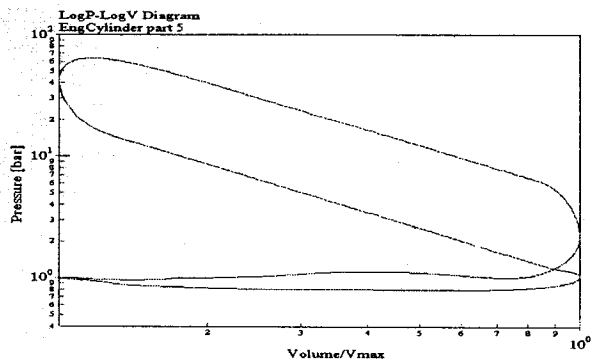

c) Early Intake Valve Opening

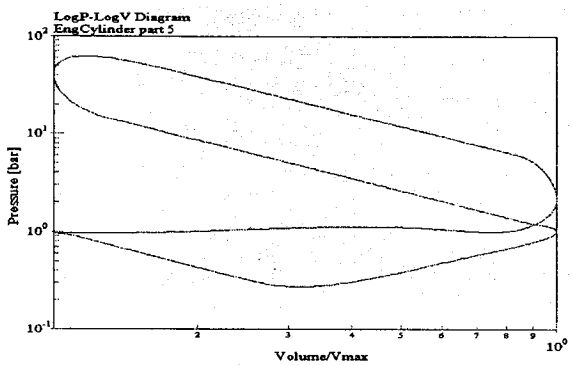

d) Late Intake Valve Opening

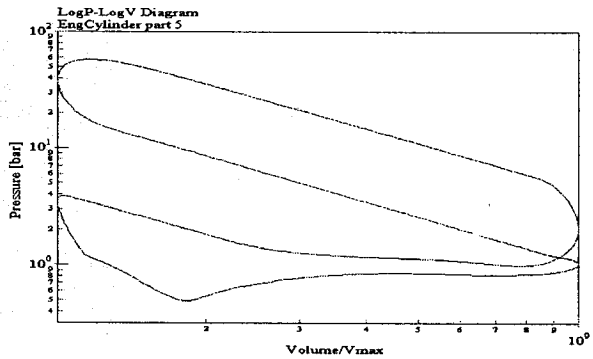

e) Early Exhaust Valve Closing

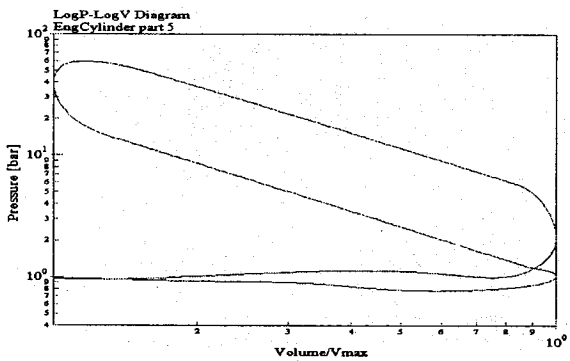

f) Late Exhaust Valve Closing

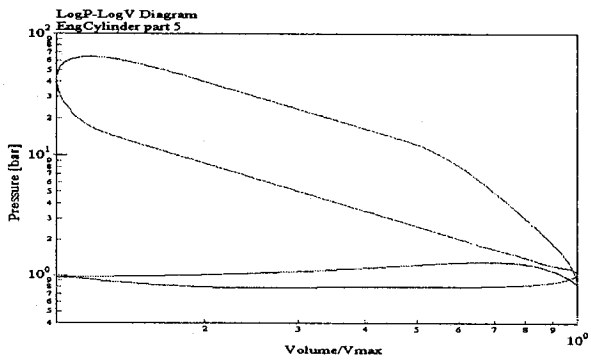

g) Early Exhaust Valve Opening

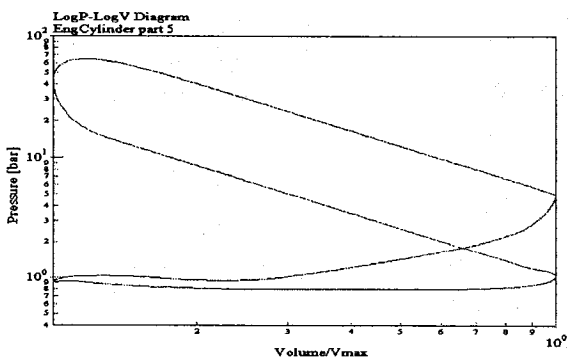

h) Late Exhaust Valve Opening

Fig. 2.28 Log P/Log V diagrams for intake and exhaust strategies

2.4 Engine Model Simulation and Analysis for Solenoid Operated Independent Actuator for Four Stroke Diesel Engine.

This section presents the analysis of computer simulation results to predict the gas flow dynamics through the intake and exhaust valves for a naturally aspirated single cylinder variable valve timed C.I. engine. One dimensional gas flow dynamic simulation studies were performed by using the GT-Power engine simulation package to verify the effects of the intake and exhaust valve opening and closing. During the simulation studies the quantity of fuel injection is held constant and the timings of intake/exhaust valves are varied.

This section describes the effects of variable valve timing (VVT) events on diesel engine performance. An investigation into the effects of inlet and exhaust valve gas dynamics is given. In particular, effects on the pressure-volume cycle and reverse flow through the intake and exhaust valves are studied. The research work of this section is published in [1].

Figures 2.30a and 2.30c show the valve lift and phase profiles for the intake and exhaust valves, respectively, for a conventional solenoid operated C.I. engine. Figure 2.30b shows the air mass flow through the intake valve into the engine cylinder. During the compression stroke after BDC and during the valve overlap, possible backflow can occur. Figure 2.30d shows the exhaust mass flow through the exhaust valve out of the engine cylinder. Figure 2.29 shows the Log P versus Log V diagram for the conventional C.I. engine. Table 2.3 lists the diesel engine specifications, and the conventional intake and exhaust valve timings.

Table 2.3 Engine Specifications (Solenoid operated CI engine)

Type of engine: 4-stroke
Number of cylinders: single cylinder
Engine speed: 4000 rpm
Bore and stroke: 100 mm respectively
Compression ratio: 16.5
Solenoid operated intake and exhaust valves
Inlet Valve reference Diameter 45.5 mm
Inlet valve opening timing: 10 degrees before TDC
Inlet valve closing timing: 60 degrees after BDC
Inlet valve lift (maximum) 4.2 mm
Exhaust valve reference diameter 37.5 mm
Exhaust valve opening timing: 60 degrees before BDC
Exhaust valve closing timing: 20 degrees after TDC
Exhaust valve Lift (maximum) 5 mm
Type of Injection: direct injection
Nozzle hole diameter 0.3 mm
Number of holes nozzle – 6
Nozzle discharge coefficient - 0.8
TDC clearance height: 3mm

For both the intake and exhaust valves, VVT is acquired by either advancing or by retarding the time of opening and closing. Controlling of the engine valve events are expressed in

seconds (time domain) and not in degrees of crank angle. Variations in intake and exhaust valve timings are described in the following.

2.4.1. Early Intake Valve Opening (EIVO)

Opening of the intake valve is the beginning of the induction stroke as well as the start of the valve overlap period. For a conventional C.I. engine, the opening of the intake valve occurs at around 20 degrees before TDC. In the case of EIVO, the intake valve opens 50 degrees earlier with respect to the conventional engine. By EIVO, the duration of the valve overlap period increases and thus the amount of backflow also increases during this period, as shown in fig. 2.31a.

Opening of the intake valve well before the end of the exhaust stroke results in an increase in the duration of the valve overlap. Some amount of burnt gases will go back into the intake manifold because of the cylinder intake manifold pressure gradient [32]. This backflow could be used for internal EGR, which is helpful for the reduction of NOx.

EIVO allows the exhaust gases to be in contact with the low-pressure intake system for a longer period of time. Thus, the manifold exhaust gases are recycled back into the cylinder at a lower temperature, which helps to reduce the formation of NOx. Because of EIVO some of the exhaust gases goes back into the intake manifold and thereby reduces the pumping losses, as shown in fig. 2.39a during the suction stroke.

According to Siewert [32], early opening of the exhaust valve increases fuel consumption, HC and CO, but reduces NOx. One of the reasons for this is because the fresh air gets diluted

with exhaust gases, which decreases the combustion temperature. Also because of air dilution, the strength of the mixture reduces and results in higher fuel consumption.

2.4.2. Late Intake Valve Opening (LIVO)

Late opening of the intake valve is obtained by opening the inlet valve 50 degrees later with respect to a conventional engine. LIVO avoids partial or full valve overlap, which results in very low or no backflow to occur during this period, as shown in fig. 2.32a.

Late opening of the intake valve tends to cause no flow connection between the cylinder and the intake manifold unless there is a pressure gradient between them. Further delay in the LIVC actually causes the cylinder pressure to dip momentarily below the intake manifold pressure [6]. The pumping losses will be increased, as shown in fig.2.39b, because of the greatly reduced cylinder pressure in the first part of the intake stroke.

Because of late intake valve opening air is brought into the cylinder with high velocity during the remaining suction stroke. This high velocity creates turbulence for the air, which assists for good combustion, and is considered as a good technique to reduce unburned hydrocarbons (UBHC) emissions.

2.4.3. Early Intake Valve Closing (EIVC)

The closing of the inlet valve represents the end of the intake stroke and the start of the compression stroke. For the conventional C.I. engine, the inlet valve closes at around 60 degrees after BDC during the compression stroke. In the case of EIVC, early intake valve closing is obtained by the closing of the intake valve 50 degrees earlier with respect to the conventional engine.

Due to early closing of the inlet valve, backflow during the compression stroke can be reduced or avoided, as shown in fig. 2.33 a. In this case pumping losses are lower, as shown in fig. 2.39c. EIVC reduces the amount of air admitted inside the engine cylinder and thereby reduces the work (or pumping loss) required for admitting this limited air and reduces the NOx emissions.

2.4.4. Late Intake Valve Closing (LIVC)

In this case, late intake valve closing is obtained by closing the inlet valve 50 degrees later with respect to a conventional engine. Due to delay in closing of the intake valve towards the end of the compression stroke, some of the air-fuel mass flows back into the intake manifold, as shown in fig. 2.34a. The amount of backflow is more when compared to the conventional engine.

Although there was no change made in the exhaust valve timing, LIVC still produces significant effects on the exhaust gas dynamics because of the air-fuel mass backflow, due to pressure gradient, which results in less air-fuel mass left for combustion. This results in less burnt gases produced after combustion, as shown in fig. 2.34b.

The pumping losses are lower, as shown in fig. 2.39d, because the vacuum created in the LIVC engine during the suction of air is not as low as in the conventional engine. The peak cylinder pressure is less, as shown in fig. 2.39d, with respect to a conventional engine. Because of the backflow of air during the compression stroke, combustion temperature and pressure will reduce, which results in lower NOx emissions.

2.4.5. Early Exhaust Valve Opening (EEVO)

For a conventional C.I. engine, opening of the exhaust valve takes place at around 60 degrees before BDC. To obtain EEVO, the exhaust valve opens 50 degrees earlier than normal. EEVO occurs well before the end of the expansion stroke. This early opening of the valve provides better scavenging for the burned gases, but it causes a reduction in the expansion work, as shown in fig. 2.39e, that reduces the power output of the engine. Therefore, it is detrimental to open the exhaust valve too early. However, there would be a reduction in the pumping work, as shown in fig. 2.39e, required to evacuate the cylinder after the piston passes through BDC. This is due to the decrease in the mass of exhaust gas during the exhaust stroke. This reduction in mass would require less force to expel this mass out of the cylinder. The quantity of mass flow rate during the exhaust stroke is less, as shown in fig. 2.34b, with respect to a conventional engine.

Early exhaust valve opening results in an increase of exhaust hydrocarbons and CO because the oxidation process has been curtailed by early opening of the valve. Because of curtailing the combustion process, maximum combustion temperature decreases, which results in the reduction of NOx.

2.4.6. Late Exhaust Valve Opening (LEVO)

To obtain LEVO, the exhaust valve is opened 50 degrees later than normal. In this case, the majority of work shifts to the exhaust stroke as shown in fig. 2.35b. Due to this work shift, a more complete blowdown takes place and greater expansion work results during the power stroke, as shown in fig. 2.39f. LEVO requires more pumping work, as shown in fig. 2.39f, because the majority of work is shifted to the exhaust stroke to expel the burnt gases from the

engine cylinder. Also, exhaust pumping work increases because of the very late opening of the exhaust valve, which restricts the exhaust gases from expelling out of the cylinder while the piston is still doing expansion work. Because of LEVO, the pressure inside the cylinder increases during the time of exhaust valve closing. Thus, there is an increase of retained residual gases inside the cylinder, which results in higher combustion time and exhaust temperatures during the exhaust valve opening, which may assist to reduce the unburned hydrocarbons (UBHC).

2.4.7. Early Exhaust Valve Closing (EEVC)

In conventional C.I. engines, the closing of the exhaust valve takes place at around 20 degrees after TDC. It is the end of the exhaust stroke as well as the end of the valve overlap period. To obtain EEVC the exhaust valve closes 50 degrees earlier with respect to a conventional engine. EEVC prevents the partial or total overlap, which reduces or prevents the backflow as show in fig. 2.37b. Because of EEVC, the total amount of burnt gases may not escape out of the engine cylinder during the exhaust stroke. In fig. 2.37b, it is noticeable that the exhaust stroke is completed before TDC by closing the exhaust valve earlier. During the end portion of EEVC, the exhaust gases gets a smaller area to flow out of the cylinder through the exhaust valve opening. This flow restriction may increase the pumping losses, as shown in fig. 2.39g. Because of EEVC, exhaust gases are not totally scavenged out of the cylinder, which causes dilution of the fresh air- fuel mixture. This results in the reduction of NOx and indicated thermal efficiency and increase in fuel consumption.

2.4.8. Late Exhaust Valve Closing (LEVC)

To obtain LEVC, the exhaust valve is closed 50 degrees later than normal. In this case, the period of the valve overlap increases. Due to this increase in valve overlap, during the intake stroke some amount of burnt gases from the exhaust manifold flows back into the cylinder, as shown in fig. 2.38b. This backflow may be called as EGR, which is useful to reduce NOx. Pumping losses are lower as shown in fig. 2.39h.

Because of mechanical constraints, retarding of exhaust valve closing (LEVC) is very marginal in view of the piston clashing with the valve. Similarly, advancing of the intake valve (EIVO) is restricted because of this mechanical constraint. This is one of the reasons why the application of VVT is restricted on diesel engines.

At high speeds more valve overlap is beneficial for scavenging of the residual gases, which gives higher engine power output. But more valve overlap is detrimental for idle quality due to the larger amount of residual gases, which flows back into the intake manifold. Backflow can be prevented or reduced by reducing the overlap, which results in an increase in torque at idle speed (low speed), but this will reduce the volumetric efficiency at higher speeds.

2.5 Summary

In this section the conventional and variable valve timing events, and their effects on gasoline and diesel engines, were discussed in detail. The effects of various valve timing strategies on the P-V cycle and exhaust emissions were analyzed by using the one dimensional flow simulation software, namely, GT-Power.

Engine model simulation and analysis were performed for:

1. Cam operated dependent actuator for four stroke gasoline engine.
2. Solenoid operated independent actuator for four stroke gasoline engine.
3. Solenoid operated independent actuator for four stroke diesel engine.

From the engine model simulation and analysis of the above three cases, it was concluded that the intake valve strategies are useful for reducing pumping losses for gasoline engines, while exhaust valve strategies are useful for reducing the exhaust emission for both gasoline and diesel engines.

In the next chapter the solenoid operated valve actuation is proposed to obtain variable valve timing of the engine. The iron core of a solenoid is replaced by a permanent magnet to obtain bidirectional motion. The next chapter emphasizes on the description and modeling of the permanent magnet core solenoid system.

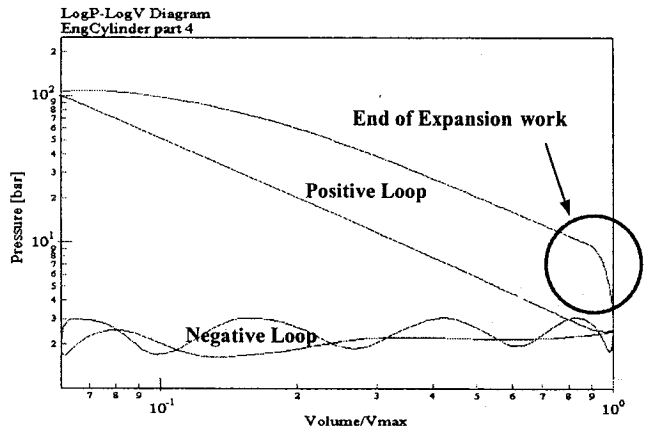

Fig. 2.29 Log-P/Log-V Diagram for Conventional CI Engine

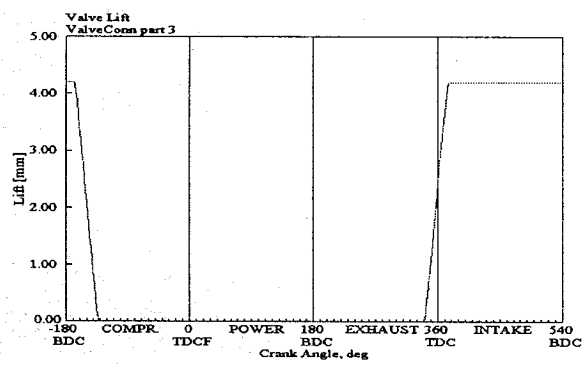

a. Intake valve lift and phase for conventional CI engine

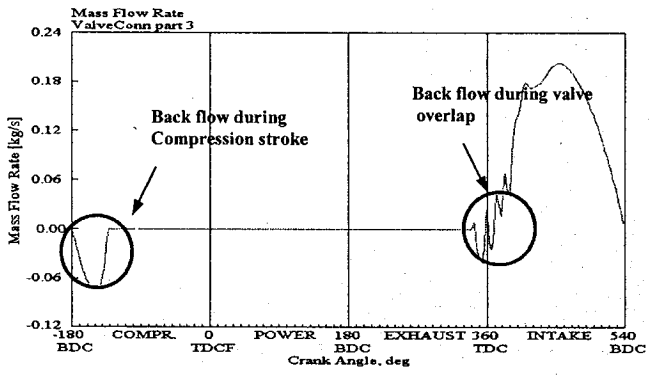

b. Flow of air mass through the intake valve into an engine cylinder. Possible backflow can occur during valve overlap and closing time of intake valve after BDC.

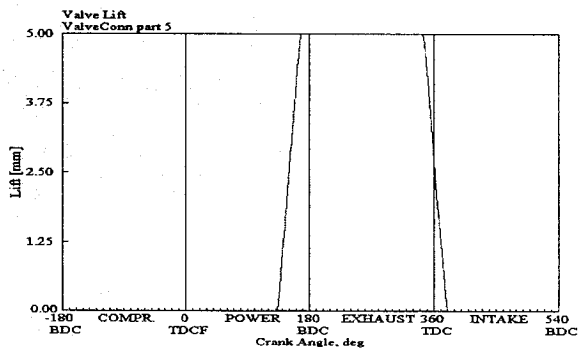

c. Exhaust valve lift and phase for conventional CI engine

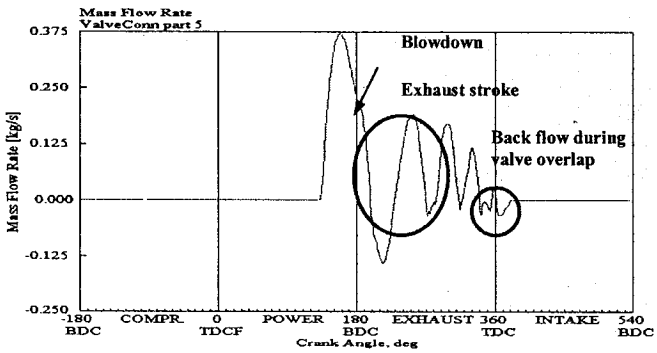

d. Flow of exhaust mass through the exhaust valve out of an engine cylinder. Possible backflow can occur during valve overlap.

Fig. 2.30 For conventional CI engine

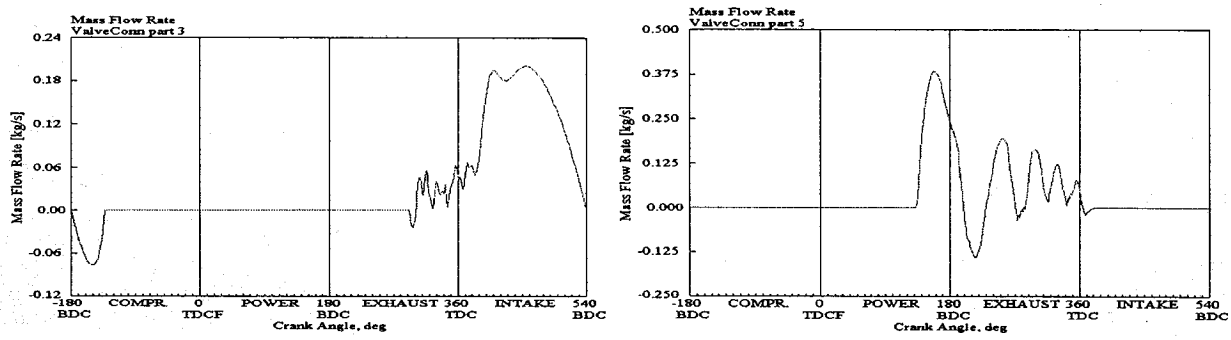

a) Flow though intake valve b) Flow through exhaust valve

Fig. 2.31 Early Intake Valve Opening (EIVO)

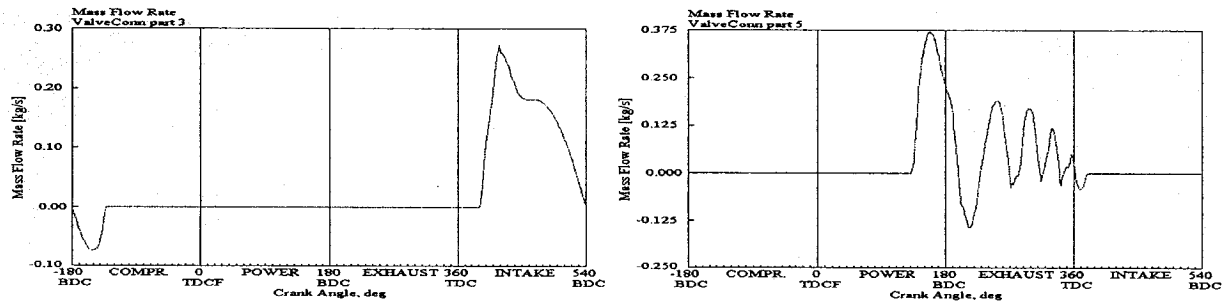

a) Flow though intake valve b) Flow through exhaust valve

Fig. 2.32 Late Intake Valve Opening (LIVO)

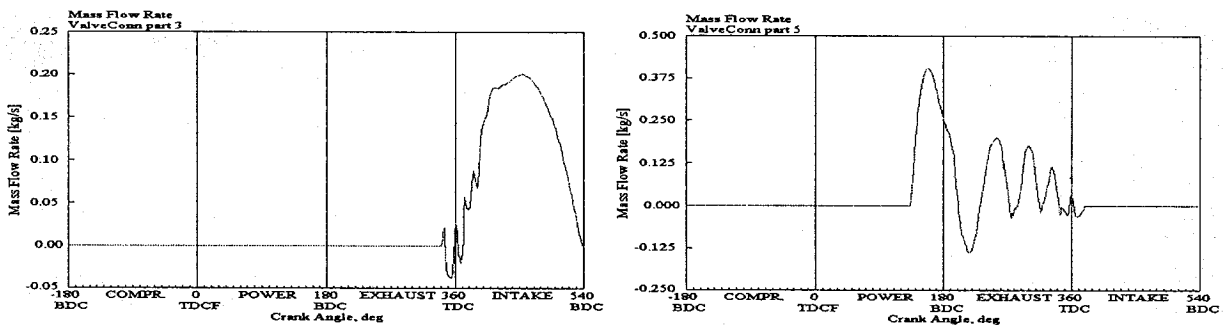

a) Flow though intake valve b) Flow through exhaust valve

Fig. 2.33 Early Intake Valve Closing (EIVC)

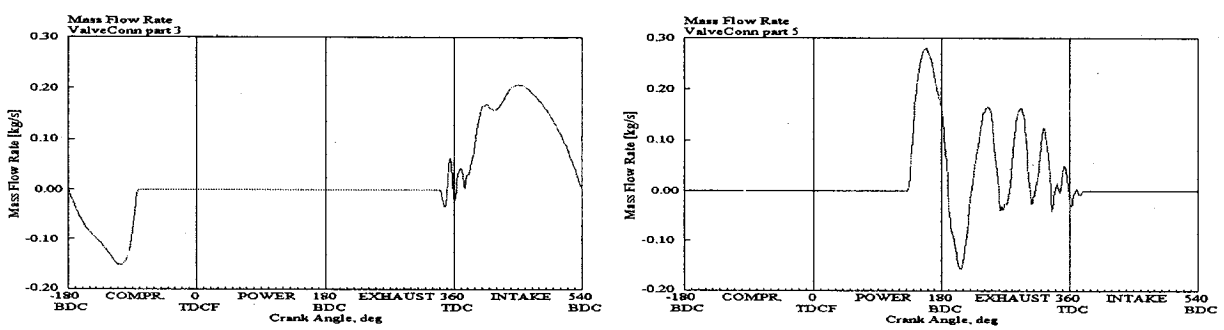

a) Flow though intake valve b) Flow through exhaust valve

Fig. 2.34 Late Intake Valve Closing (LIVC)

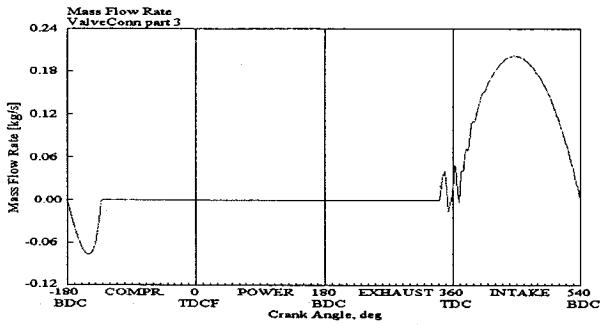

a) Flow though intake valve

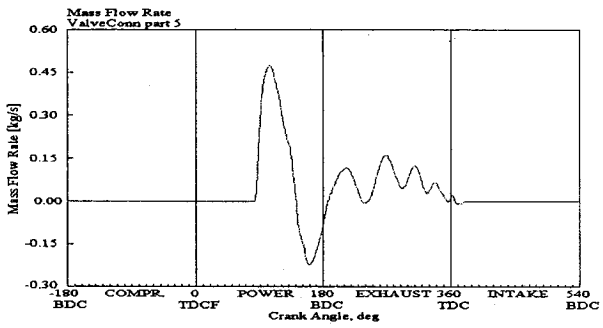

b) Flow through exhaust valve

Fig. 2.35 Early Exhaust Valve Opening (EEVO)

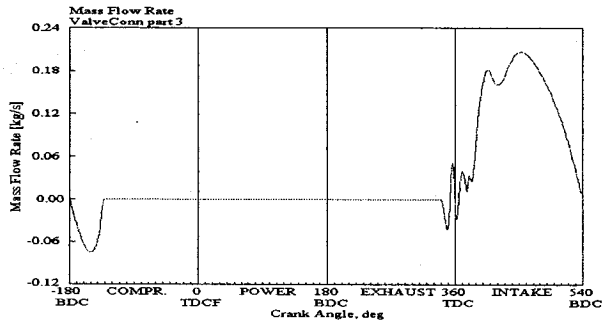

a) Flow though intake valve

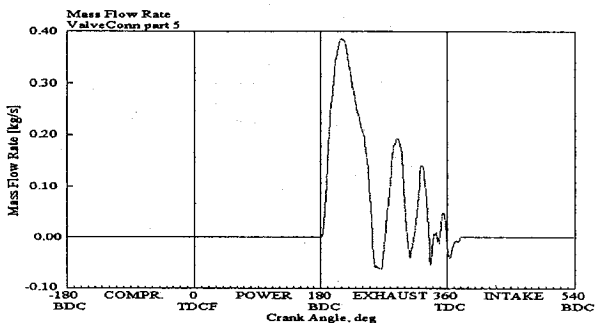

b) Flow through exhaust valve

Fig. 2.36 Late Exhaust Valve Opening (LEVO)

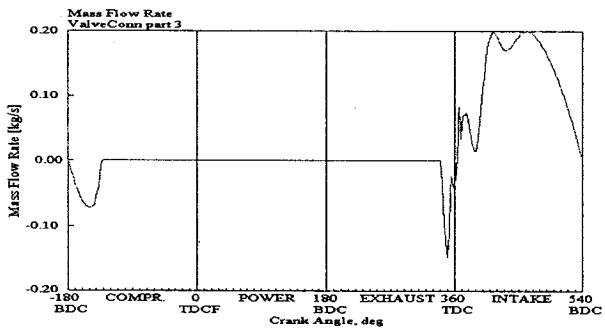

a) Flow though intake valve

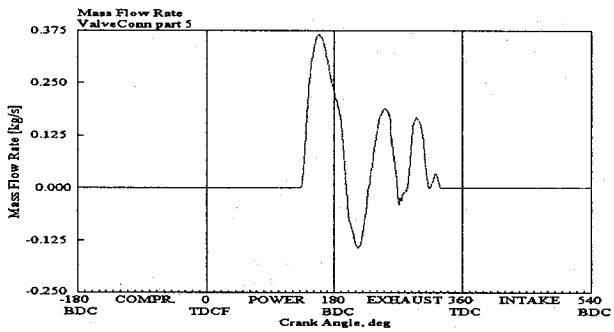

b) Flow through exhaust valve

Fig. 2.37 Early Exhaust Valve Closing (EEVC)

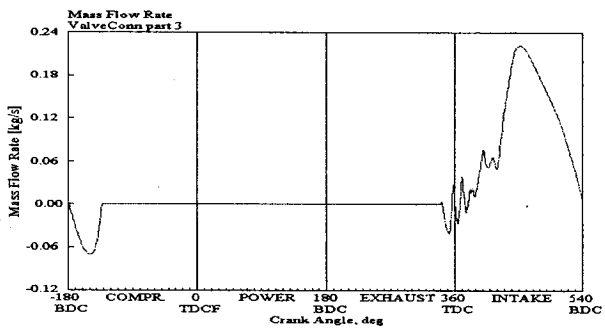

a) Flow though intake valve

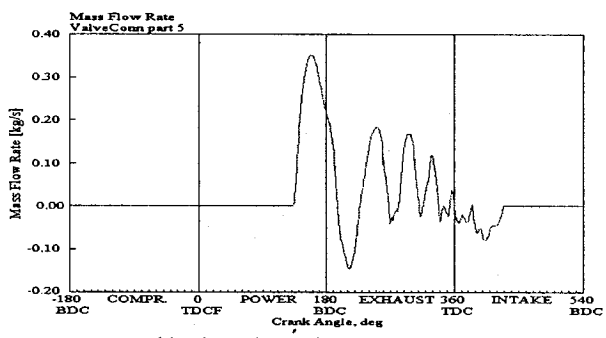

b) Flow through exhaust valve

Fig.2.38 Late Exhaust Valve Closing (LEVC)

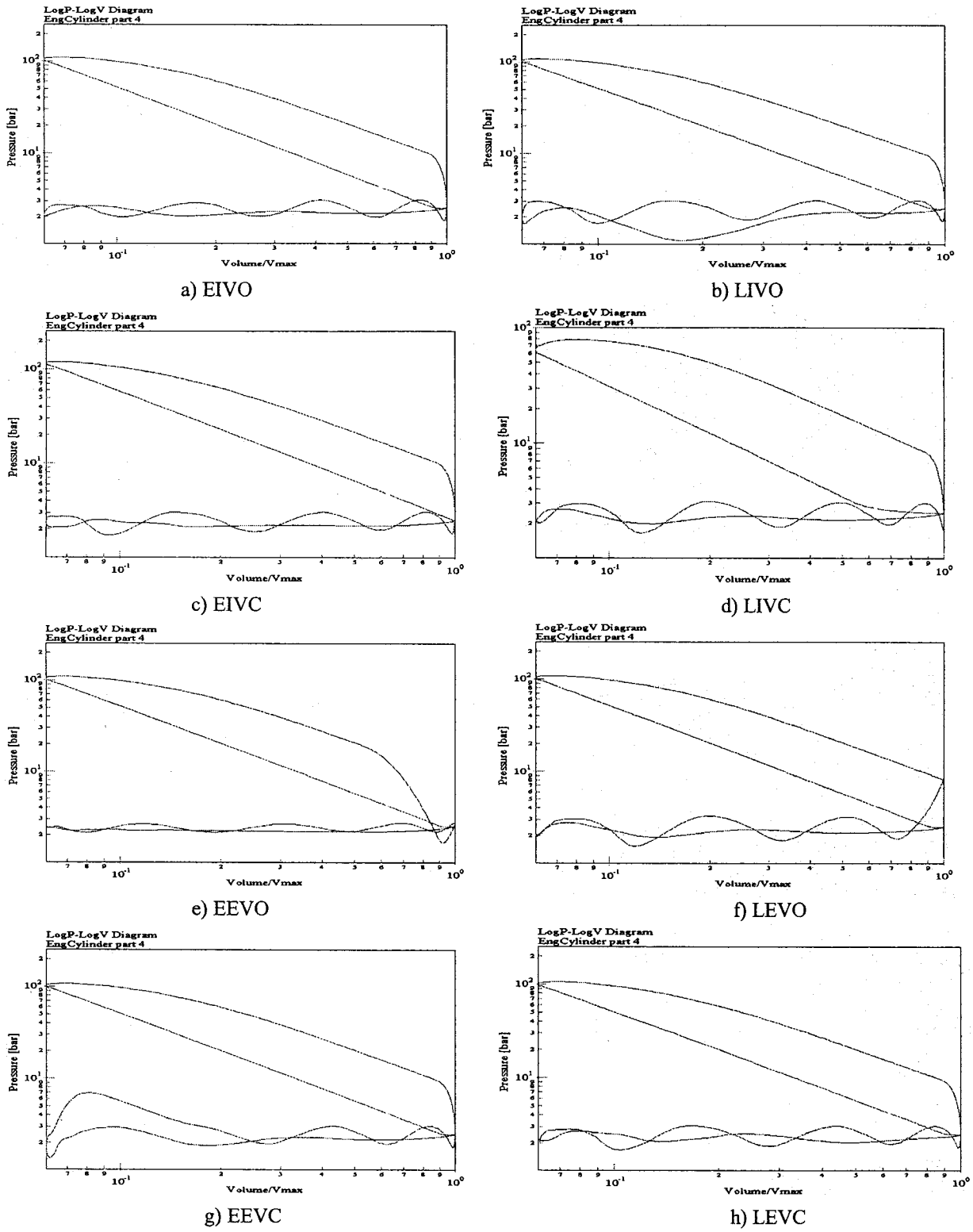

Fig. 2.39 Log-P/Log-V diagram for variable valve timed CI engine

CHAPTER 3

PERMANENT MAGNET CORE SOLENOID SYSTEM DESCRIPTION AND MODELLING

3.1 Introduction

Electromagnet valve actuators (EMVA) are recently receiving much attention from engine manufacturers due to their flexibility, fast response and ease in control. Current applications in EMVA's are basically ON/OFF devices, while more sophisticated research work is under going, as for example in the current control to reduce the valve impact forces. The electromagnet valve actuator proposed in this research is novel in that one single solenoid with a permanent magnet core will allow bi-direction motion of a valve stem attached to the core. In addition, with proper feedback control, the valve can be commanded to move to any desired position for true variable valve actuation and timing. As well, controlling the current applied to the permanent magnet, the valve can be decelerated to reduce impact forces upon its seat to reduce wear and noise. Even when the solenoid is not energized, the force of attraction provided by the permanent magnet can be used to latch the valve in its closed position.

In this chapter, the governing equations describing the solenoid and the permanent magnet, and their interactions, are derived. In the following chapter, experimental results are compared to show the validity of the equation derived from this chapter.

3.2 Characteristics of Solenoid Actuator and Permanent Magnet

An existing commercial linear solenoid actuator, Lisk Model L12-B-M3-L-E4-12-P-24, rated at 420 W, 24 V nominal, for 10% pulse duty cycle (34 sec. maximum ON time), was selected

for analysis, and its cross sectional view is shown in fig. 3.1. The solenoid, as for all electromagnets, can only produce pulling forces when electrically actuated.

The carbon steel moving core of the solenoid is replaced by a high energy rare earth permanent magnet, Neodymium-Iron-Boron (NdFeB), specially manufactured to the same shape and dimensions as the original core. The NdFeB permanent magnet was selected because it has the highest available energy among the other permanent magnetic materials with a large value of coercive force (defined as the field strength in amperes/meter required to demagnetize the permanent magnet to zero flux density). In particular, this material has linear demagnetization characteristics throughout the entire second quadrant in its magnetic characteristics curve of flux density versus applied field strength (ie: *BH* hysteresis curve). This means that recoil lines of the NdFeB magnet in the operating region are straight-lines with a slope of $1.06\mu_0$ [57] (where μ_0 is the permeability of vacuum), which provides a simplification to its modeling and use. Other types of permanent magnets having nonlinear second quadrant characteristics require a more complicated system model.

The NdFeB permanent magnet core is manufactured by Dexter Magnetic Technologies. The grade of the material is ND48 with the maximum energy product of $BH_{\max} = 380kJ/m^3$; the remanent magnetization of $B_r = 1.35T$ (ie: flux density at zero applied field strength); the coercive force of $H_c = 820kA/m$, and the maximum operating temperature of 150° C.

3.3 Magnetic Circuit Analysis of Permanent Magnet Core Solenoid

Figure 3.1 shows the sectional view of the coil-wound cylindrical solenoid. The pole end of the solenoid and the facing moving carbon steel core are conical in shape to increase the electromagnetic force of attraction since force is directly proportional to the square of magnetic flux and area. For a solenoid with a steel core, the electromagnetic force always tends to reduce the air gap and is independent of the applied current (and resulting flux) direction. To achieve bi-directional core motion, the steel core is replaced by a permanent magnet of similar shape to that of the original core. Depending on the direction of the applied current, the permanent magnet core will be either pushed away from the solenoid pole end, or will be attracted to it. The derivation of push and pull forces will be described in Section 3.4.

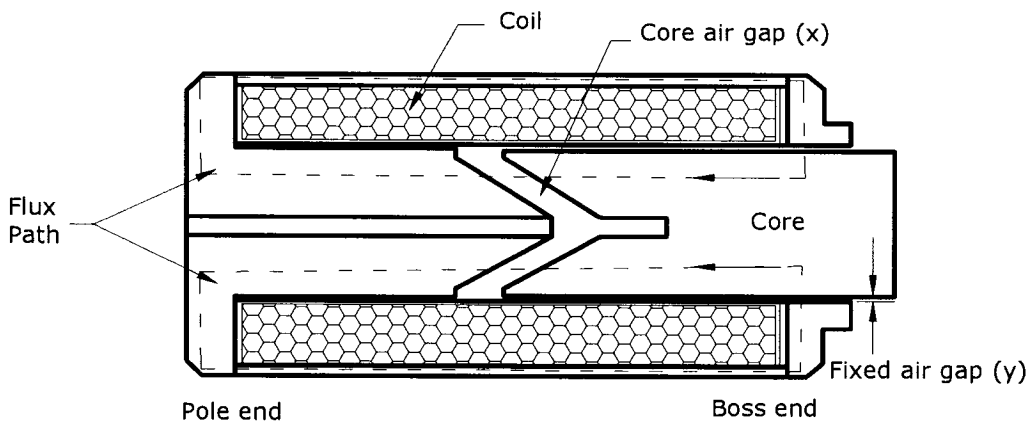

Fig. 3.1. Magnetic circuit for solenoid

With reference to fig. 3.1 for the solenoid with a moving permanent magnet core, the path of the magnetic flux passes through the outer metal casing enclosing the coil windings, through the solenoid metal conical pole end, across the variable air gap and through the moving permanent magnet, through the fixed boss end air gap, and the magnetic circuit is completed

by the flux returning to the casing through the metal boss end. The total reluctance R_t for the magnetic circuit can be expressed as the sum of the individual reluctances in series, given by:

$$R_t = R_m + \frac{l_x}{\mu_0 A_x} + \frac{l_y}{\mu_0 A_y} + \frac{l_C}{\mu_C A_C} \tag{3.1}$$

where, R_m represents the reluctance through all the metallic material, l_x is the length and A_x is the area of the air gap reluctance due to the core displacement, l_y is the length and A_y is the area of the boss end air gap reluctance, and l_C is the length and A_C is the area of the magnet core reluctance. Because the permeability of the permanent magnet is $\mu_C = 1.06\mu_0$ [57], its value is taken to be the same as that of air μ_0. As a result, the magnetic flux passes through a large length consisting of permeability μ_0, and hence the reluctance due to the air gaps plus magnet core are much larger as compared to that of metal, and thus reluctance R_m can be neglected. In addition, since the permeability of the pole end air gap is the same as that of the permanent magnet, there is no longer a variable reluctance due to l_x. Thus, the total reluctance may be considered as a constant and is independent of the core motion, given by:

$$R_t = \frac{l_y}{\mu_0 A_y} + \frac{l_C}{\mu_0 A_C} \tag{3.2}$$

where l_C is the constant length from the solenoid pole end to the boss end.

For the magnetic circuit of fig. 3.1, the magnetomotive force (mmf) is related to the magnetic flux through the total reluctance given by equation (3.2), as:

$$Ni = \phi\left(\frac{l_y}{\mu_0 A_y} + \frac{l_C}{\mu_0 A_C}\right) \tag{3.3}$$

where, N is the total number of coil windings, i is the applied current, and ϕ is the magnetic flux.

3.4 Mathematical Model of Solenoid Transient Characteristics

The equivalent circuit for the solenoid coil [58, 59] with a steel moving core is shown in fig. 3.2. The variable resistance R_C across the coil inductance accounts for eddy current losses due to the solenoid metal, which is ohmic in nature. By considering eddy current losses, hysteresis is introduced into the magnetization curve of the solenoid model. The leakage inductance L_i in series with the coil accounts for flux leakages, which tends to increase the system overall inductance. The series resistor R_i represents the internal resistance of the coil wire. The number N of coil windings is applied in order to obtain the resistance R_i for rated power. $L(\phi, x)$ represents the coil inductance, which is a function of the magnetic flux ϕ and core displacement producing air gap x. The current supplied from the source is termed the "exciting current" i_e, while the current through the coil that produces the magnetic flux is termed the "magnetizing current" i_m. The difference, $i_e - i_m$, is the core-loss component of current.

In general, the eddy current loss component R_C and the leakage inductance L_i are unknown, and values are assumed so that experimental values of current and magnetic force can agree with analysis. In the following model for the solenoid with a moving permanent magnet core, these two components are neglected, and hence the governing equations are derived from the simplified equivalent circuit.

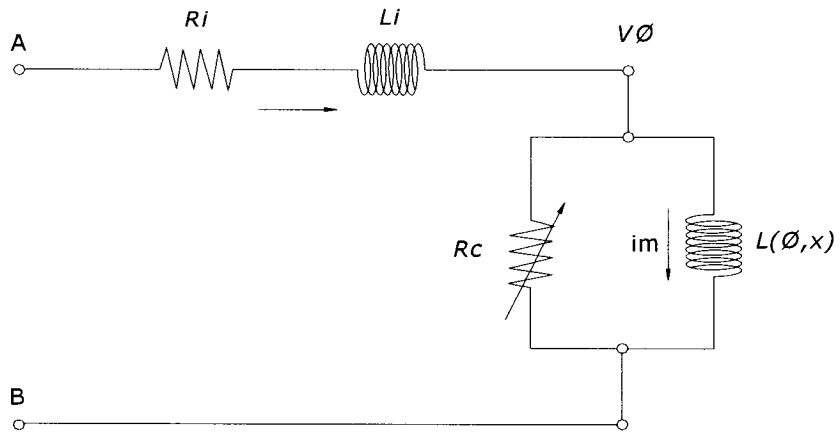

Fig . 3.2. Equivalent circuit for solenoid

The applied voltage V across the solenoid terminals AB is:

$$V = iR_i + V_\phi \tag{3.4}$$

where the induced voltage across the coil due to the changes from the magnetic flux, based on Faraday's law, is:

$$V_\phi = N\frac{d\phi}{dt} \tag{3.5}$$

Taking the derivative of equation (3.3) with respect to time, and substituting equation (3.5) into (3.4), results in:

$$V = iR + L\frac{di}{dt} \tag{3.6}$$

where the coil inductance L is constant and is given by:

$$L = \frac{N^2}{R_t} = \frac{N^2}{\frac{1}{\mu_0}\left(\frac{l_y}{A_y} + \frac{l_C}{A_O}\right)} \tag{3.7}$$

It should be noted that once the current has been determined as a result of the applied voltage, as given by equation (3.6), the magnet flux can then be determined from equation (3.3).

3.5 Force Exerted by Cylindrical Permanent Magnet

According to the Biot-Savart's law [60], the value of the magnetic flux density B_z at a distance l_x from the end of a cylindrical magnet of length l_m and radius r, can be evaluated from:

$$B_z = \frac{B_r}{2}\left[\frac{l_x + l_m}{\sqrt{(l_x + l_m)^2 + r^2}} - \frac{l_x}{\sqrt{l_x^{\,2} + r^2}}\right] \tag{3.8}$$

where B_r is the residual flux density of the permanent magnet. Although the actual shape of the permanent magnet that is used has a female conical end, as shown in fig. 3.3, equation (3.8) is assumed to still apply.

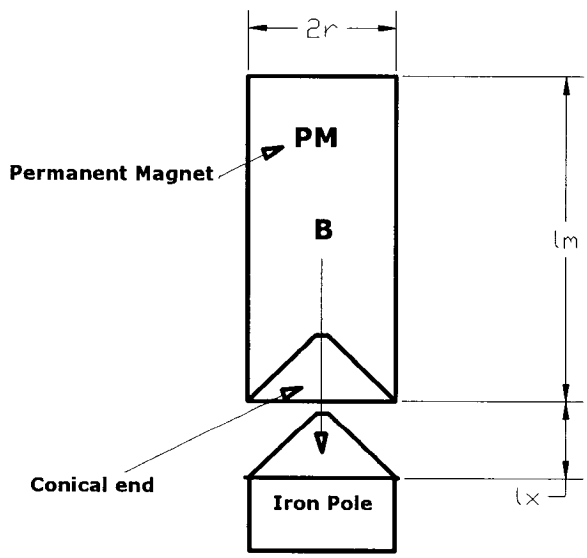

Fig. 3.3. Permanent magnet with conical pole face

Therefore, the force of attraction exerted by the magnet to ferromagnetic material can be calculated by [61]:

$$F_{mag} = \frac{\phi^2}{2\mu_0 A} \tag{3.9}$$

Since the flux density is defined as flux per area, $B_z = \phi / A$, equation (3.9) can be equivalently written as:

$$F_{mag} = \frac{B_z{}^2 A}{2\mu_0} \tag{3.10}$$

where the magnet flux density B_z of the permanent magnet is determined from equation (3.8).

3.6 Force due to Solenoid Coil Incorporating Cylindrical Permanent Magnet

When a permanent magnet is placed within an externally applied magnetic field, the total force acting on the permanent magnet is given by [62]:

$$F = \int (-\nabla \bullet M) B_0 dV + \int n \bullet M B_0 dA \tag{3.11}$$

where, B_0 is the external magnetic field due to all sources except that from the permanent magnet itself, dV is the element of permanent magnet volume in the field, dA is the area of the element through which the field passes, M is the magnetization of the permanent magnet. $-\nabla \bullet M$ is the magnetic volume charge density, and $n \bullet M$ is magnetic surface charge density.

The magnetization M of the cylindrical permanent magnet is considered uniform along its cylindrical axis. For a permanent magnet inside a cylindrical solenoid, the external field B_0

is acting on the permanent magnet along its cylindrical axis. In this case, the magnetic volume and surface charge densities are [63]:

$$-\nabla \bullet M = 0 \tag{3.12}$$

$$n \bullet M = M \tag{3.13}$$

By substituting equation (3.12) and (3.13) into (3.11), the coil external magnetic field produces a force on the permanent magnet, given as:

$$F_{(i,x)} = \int_A MB_{coli}(i,x)dA$$

$$= MA\left(B_{coil}(i,x)\big|_{x1} - B_{coil}(i,x)\big|_{x2}\right) \tag{3.14}$$

where, $B_{coil}(i,x)\big|_{x1}$ and $B_{coil}(i,x)\big|_{x2}$ are, respectively, the magnetic fields due to the coil at the two ends of the permanent magnet. The permanent magnet has one end inside and very much close to the center of the solenoid, and the magnetic field around the center of the solenoid is considered uniform and equal in magnitude. The other end of the permanent magnet is outside of the solenoid boss end, where the field $B_{coil}(i,x)\big|_{x2}$ is considered zero. Thus, the magnetic field produces a force on the permanent magnet, by the simplification of equation (3.14) to:

$$F_{coil}(i) = MAB_{coil}(i) \tag{3.15}$$

which is independent of its end position x because of the uniformity of the external magnet flux in the longitudinal central vicinity of the solenoid.

To support this fact, fig. 3.4 shows a long uniform solenoid situated in air with NI amp-turns and a length L. The flux density B at the center is nearly constant while it gradually decreases near its two ends [64].

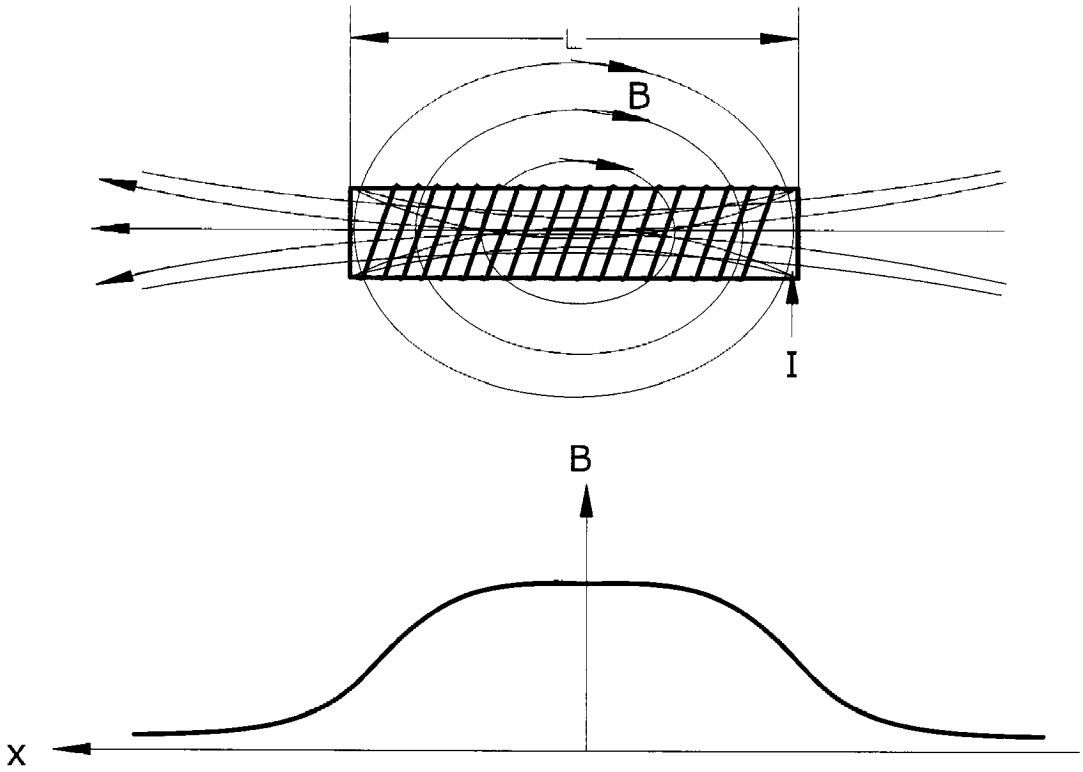

Fig. 3.4. Magnetic field along the longitudinal axis of an air solenoid

3.7 Permanent Magnet Characteristics

Until recently, the proper utilization of hard magnetic materials has been considered with a bit of mystery, poor understanding, and its use has been accomplished largely as a result of trial-and-error methods. These impressions are gradually being voided as the modern magnet materials receive greater attention, and from many applications it becomes evident that

magnet performance is quite predictable. There are many characteristics of a permanent magnet that need to be considered in its design for actuators. Its shape contains information on how the magnet will behave under static and dynamic operating conditions, and in this sense the material characteristic will constrain what can be achieved in the actuator mechanism.

The B versus H (flux density versus magnetomotive force) curve of any permanent magnet has some portions which are almost linear, while other portions of its characteristics are highly nonlinear, as shown in fig. 3.5. The shapes of these B versus H curve and its demagnetization portion (second quadrant) give considerable ideas to researchers about the suitability of the material for a given application. From fig. 3.5, Hm along the horizontal axis is defined as the magnetic field intensity, Bm along the vertical axis is defined as the magnetic field density, Br is the residual magnetism, Hc is the coercive force, and BsHs is the saturation point.

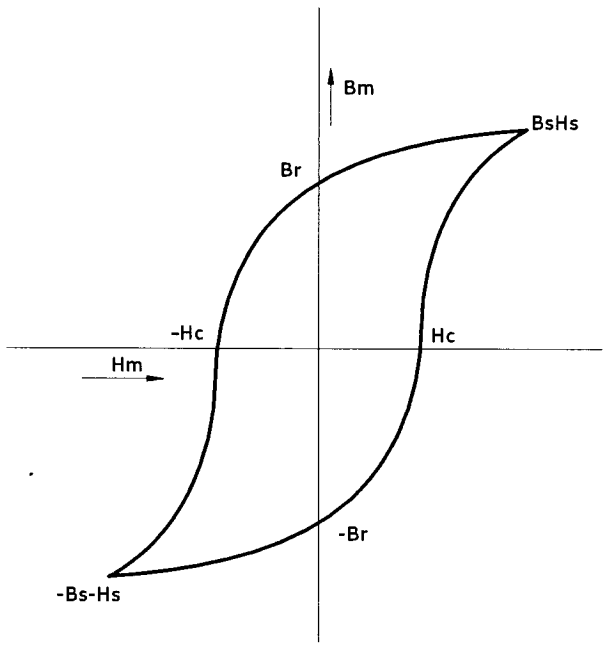

Fig. 3.5. B-H curve

The flux for the combination of a solenoid and a permanent magnet is divided into two parts; one is flux due to the solenoid coil and the other is due to the permanent magnet. When an external field is applied to a permanent magnet, the magnetic flux density is given by:

$$B_m = \mu_0 (H_m + M) \tag{3.16}$$

where, H_m is the external magnetic field strength, μ_0 is the permeability of air, and M is the magnetization of the permanent magnet. Magnetization M of the magnet is considered as a constant as demagnetization lines are straight in the operating region. Also, since the magnet is considered as uniformly magnetized, the remanent magnetization (or residual magnetism) B_r at $H_m = 0$, can be written as:

$$B_r = \mu_0 M \tag{3.17}$$

3.8 Total Force of Attraction

The total force of attraction created by the solenoid producing an external field which acts on the permanent magnet, and by the permanent magnet attraction to the solenoid metal core, can be expressed respectively, as:

$$F_{total} = F_{coil}(i) + F_{mag} \tag{3.18}$$

By the substitution of equations (3.15) and (3.10) into (3.18), the total force is:

$$F_{total} = MAB_{coil}(i) + \frac{B_x^2 A}{2\mu_0} \tag{3.19}$$

The above analysis assumes that the permanent magnet south-pole is within the external magnetic field traveling from left to right, with the solenoid metal core to the left of the permanent magnet.

3.9 Total Force of Repulsion

By changing the applied voltage polarity the current direction reverses, which in turn causes the coil flux to change direction. The external magnetic field now travels from right to left, which will tend to push the south-pole of the permanent magnet. The south-pole of the permanent magnetic will still attract the solenoid metal pole. Therefore, the total force of repulsion can be expressed as:

$$F_{total} = -F_{coil}(i) + F_{mag} \tag{3.20}$$

$$F_{total} = -MAB_{coil}(i) + \frac{B_x^2 A}{2\mu_0} \tag{3.21}$$

3.10 Summary

In this chapter the system of the solenoid incorporating a permanent magnet was described and modeled mathematically. It was noted that the force is not a function of the permanent magnet core displacement since the permeability of the permanent magnet is considered equal to that of air. In addition, to be independent of core displacement requires that the magnetic field along the longitudinal axis at the center of the solenoid be equal in magnitude. The total force of attraction or repulsion is dependent upon the direction of flux lines from the magnetic field created by the solenoid coil and permanent magnet.

In the next chapter; the experimental set up for transient force and current characteristic measurements are described. Also, the model simulation results are validated by comparing to those from experiments.

CHAPTER 4

EXPERIMENTAL SETUP AND COMPARISON BETWEEN TEST AND SIMULATION RESULTS FOR PERMANENT MAGNET CORE SOLENOID

4.1 Experimental Setup for Current and Force Transient Measurements

The experimental setup to measure the solenoid force and current transient characteristics at various fixed air gaps is shown in fig. 4.1. The test-stand consists of an aluminum cylinder housing the solenoid and piezoelectric load cell. The electrical solenoid sits on top of a brass T-pin which in turn is placed inside and sits on the brass holder. The T-pin is manufactured as one piece, consisting of a disk as its base and a pin at its center. The pin protrudes through a hole on the solenoid pole end so that the permanent magnet can sit on top of the pin. Various T-pins are manufactured with different pin lengths which determine the air gap length between the magnet and solenoid pole end. A brass cap is placed on top of the solenoid boss end and is threaded into the holder to secure the solenoid in the vertical position and to ensure that the T-pin provides a fixed air gap. The holder is made to stand vertically using a brass threaded rod which in turn is threaded into the base of the aluminum cylinder. A brass nut is used to lock the holder so that its position remains rigid, while a second nut solidly locks the assembly to the cylinder base. A brass cylindrical spacer sits on top of a brass disk spacer, which are placed on top of the permanent magnet. The length of the cylinder spacer is to avoid flux leakage from the solenoid and magnet because the load cell casing is made out of steel. A threaded rod through the cylinder housing is used to preload the load cell and solenoid assembly. Once the compression preload has been set by turning the threaded rod, it is then locked by a nut. By preloading the load cell, push and pull forces can be measured about the preload.

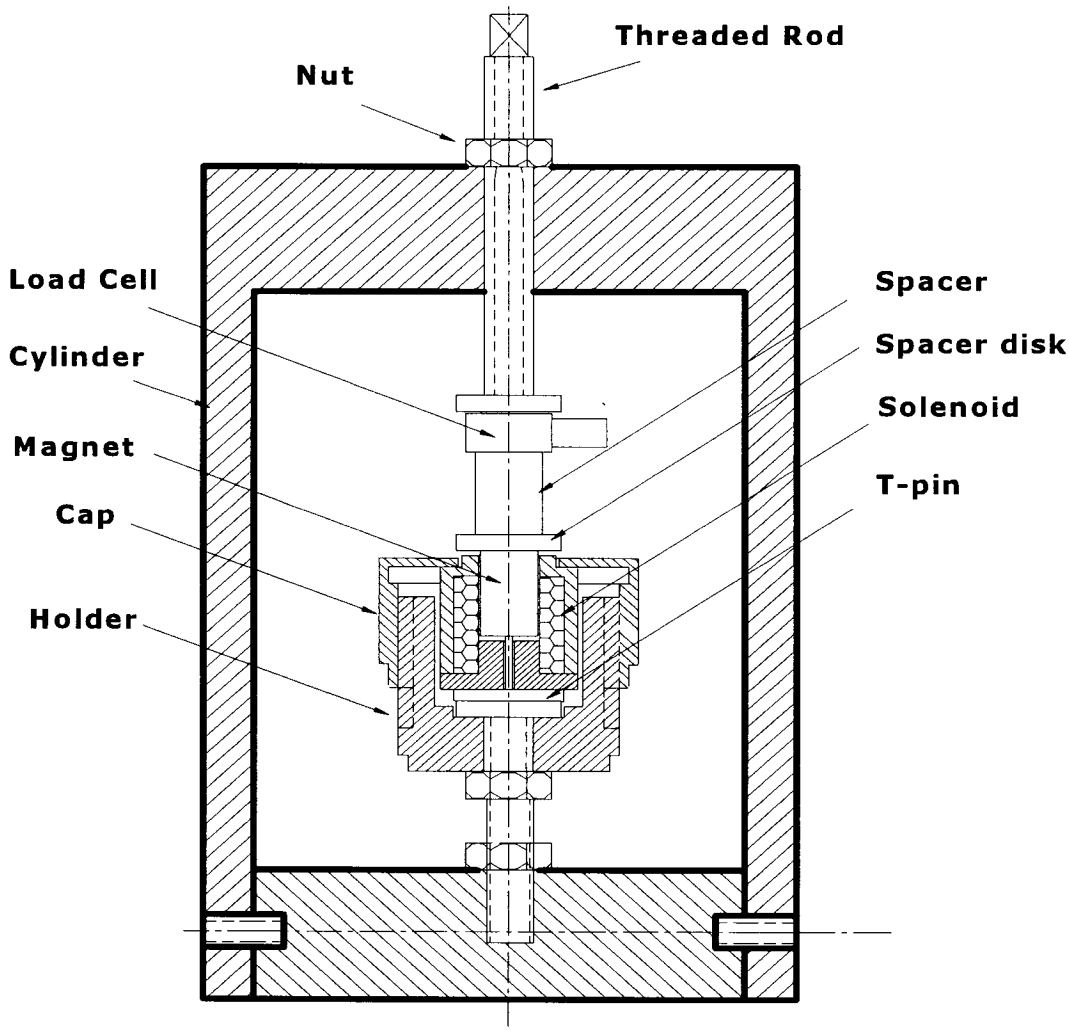

Fig. 4.1. Schematics of experimental fixture

Appendix A shows the calibration curve for the load cell. All component parts within the aluminum housing are made of brass to ensure that the electromagnet and permanent magnet magnetic flux are not disturbed. The walls of the cylindrical housing are made sufficiently thick so that the solenoid force does not produce any deflections on the housing and therefore all the solenoid force will be transmitted to the load cell.

Voltage supplies are connected in series to obtain solenoid coil input voltages of various values. The power supply is connected to one terminal of the solenoid coil, while the other terminal is connected to two power NMOS transistors in parallel. Two transistors are used to reduce the NMOS resistance while they are ON. Although the NMOS transistors only require a positive 6 V gate-to-source voltage to turn ON and zero voltage to turn OFF, a ±20 V (higher and lower) was used to speed up the transistor turn ON and to ensure the transistors are turned OFF. A flyback diode is connected across the coil to protect the two NMOS switches from positive voltage spikes.

A clamp-on meter around the solenoid coil terminal wire is used to measure the applied current through the coil. The output of the clamp-on meter is connected to the data acquisition port of LABVIEW. The wires from the piezoelectric load cell are connected to a charge amplifier, and in turn the wires of the amplifier are connected to a second data acquisition port of LABVIEW. After recording of the experimental data from LABVIEW, the data file is imported into MATLAB for filtering of the noisy signals.

4.2 Experimental Set-up to Measure Permanent Magnet Pulling Force

The experimental set-up to measure the pulling force contributed only by the permanent magnet at various air gaps is shown in fig. 4.2. The solenoid is placed inside the brass holder and is kept in the vertically aligned position by threading the brass cap onto the holder. A brass threaded rod is screwed into the bottom of the holder and is secured in position by a brass nut. The same rod with a fine pitch is threaded through the base of the test-stand where a graduated disk is attached. The piezoelectric load cell is placed on top of the test-stand

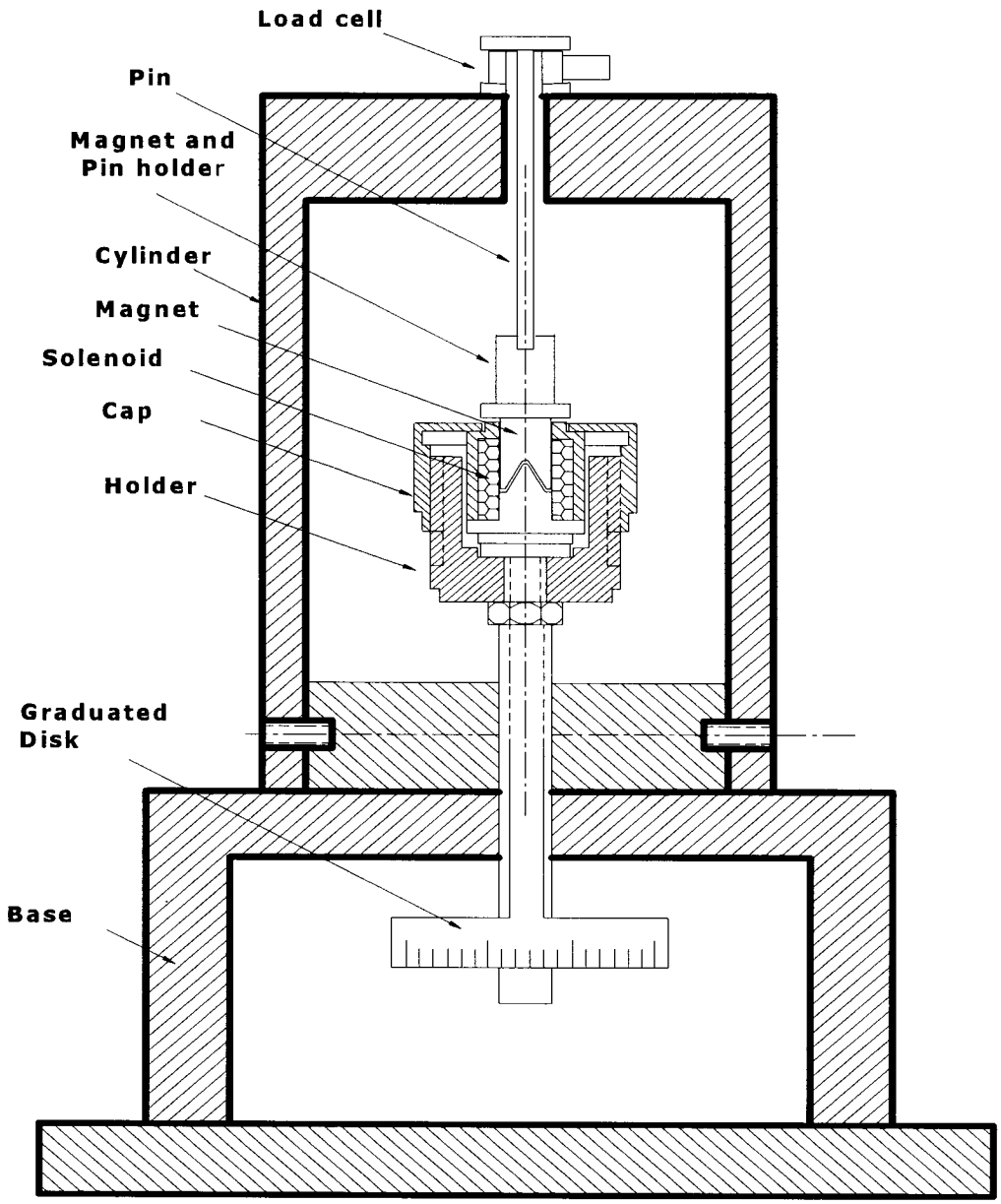

Fig. 4.2. Schematic of the fixture to measure permanent magnet force

housing, and a disk with a long pin attached sits on the load cell. Attached to the end of the long pin is the permanent magnet holder in which the magnet is inserted and is held in place by two side set-screws. To measure the force of attraction by the permanent magnet with respect to the solenoid pole end, the air-gap is first adjusted to 1.0 mm and the compression

force on the load cell is measured from an oscilloscope. By turning the graduated disk, the air gap is increased and various forces per air gap distances are recorded.

4.3 Test Measurements of Permanent Magnet Pulling Force

Figure 4.3 shows the experimental (dots) pulling force of the permanent magnet on the solenoid steel pole end with respect to different air gaps. The solid line represents the magnet pulling force as calculated from theory with respect to the magnetic flux determined from equation (3.8) and the force calculated from equation (3.10). The theoretical values are in good correlation with those from test results.

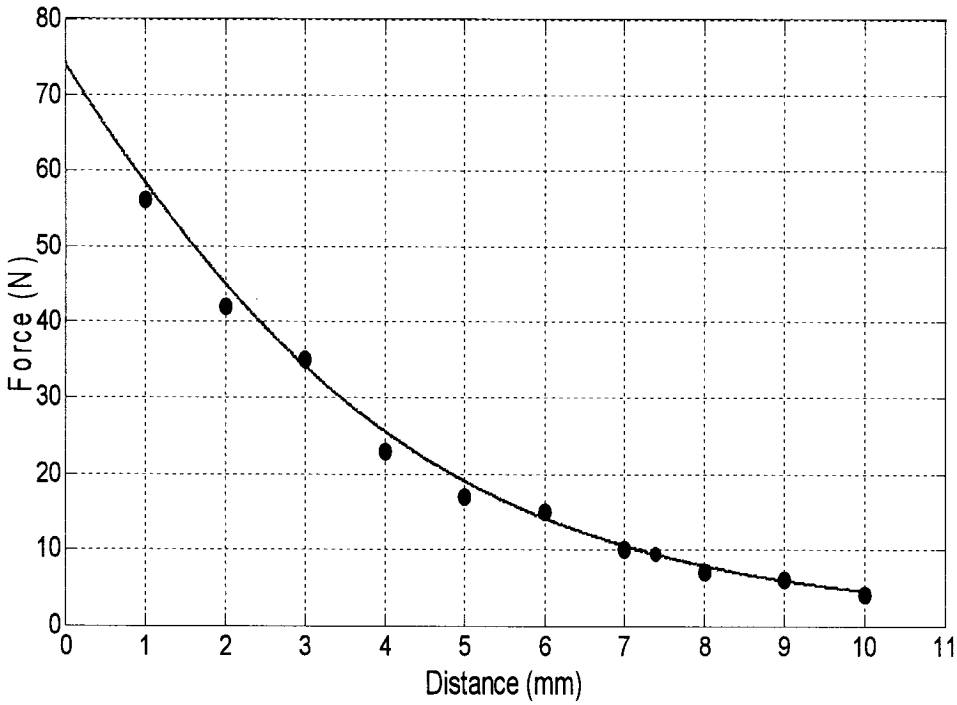

Fig. 4.3. Permanent magnet force versus air gap

4.4 Test and Simulation Results for Permanent Magnet Force and Current at Various Applied Voltages and Air Gap Positions

The transient force and current are measured for the solenoid with the permanent magnet core fixed at eight different air-gap positions from 1 mm to 8 mm at steps of 1 mm increments. At each air gap, the voltage applied to the solenoid was 11 V, 27 V, 38 V, 46 V and 56V. To reduce the amount of data to be presented, only the current and force measurements and from simulation for three different air gaps at 1 mm, 4 mm and 8 mm are illustrated, and are shown in figures 4.4 to 4.9, respectively.

Figures 4.4 to 4.6 show the solenoid transient responses for the solenoid under pulling action, in which the magnet is attracted to the solenoid pole. A comparison of the experimental results for the three figures of current and three figures of force at different air gaps show that the transients and steady state values are essentially the same. This proves the fact that the current and force responses are independent of air gap positions because the permeability of the permanent magnet is approximately the same as that of air.

When comparing the current transients, it is noticed that especially for large applied voltages, the current rises to a maximum and then gradually decreases. This is because the voltage supplies are being loaded and are not ideal because of its series internal resistance [66]. The rise of the current profile from time zero is shown to be not exponential because the coil inductance is a nonlinear function of flux. A comparison of the force transients show that the profiles are similar to that of the current profiles, since force is related to flux (or current).

The simulation results of current are exponential in shape because the magnetic circuit model is a linear first order system. The transients could be corrected to be more comparable to actual results by introducing a nonlinear reluctance element as a function of flux, such as taking into account the hysteresis BH shape of the metal material of the solenoid. This will in turn introduce a nonlinear variable term into the circuit inductance. The deviations from the maximum current as compared to the peak experimental current values can be contributed to the inaccurate estimation of the coil resistance, and unaccounted resistances in the circuit and the resistances contributed from the NMOS transistors. Since force is related to current, the simulated force responses are similar in shape to the simulated current profiles. The deviations of the simulated maximum force values as compared to experimental values can be corrected by adjusting the magnetization value M of the permanent magnet. This is because the manufacturer gives a range for the remanent magnetization B_r, and also because the induced magnetization by the magnetic field of the coil was not considered.

Figures 4.7 to 4.9 show the pushing action of the permanent magnet when the applied voltage polarities are reversed on the solenoid coil. The experimental current plots for the three different air gaps are essentially the same since the system is independent of air gap position. Also, comparisons of the current profiles for magnet pushing action to the current profile for magnet pulling action are essentially the same. This is because the system is the same, and only the voltage polarity has been reversed. This comparison also applies for the forces under magnet pulling and pushing action. The deviations between the simulated current and force profiles as compared to experimental values are due to the same reasons as previously described for the magnet pulling action.

4.5 Summary

In this section the experiments were performed to measure the force and current characteristics of the solenoid incorporating a permanent magnet. The force and currents were measured for eight different air gaps from 1 mm to 8 mm in incremental steps of 1 mm. The major deviation between the simulated and experimental results occurs during the initial rise time of the current profile. This difference can be attributed to unaccounted nonlinearities contributed to the changing inductance created by the hysteresis BH shape of the metal material of the solenoid. Since the pulling and pushing forces are directly related to current, these deviations are also reflected in the force profiles. Experiments also confirmed that the pulling and pushing forces are independent of the permanent magnet core displacement.

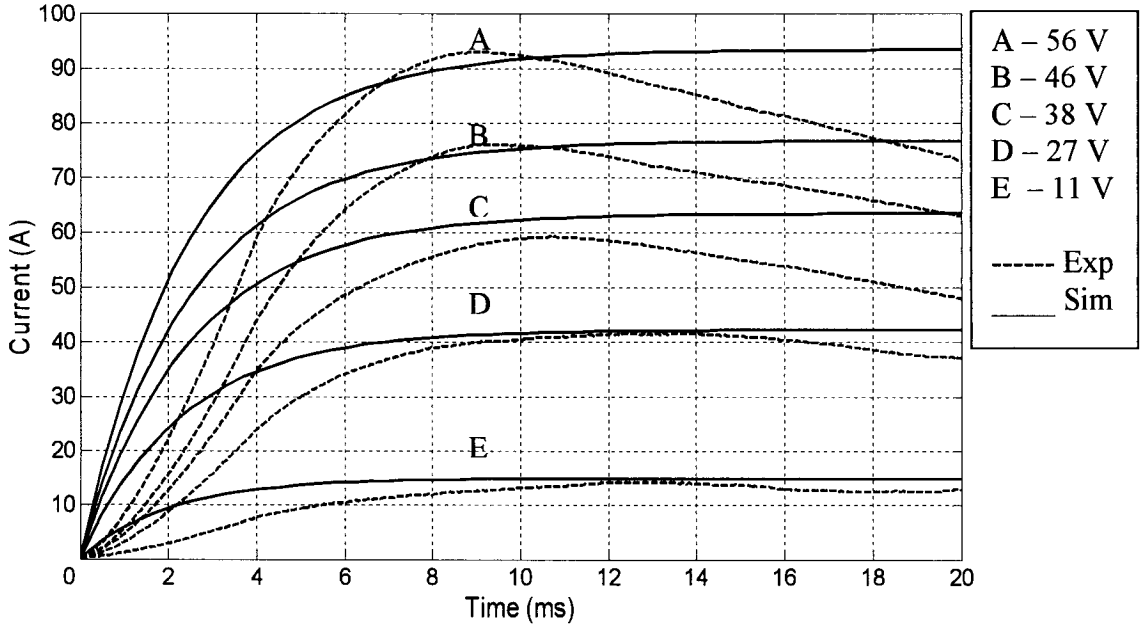

Fig 4.4a. Pulling current due to the coil at 1 mm of air gap

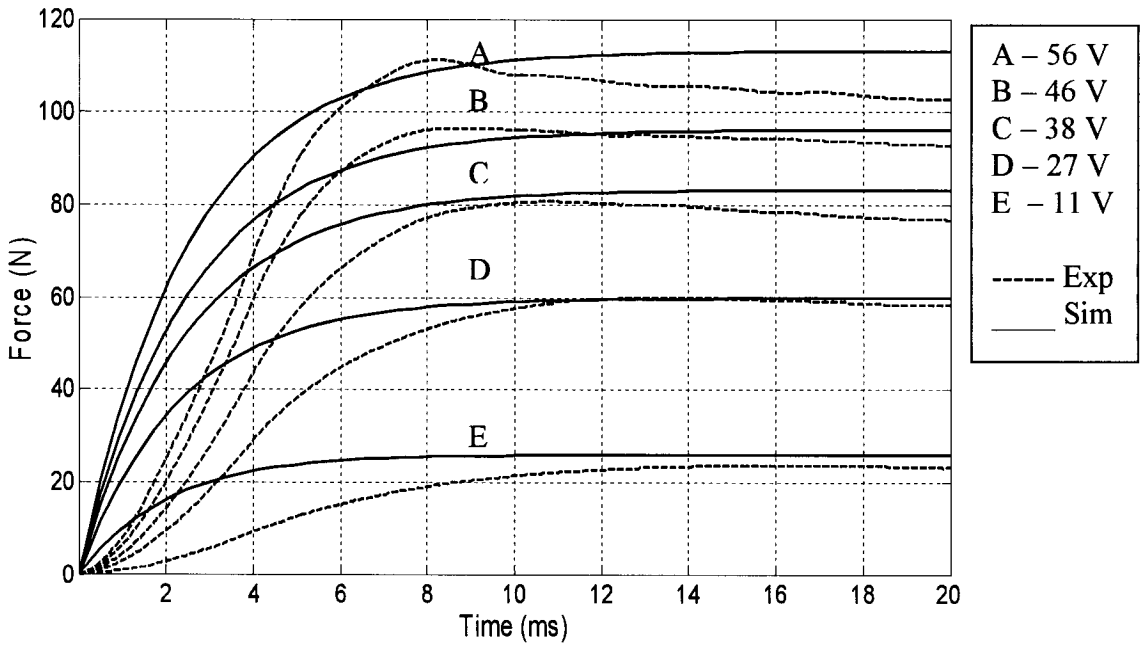

Fig 4.4b. Pulling force due to the coil at 1 mm air gap

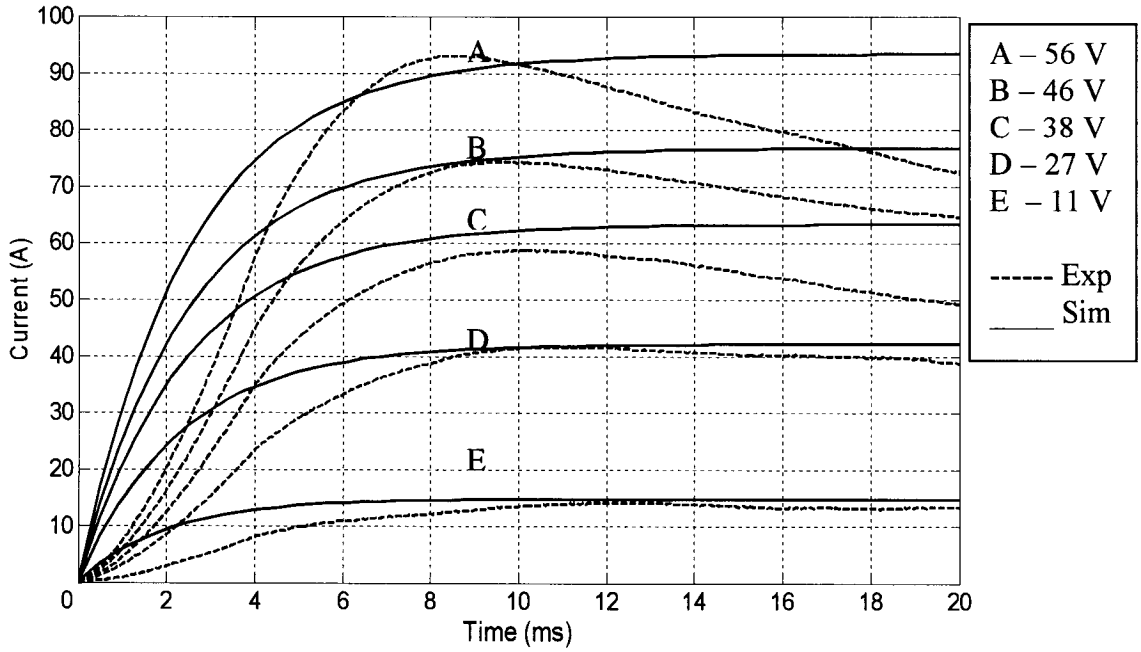

Fig 4.5a. Pulling current due to the coil at 4 mm of air gap

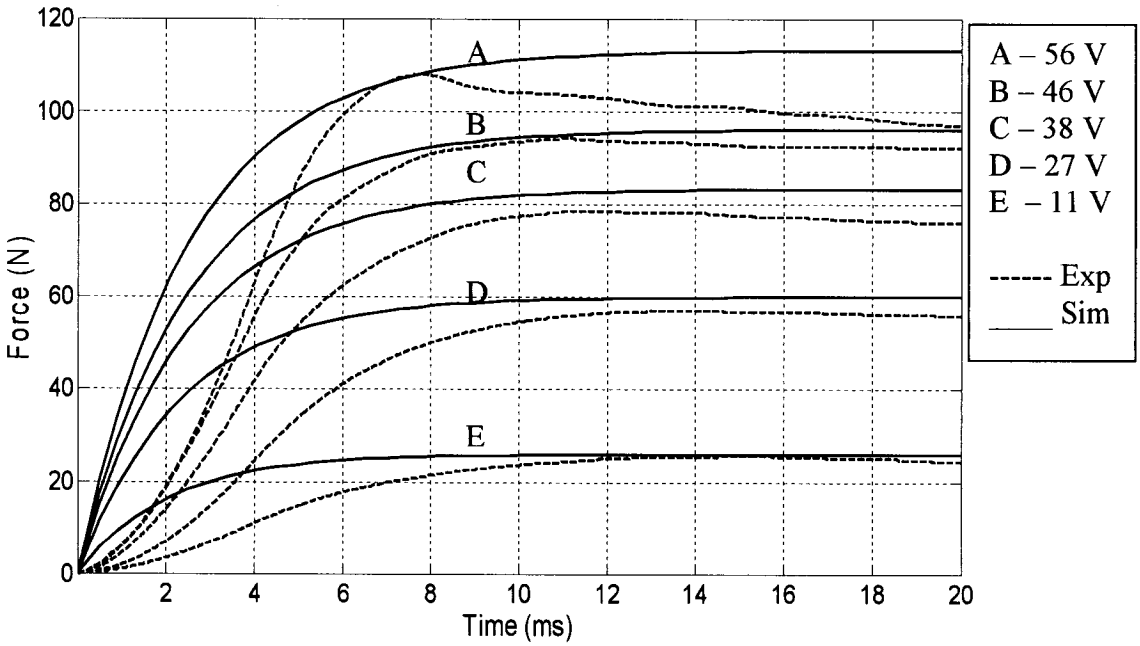

Fig 4.5b. Pulling force due to the coil at 4 mm of air gap

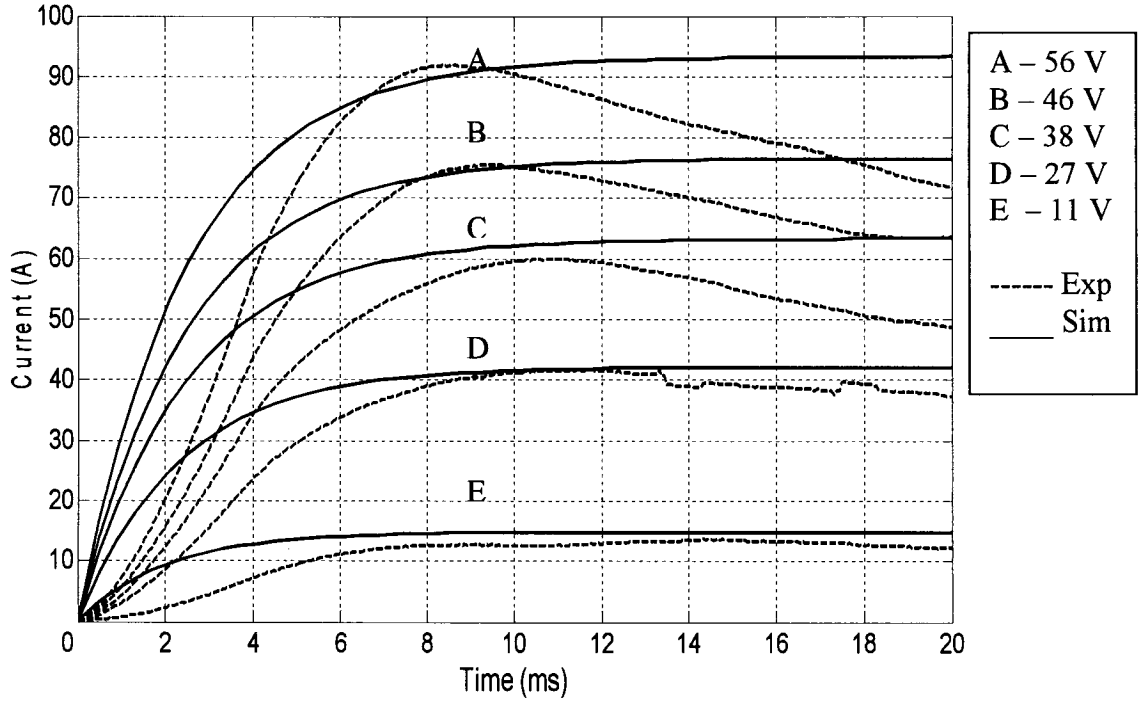

Fig 4.6a. Pulling current due to the coil at 8 mm of air gap

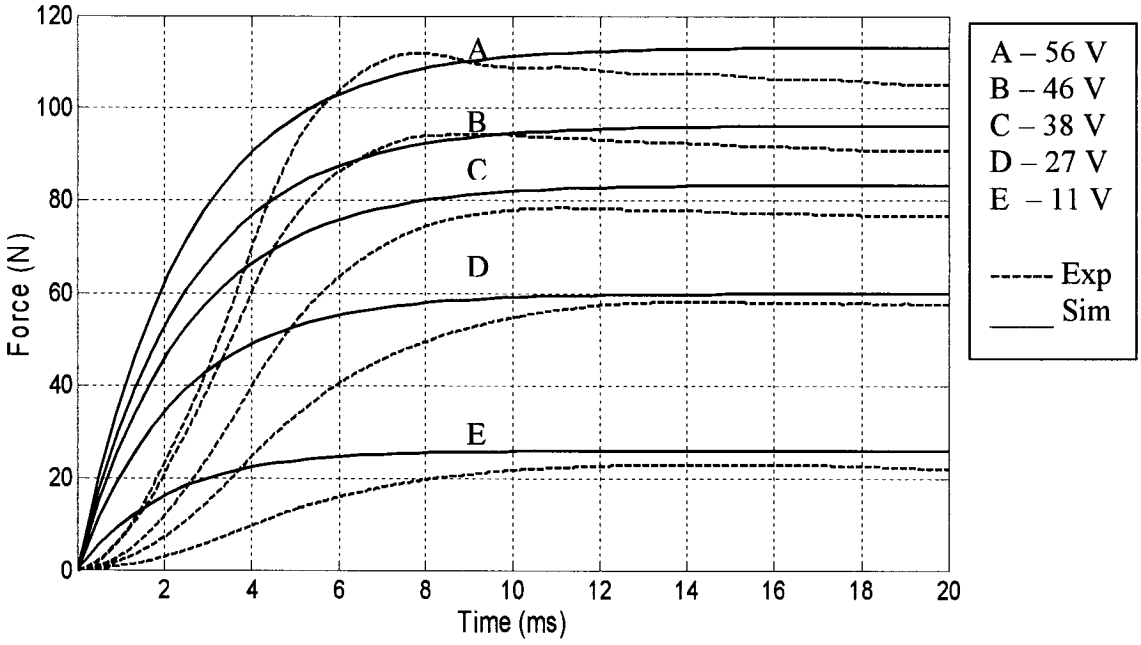

Fig 4.6b. Pulling force due to the coil at 8 mm of air gap

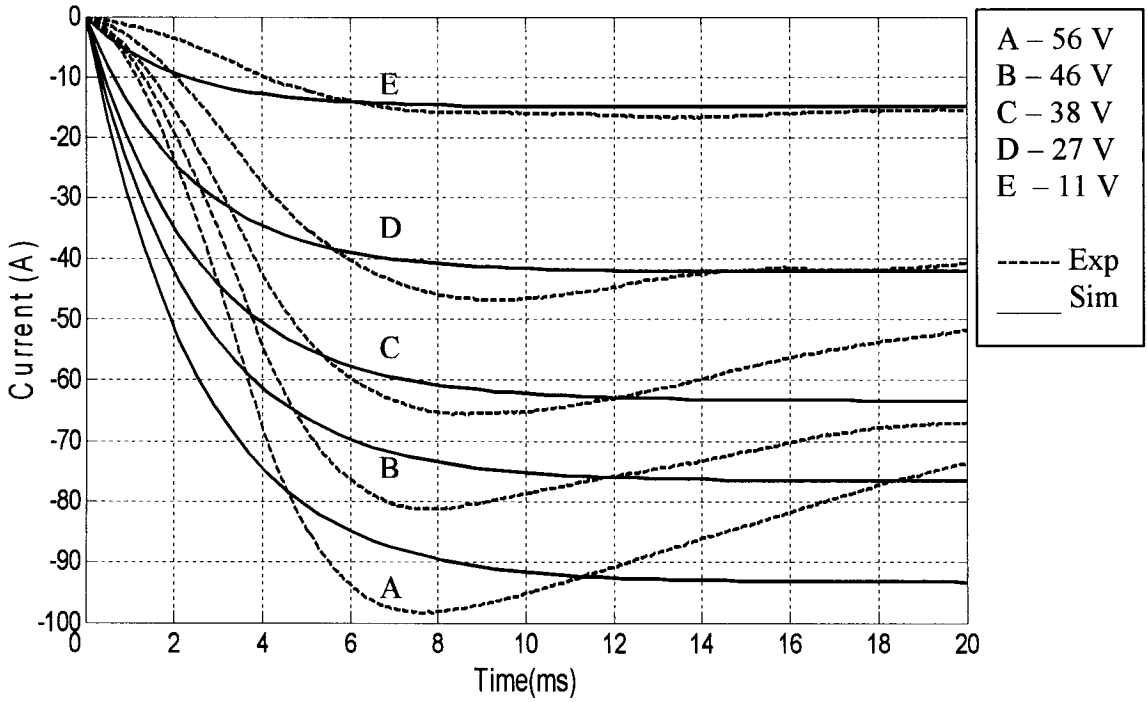

Fig 4.7a. Pushing current due to the coil at 1 mm of air gap

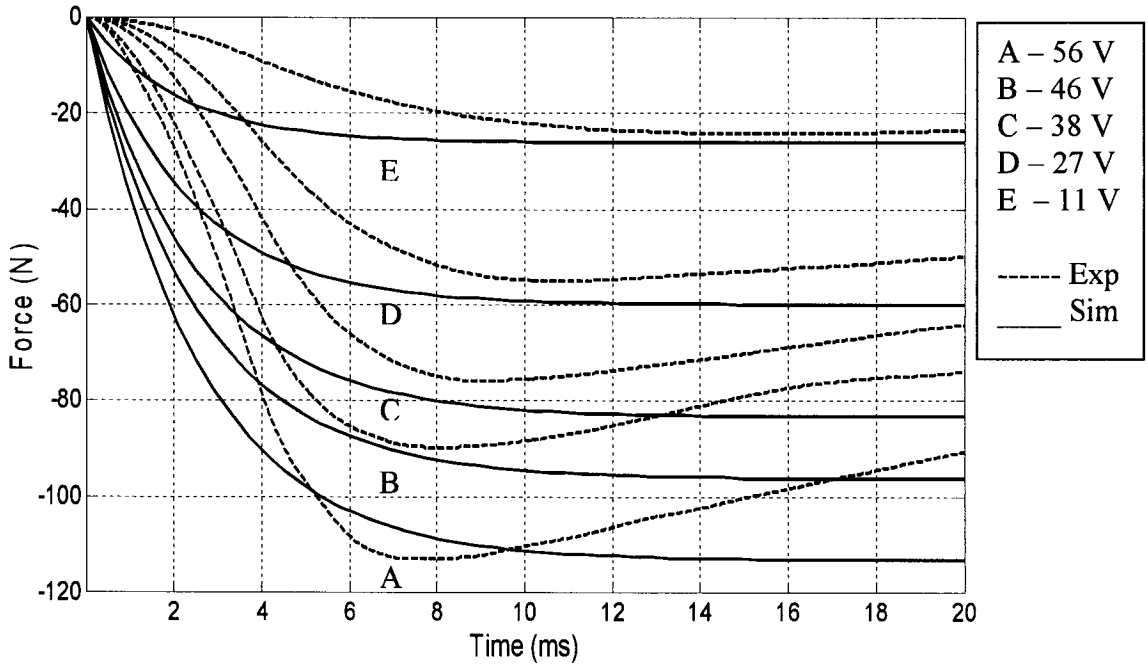

Fig 4.7b. Pushing force due to the coil at 1 mm of air gap

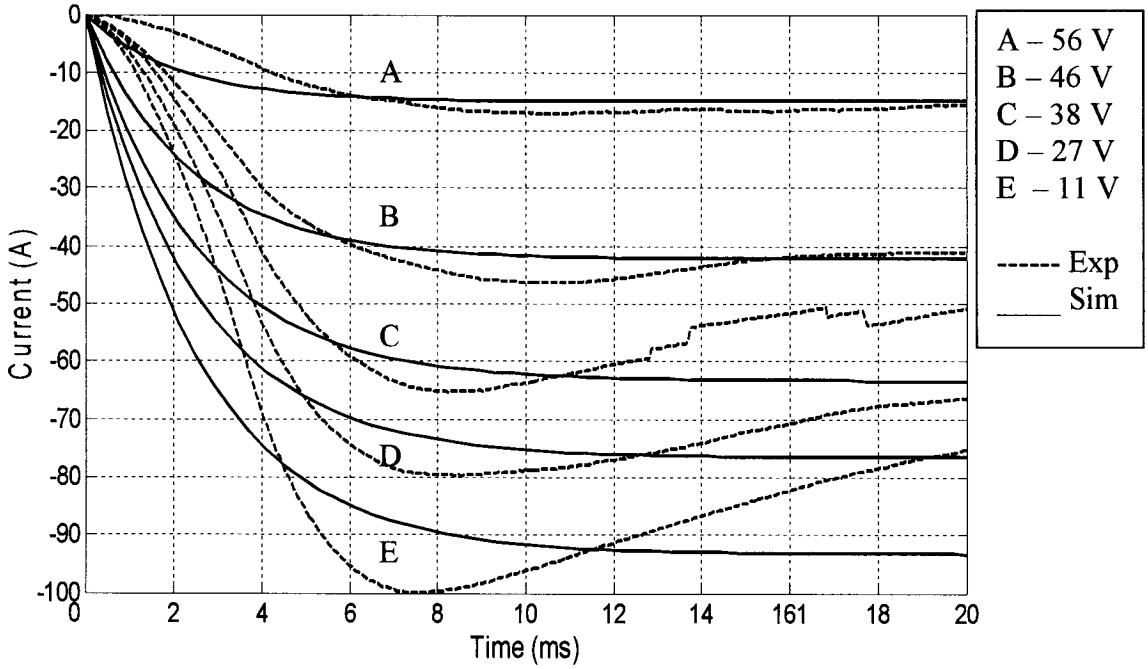

Fig 4.8a Pushing current due to the coil at 4 mm of air gap

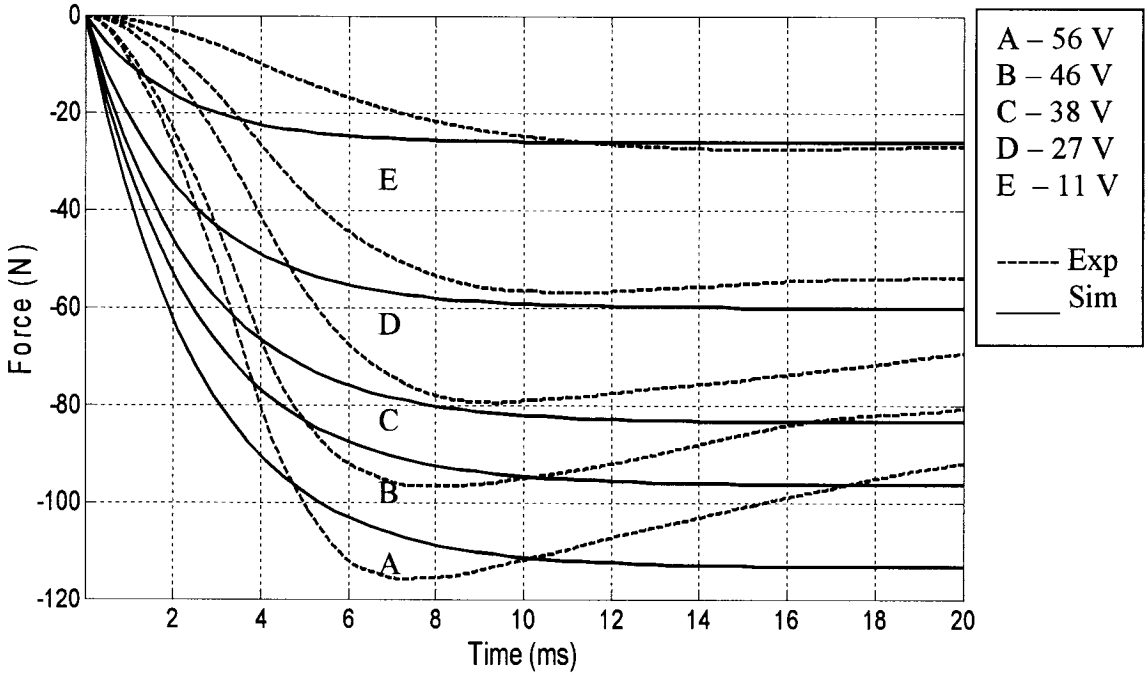

Fig 4.8b. Pushing force due to the coil at 4 mm of air gap

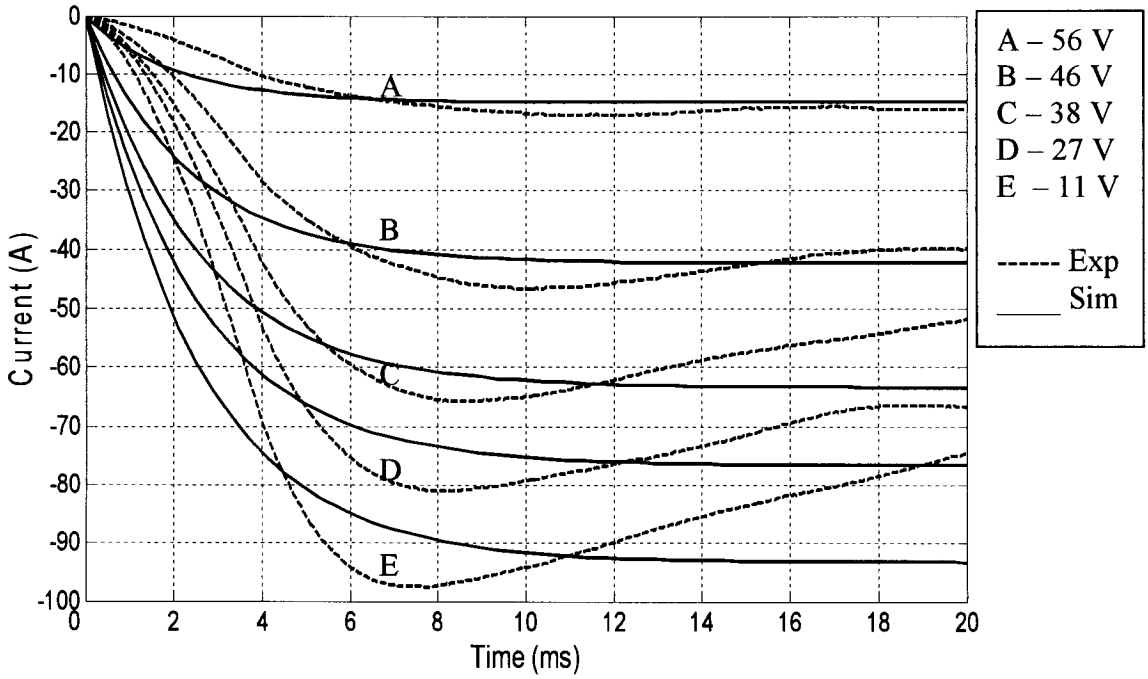

Fig 4.9a. Pushing current due to the coil at 8 mm of air gap

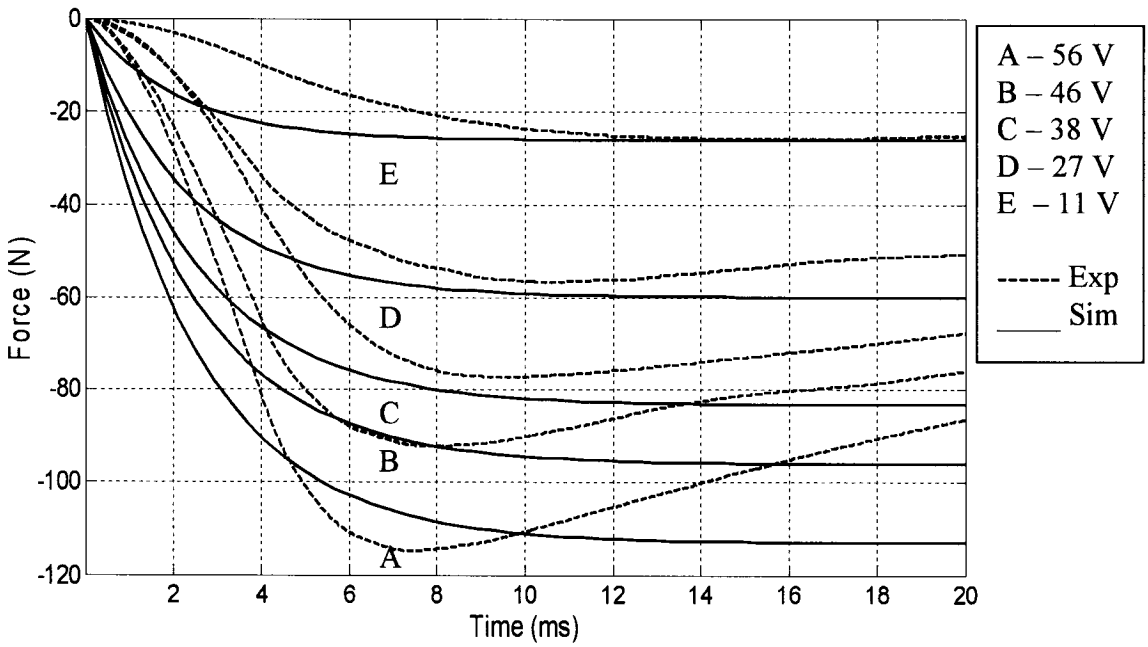

Fig 4.9b. Pushing force due to the coil at 8 mm of air gap

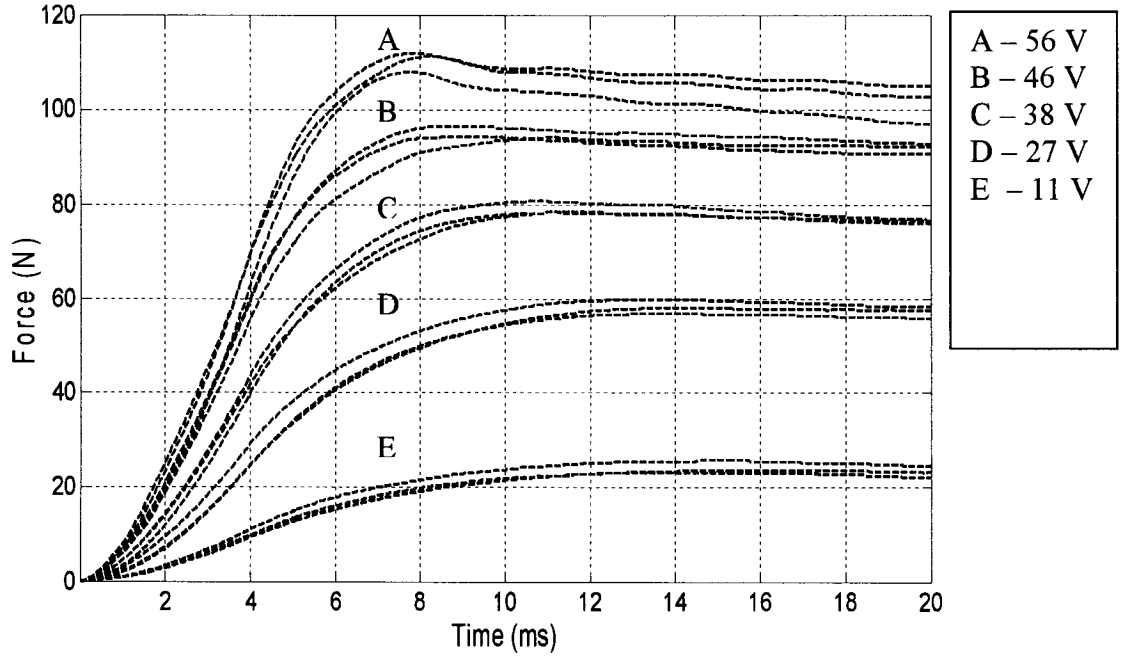

Fig 4.10a. Pulling force due to the coil at 1mm, 4mm, and 8 mm of air gap

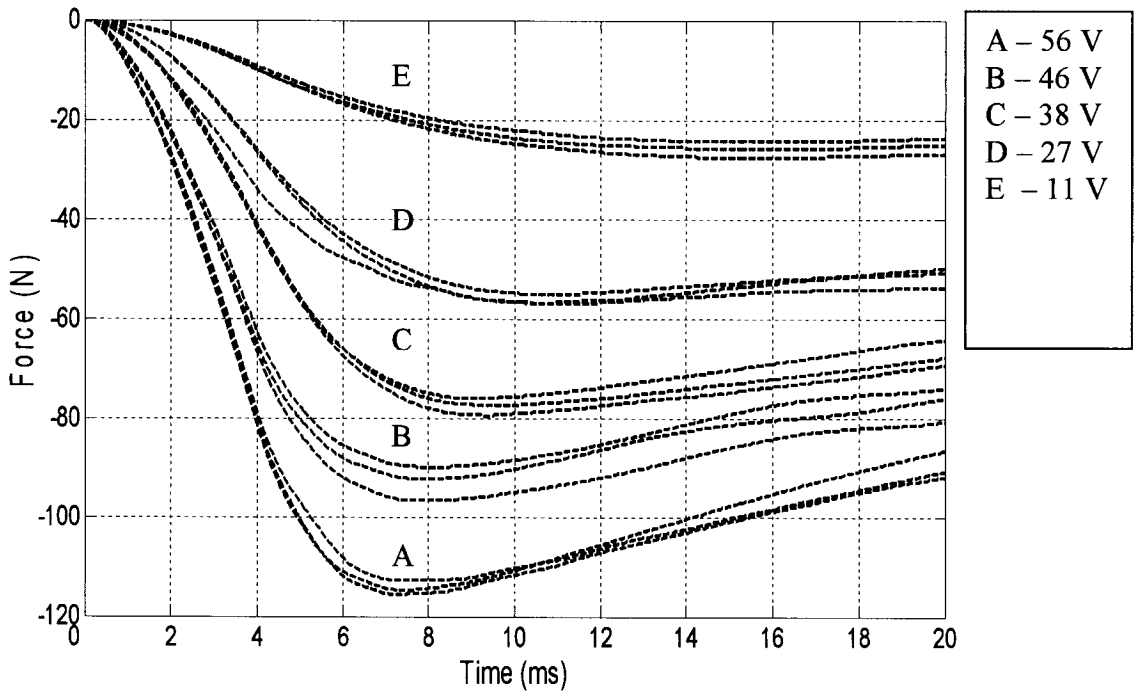

Fig 4.10b. Pushing force due to the coil at 1mm, 4mm, and 8 mm of air gap

CHAPTER 5

CONCLUSION AND RECOMMENDATIONS

5.1 Conclusions

A wide variety of intake and exhaust valve timing strategies have been discussed, each having its own advantages and limitations. A combination of theoretical and experimental studies is necessary to determine the true potentials of the various strategies.

The pumping loop of the PV diagrams and gas flow dynamics through intake and exhaust valve lift and timing are predicted through computer simulation by using the GT-Power simulation software. The presentation by PV and flow diagrams is helpful to identify the potentials of valve timing. The results obtained by simulation perfectly match those discussions from the papers reviewed for various valve strategies.

It has been seen that intake valve timing is the single most important parameter to measure the low-speed and high-speed volumetric efficiency. The pumping losses in gasoline engines are greater than those in diesel engines. In gasoline engines pumping losses occur due to inhaling of the sub-atmospheric gases (intake pumping loss) during the suction stroke and expelling the exhaust gases (exhaust pumping loss) during the exhaust stroke. While in the case of diesel engines, even though the intake pumping losses are lower due to the absence of the throttle valve, exhaust pumping losses will be similar as in gasoline engines, and sometimes even more due to the high in-cylinder pressure. Therefore, the reduction of exhaust pumping losses is one of the parameters to be taken into account for diesel engines. In addition, as a consequence of high compression ratios required for diesel engines, there is very little clearance between the

piston and valves. Thus, it can be predicted that conventional camshaft phasers have limited use in diesel engines. The systems, which independently control the valve opening and closing with variable lift and duration, are more applicable. The transient gas flow behavior for a diesel engine is further complicated and is difficult to fully understand. The pumping loop waivers and may be due to the direct injection of diesel fuel at very high pressure which interacts with the flow dynamics of the air inhaled. In general, it will be useful to continue the study of variable valve timing and its effects on the behavior of gases during the suction and exhaust strokes, which will help to understand gas dynamics effects on the engine volumetric efficiency, emissions and performance.

The review has also shown that LIVC and EIVC are the two strategies where most research has been done. For reducing exhaust emissions, more work is still required with respect to valve overlap and exhaust strategies. Especially for diesel engines, combustion takes place at very high temperature and pressure and this process of combustion assist to form NOx emissions. One of the greatest advantages of VVT is that, by the manipulation of valve timing it is possible to get internal EGR, which has the potentials to reduce NO_X emissions. According to simulation studies it has been shown that internal EGR can be obtained by EIVO and LEVC, while EIVC, LIVC, EEVC and EEVO can also be useful for this purpose. Whereas, LIVO and LEVO are useful to reduce UBHC.

Effects of VVT on an engine are very much dependent on the type of actuator used. Mechanical mechanisms are overly complicated and true variable timing has not been achieved as yet. Electromechanical actuation can achieve this goal. The development of true variable valve timing by electromagnetic valve actuation will give unique opportunities to

understand the characteristics of VVT on actual engines and to confirm VVT engine mathematical models for further engine advancement and development.

To achieve these goals, the design of a solenoid actuator with a permanent magnet moving core has been proposed. The magnet core is able to move bi-directionally depending on the flux direction created by the polarity of the applied voltage on the solenoid. A rare earth permanent magnet of type NdFeB was selected with a linear recoil line of $1.06\mu_0$ so that the solenoid force created is independent of the air gap and to simplify the system modeling equations. Also to be necessary to be independent of the air gap, the pole of the permanent magnet must operate within the area where the solenoid magnetic flux density is uniform and equal in magnitude.

The mathematical model of the permanent magnet solenoid has been simulated to determine its current and force characteristics at various fixed air gaps. A prototype permanent magnet solenoid has been built, where the magnet manufacturer made the NdFeB magnet core according to the dimensions to fit the off-the-shelf solenoid that was purchased. Experiments performed on the prototype confirmed the model current and force characteristics, and the capability of bi-directional motion because of the bi-directional force that was created. The major deviations between test and simulation results occur during the current and force transient rise time which is accounted to the nonlinearity of the system inductance.

By connecting the stem of the engine valve to the moving permanent magnet core, and with a proper force control strategy, true variable valve motion and timing can be achieved. In

addition, force control can achieve reduced valve to seat impact forces for soft landing to alleviate noise and wear.

In summary, VVT is a rich field and much research has been done to recognize its potentials. To get the full benefits from VVT, two important aspects are necessary. One is the manufacturing of cost effective, less complex, and reliable valve timing mechanisms. The second is to understand the benefits from the manipulation of valve timing and its effects on the PV cycle of an engine. With proper VVA mechanism design and control, it can be expected that the PV cycle of any VVT engine can achieve near-zero pumping losses, maximum volumetric efficiency, and the minimization of exhaust pollutions.

5.2 Recommendations for Future Work

The following recommendations could be made regarding the short-term follow-up of this research work:

1. Enhance the mathematical model of the permanent magnet solenoid to include the dynamics of the valve for use to establish the necessary pulse width modulation (PWM) applied voltage and feedback control strategy for position (VVT) and soft landing force control. The study will also help to establish the necessary sensors for feedback control.
2. From the analytical study of (1) above used to establish design parameters, manufacture a permanent magnet solenoid operated valve prototype for experimental testing to confirm the expected results and adjust design parameters.
3. From the analytical study of (1) above, implement the PWM control strategy onto a microcontroller system necessary for the experimental study of (2) above.

4. Implement the solenoid prototype of (2) above and controller of (3) above for actual engine testing on a modified 1-cylinder diesel and 1-cylinder gasoline engine to study, confirm and enhance the knowledge of the effects of various intake/exhaust valve strategies as discussed in this thesis.

REFERENCES

1. Parvate-Patil, G. B., Hong, H., Gordon, B.W., "Analysis Variable Valve Timing Events and Their Effects on Single Cylinder Diesel Engine", 2004-01-2965, SAE Transactions, Journal of Engines, 2004.

   Also published in SAE Special Publication- 1900, ISBN number 07680-1522-7

   Judged among the most outstanding SAE paper of 2004

2. Parvate-Patil, G. B., Hong, H., Gordon, B. W., " An Assessment of Intake and Exhaust Valve Strategies for Variable valve timing", 2003-32-0078, SAE Transactions, Journal of Engines, Sec.3, Vol. 112, pp.2174-2190, 2003.

   Judged among the most outstanding SAE paper of 2003

3. Parvate-Patil, G. B., Hong, H., Gordon, B. W., " Effects of Late Intake Valve Closing on Four Stroke Gasoline Engines", 2004 ASME Heat Transfer/Fluids Engineering Summer Conference Westin Charlotte & convention Center, Charlotte, North Carolina, USA, July 11-15, 2004.

4. Hong, H., Parvate-Patil, G. B., Gordon, B. W., "Review and Analysis of Variable Valve Timing Strategies- Eight Ways to Approach", *IMechE*, Vol. 218 Part D: Journal of Automobile Engineering, 2004.

5. Tuttle, J.H., "Controlling Engine Load by Means of Late Intake-Valve Closing", SAE paper no. 800794, 1980.

6. Asmus, T.W., "Valve Events and Engine Operation", SAE paper no. 820749, 1982.

7. Rabia, S.M. and Kora, N.S., "Knocking Phenomena in Gasoline with Late-Intake Valve Closing", *SAE* paper no. 920381, 1992.

8. Ahmad, T. and Theobald, M.A., "A Survey of Variable-Valve-Actuation Technology", *SAE* paper no. 891674, 1989.

9. Sunders, R.J. and Abdual-Wahab, E.A., "Variable Valve Closure Timing for Load Control and the Otto Atkinson Cycle Engine", *SAE paper* no. 890677, 1989.

10. Blakey, S.C., Foss, P.W., Basset, M.D. and Yates, P.W., "Improved Automotive Part Load Fuel Economy Through Late Intake Valve Closing", *XIV proceedings of Internal Combustion Engine and Combustion,* India, 1995.

11. Blakey, S.C. and Saunders, R.J., "A Design and Experimental Study of an Otto Atkinson Cycle Engine Using Late Intake Valve Closing", *SAE* paper no. 910451, 1991.

12. Ma, T.H., "Effect of Variable Engine Valve Timing on Fuel Economy", *SAE* paper no. 880390, 1988.

13. Seiichi, S., Kenji, N., Shizuo, Y., Youichi, M., Yoshiharu, Y., Hisao, N., Tsuneaki, I., Tomio, O. and Mikiya, A., "Application of Over-Expansion Cycle to a Larger Gasoline Engine with Late-Closing of Intake Valves", *ASME* 2002, *ICEF* 2002-484.

14. Shiga, S., Morita. M., Yagi, S., and Matsumoto, T., "Effect of Early-closing of Intake-valve on the Engine Performance in a Spark-ignition Engine", *SAE* paper no. 960585, 1996.

15. Soderberg, F. and Johansson, B., "Fluid Flow Combustion and Efficiency with Early or Late Intake Valve Closing", *SAE* paper no. 972937, 1997.

16. Soderberg, F. and Johansson, B., "Load Control using Late Intake Valve Closing in a Cross Flow Cylinder Head", *SAE* paper no. 2001-01-3554, 2001.

17. Saunders, R.J. and Rabia, S.M., "Part load efficiency in Gasoline Engines, Practical Limits of Efficiency of Engine", *IMechE*, pp. 55-62, 1986, Part D: Journal of Automobile Engineering, 1986.

18. Elord, A.C. and Nelson, M.T., "Development of Variable Valve Timed Engine to Eliminate Pumping Losses Associated with Throttled Operation", *SAE* paper no. 860537, 1986.

19. Haugen, D.J., Blackshear, P.L., Pipho, M.J. and Esler, W.J., "Modifications of a Quad 4 Engine to Permit Late Intake Valve Closure", *SAE* paper no. 921663, 1992.

20. Stein, R.A., Galietti, K.M., and Leone, T.G., "Dual Equal VCT- A Variable Camshaft Timing Strategy for Improved Fuel economy and Emissions", *SAE* paper no. 950975, 1995.

21. Ham, Y.Y. and Park, P., "The Effects of Intake Valve Events on Engine Breathing Capability", *The Sixth International Pacific conference on Automotive Engineering, Seoul, Korea,* paper number 912470, 1991.

22. Tuttle, J.H., "Controlling Engine Load by Means of Early Intake-Valve Closing", *SAE* paper no. 820408, 1982.

23. Urata, Y., Umiyama, H., Shimizu, K., Fujiyoshi, Y., Sono, H. and Fukuo. K., "A Study of Vehicle Equipped with Non-Throttling S.I Engine with Early Intake Valve Closing Mechanism", *SAE* paper no. 930820, 1993.

24. Gray, C., "A Review of Variable Engine Valve Timing", *SAE* paper no. 880386, 1988.

25. Hans, P.L., Llaus, W. and Dusan, G., "Variable Valve Timing – A Possibility to Control Engine Load Without Throttle", *SAE* paper no. 880388, 1988.

26. Stivender, D.L., "Intake Valve Throttling (IVT) – A Sonic Throttling Intake Valve Engine", *SAE* paper no. 680399, 1968.

27. Moro, D., Ponti, F. and Serra, G., "Thermodynamic Analysis of Variable Valve Timing Influence on SI Engine Efficiency", *SAE* paper no. 2001-01-0667, 2001.

28. Diana, S., Lorio, B., Giglio, V. and Police, G., "The Effect of Valve Lift Shape and

Timing on Air Motion and Mixture Formation of DISI Engines Adopting Different VVA Actuators", *SAE* paper no. 2001-01-3553, 2001.

29. Sellnau, M. and Rask, E., "Two-step Variable Valve Actuation for Fuel Economy, Emissions, and Performance", *SAE* paper no. 2003-01-0029, 2003.

30. Vogel, O., Roussopoulos, K., Guzzella, L. and Czekaj, J., "Variable Valve Timing Implemented with a Secondary Valve on a Four Cylinder SI Engine", *SAE* paper no. 970335, 1997.

31. Badami, M., Marzano, M.R. and Nuccio, P., "Influence of Late Intake-Valve Opening on the S.I. Engine-Performance in Idle Condition", *SAE* paper no. 960586, 1996.

32. Siewert, R.M., "How Individual Valve Timing Events Affect Exhaust Emissions", *SAE* paper no. 710609, 1971.

33. Hara, S., Nakajima, Y. and Naguma, S., "Effects of Intake-Valve Closing Timing on Spark-Ignition Engine Combustion", *SAE* paper no. 850074, 1985.

34. Law, D., Kemp, D., Allen, J., Kirkpatrick. G. and Copland, T., "Controlled Combustion in an IC-Engine with a Fully Variable Valve Train", *SAE* paper no 2000-01-0251, 2000.

35. Chapman, M., Novak, J.M. and Stein, R.A., "Numerical Modeling of Inlet and Exhaust Flows in Multi-Cylinder Internal Combustion Engines", *Flows in Internal Combustion*

Engines, ASME, 1982.

36. Heywood, J.B., "Internal Combustion Engines", *McGraw-Hill Publishing Co.*, pp. 215-220, 1988.

37. Davis, G.C., Tabaczynski, R.J. and Belaire, R.C., "The Effect of Intake Valve Lift on Turbulence Intensity and Burnrate in S.I. Engines - Model versus Experiment", *SAE* paper no. 840030, 1984.

38. Dresner, T. and Barkan, P., "A Review and Classification of Variable Valve Timing Mechanisms", *SAE* paper no. 890667, 1989.

39. Sandquist, H., Wallesten, J., Enwald, K. and Stromberg, S., "Influence of Valve Overlap Strategies on Residual Gas Fraction and Combustion in a Spark-ignition Engine at Idle", *SAE* paper no. 972936, 1997.

40. Kreuter, P., Heuser, P. and Schebitz, M., "Strategies to Improve SI-Engine Performance by Means of Variable Intake Lift, Timing and Duration", *SAE* paper no. 920449, 1992.

41. Lancefield, T., Methely, I., Rase, U. and Kuhn, T., "The Application of Variable Event Timing to a Modern Diesel Engine", *SAE* paper no. 2000-01-1229, 2000.

42. Tai, C., Tsao, T., Schorn, N. and Levin, M., "Increasing Torque Output from a Turbodiesel with Camless Valvetrain", *SAE* paper no. 2002-01-1108, 2002.

43. Endo, S., Otani, T. and Kakinal, A., "An Improvement of Pumping Loss of High Boosted Diesel Engines", *SAE* paper no. 885102, 1988.

44. Hu, H., Israel, M. and Vorih, M., "Variable Valve Actuation and Diesel Engine Retarding Performance", *SAE* paper no. 970342, 1997.

45. Benajes, J., Reyes, E. and Lujan, J., "Intake Valve Pre-lift Effect on the Performance of a Turbocharged Diesel Engine", *SAE* paper no. 960950, 1996.

46. Stas, M., "Effect of Exhaust Blowdown Period on Pumping Losses in a Turbocharged Direct Injection Diesel Engine", *SAE* paper no. 1999-01-0188, 1999.

47. Charlton, S., J., Stone, C. R., Elliott, C. and Newman, M. J., "Transient Simulation of a Highly Turbocharged Diesel Engine with Variable Valve Timing", *IMechE*, C430/016, Part D: Journal of Automobile Engineering, 1991.

48. Fukutani, I. and Watanabe, E., " An Analysis of the Volumetric Efficiency Characteristics of 4- Stroke Cycle Engines Using the Mean Inlet Mach Number Mim", *SAE* paper no. 790484, 1979.

49. Lequesne, B., Henry, R., Kamal, M., "Magnavalve: A New Solenoid Configuration Based on a Spring-Mass Oscillatory System for Engine Valve Actuation", GM Research Report, E3-89, june 17, 1988.

50. Vaughan, N. D, and Gamble, P., " The Modeling and Simulation of a Proportional Solenoid Valve", Transactions of ASME, March 1996, Vol. 118, pp. 120-125.

51. Masoud, K., Lawrence, P., Sassani, F., "Nonlinear Modeling and Validation of Solenoid-Controlled Pilot-Operated Servovalves", IEEE/ASME Transactions on Mechatronics, Vol. 4, No. 3, September 1999.

52. Cheung, N., Lim, C., Rahaman., " Modeling a Linear and Limited Travel Solenoid", IEEE, 19th International Conference on Industrial Electronics, 1993.

53. Lequesne, B., "Fast-Acting, Long-Stroke Solenoids with Two Springs", IEEE Transactions on Industry Applications, Vol. 26, No.5, September/October, 1990.

54. Wang, Y., Stefanopoulou, A., Haghgooie, M., Kolmanovsky, I., Hammoud, M., "Modeling of an Electromagnetic Valve Actuator for a Camless Engine", Proceedings 5th Int'l Symposium on Advanced Vehicle Control, no. 93, Aug 2000.

55. Hofmmann, W., Stefanopoulou, A., "Valve Position Tracking for Soft Landing of Electromagnetic Camless Valvetrain", Proceedings on IFAC workshop on Automotive Control, pp 305-310, Kalsruhe, March 2001.

56. Giglio, V., Iorio, B., Police, G., "Analysis of Advantages and of Problems of Electronechanical Valve Actuators", *SAE* Paper 2002-01-1105, 2002.

57. Dexter Magnetic Technologies reference and design manual, http://www.dextermag.com

58. Hambley. A.R., "Electrical Engineering- Principles and Application", Prentice Hall, Englewood Cliffs, New Jersey, 1997.

59. Hong, H., Krepec, T., and Chen, R. M. H., "Transient Response of Fast Acting Solenoid in Automotive Applications", Journal of Circuits, Systems, and Computers, Vol.4, No. 4, 1994, pp. 415-428.

60. Rao, N. N., "Elements of Engineering Electromagnetics", Prentice Hall, 1991.

61. McCaig, M., "Permanent Magnets in Theory and Practice", A Halsted Press Book, 1989.

62. Brown Jr. W. F, "Electric and Magnetic Forces: A Direct Calculation. I", American Journal of Physics, Vol. 19, 1951, pp. 290-304.

63. Haus, H. A., Melcher, J. R., "Electromagnetic fields and energy", Prentice Hall, 1989.

64. Plonus, M. A., "Applied Electromagnetics", McGraw-Hill Book Company, 1978.

65. E. P Furilani, J. K. Lee, and D. Dowe, " Predicting the dynamic behaviour of moving magnet actuator", J. Appl. Phys. April 1993, pp. 3555-3557.

66. H. Hong., "Optimum Performance of Solenoid Injectors for Direct Injection of Gaseous Fuels in IC Engine", Ph.D. Thesis, Concordia University, 1995.

APPENDIX A

DESCRIPTION AND CALIBRATION OF PIEZO-CELL FORCE TRANSDUCER

A piezoelectric load cell was used to measure the electromagnetic force of attraction and repulsion in the experimental set-up as shown in figure 4.2 of Chapter 4.

The specifications of the load cell are as follows:

Manufacturer: Kistler, type 9001

Range: from 0 to 7500 N

Sensitivity: - 4.29 pC/N

Linearity: $\leq \pm$ 0.4 % FSO

Operating Temperature Range: - 196 to 200 ° C

The converter used is the charge amplifier is produced by Kistler, model 504E.

In the calibration of the force transducer, dead weights were gradually applied from 0 to 78.48 N to load the cell under compression, and the electrical output from the cell was recorded. Figure A.1 plots the calibration curve for the transducer.

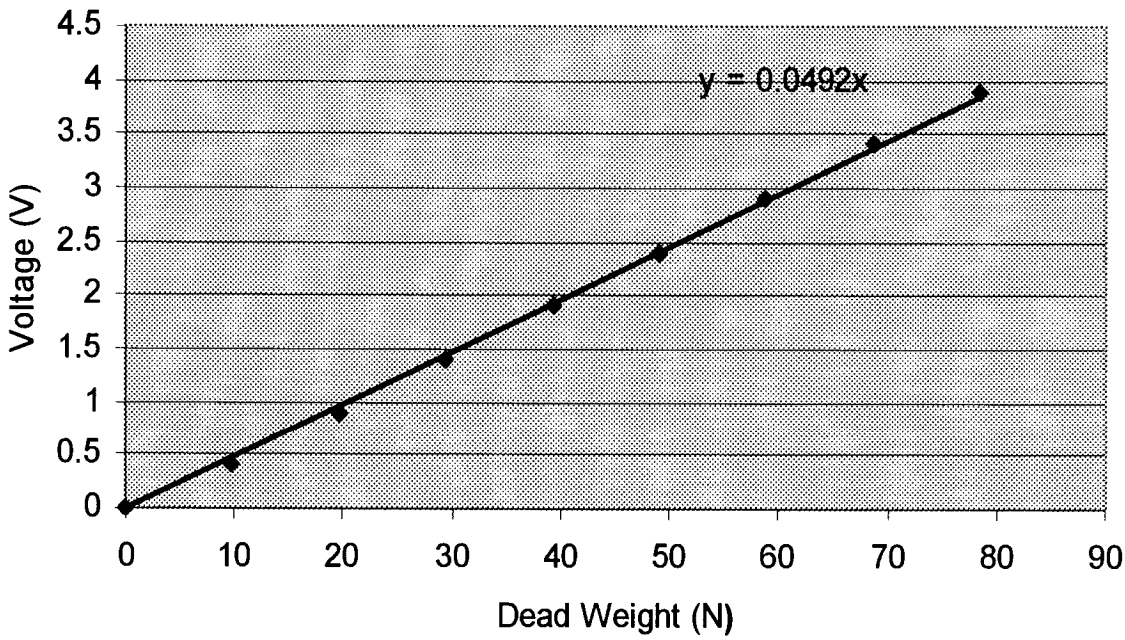

Fig. A.1 Piezo-cell force transducer calibration curve